

2016

# Brain networks involved in decision making: an electroencephalography and magnetic resonance imaging study

---

<https://hdl.handle.net/2144/19055>

*Boston University*

BOSTON UNIVERSITY  
SCHOOL OF MEDICINE

Dissertation

**BRAIN NETWORKS INVOLVED IN DECISION MAKING: AN  
ELECTROENCEPHALOGRAPHY AND MAGNETIC RESONANCE IMAGING  
STUDY**

by

**DANIELLE CHRISTINA FARRAR**

B.S., University of Washington, 2003  
M.A, Boston University, 2008

Submitted in partial fulfillment of the  
requirements for the degree of  
Doctor of Philosophy

2016

© 2016  
DANIELLE FARRAR  
All rights reserved

Approved by

First Reader

---

Ronald Killiany, Ph.D.  
Associate Professor of Anatomy and Neurobiology

Second Reader

---

Andrew Budson, M.D.  
Professor of Medicine

## **DEDICATION**

I would like to dedicate this work to my husband Spencer and to my son Skyler.

**BRAIN NETWORKS INVOLVED IN DECISION MAKING: AN  
ELECTROENCEPHALOGRAPHY AND MAGNETIC RESONANCE IMAGING  
STUDY**

**DANIELLE CHRISTINA FARRAR**

Boston University School of Medicine, 2016

Ph.D. degree requirements completed in 2016

Dual M.D./Ph.D. degrees expected in 2018

Major Professor: Ronald Killiany, PhD, Associate Professor of Anatomy and  
Neurobiology

**ABSTRACT**

Executive function describes high-level cognitive-abilities including planning, decision-making, set switching and response inhibition. Impairments of the executive functions in disease states may be subtle but can greatly reduce the quality of life and independence. The overarching theme of this project was to investigate the network of brain regions that are needed to support executive function. This was undertaken using a two-fold approach: one, to apply network analysis to resting state functional Magnetic Resonance Imaging (rs-fMRI) and Diffusion Tensor Imaging (DTI) data in order to describe how differences in morphometry and connectivity correlate to executive function differences of individuals with Mild Cognitive Impairment (MCI), and two, to describe the brain networks involved in one form of executive function, decision-making under uncertain conditions, in young, healthy individuals. Impaired decision-making can dramatically impact day-to-day functioning and understanding the underlying network of regions that support this task can provide a target for future intervention studies.

Data from the Alzheimer's Disease Neuroimaging Initiative (ADNI) were used in the studies of MCI. Individuals were grouped by their executive abilities. A regions-of-interest approach was used to parcel and label various brain regions and a network of connections was constructed out of these regions. Differences between the networks were then compared between the MCI subjects with good and poor executive functions. Those with high executive abilities showed decreased functional network connectivity and increased structural network connectivity.

The second arm of these studies was based on an original decision-making paradigm that was used to compare networks involved in decision-making at times of uncertainty in healthy young individuals using both electroencephalography (EEG) and task-based functional magnetic resonance imaging (fMRI). Overall we found greater network connectivity in the uncertain condition of the task than in the certain condition. This suggests that with increased uncertainty comes increased organized connectivity. Taken together, the results of this study re-iterate the notion that cognition depends upon the efficient communication between a network of brain regions rather than on isolated regions. They also highlight the importance of having a well-defined network of nodes and connections for optimal executive functioning.

## TABLE OF CONTENTS

<b>DEDICATION.....</b>	<b>iv</b>
<b>ABSTRACT.....</b>	<b>v</b>
<b>TABLE OF CONTENTS.....</b>	<b>vii</b>
<b>LIST OF TABLES.....</b>	<b>x</b>
<b>LIST OF FIGURES.....</b>	<b>xii</b>
<b>LIST OF ABBREVIATIONS.....</b>	<b>xvi</b>
<b>CHAPTER ONE: INTRODUCTION TO HIGH VERSUS LOW EXECUTIVE ABILITIES IN MILD COGNITIVE IMPAIRMENT .....</b>	<b>1</b>
<b>CHAPTER 2: DIFFERENCES IN EXECUTIVE ABILITIES ARE ACCOUNTED FOR BY ALTERATIONS IN FUNCTIONAL NETWORKS .....</b>	<b>6</b>
<b>Background .....</b>	<b>6</b>
<b>Methods.....</b>	<b>7</b>
Participants.....	7
Procedure .....	8
<b>Results .....</b>	<b>11</b>
<b>Discussion .....</b>	<b>14</b>



<b>CHAPTER 3: STRUCTURAL DIFFERENCES IN MCI PATIENTS WITH DISPARATE EXECUTIVE ABILITIES.....</b>	<b>19</b>
<b>Introduction .....</b>	<b>19</b>
<b>Methods.....</b>	<b>21</b>
MRI acquisition .....	22
Analysis .....	22
<b>Results .....</b>	<b>23</b>
<b>Discussion .....</b>	<b>33</b>
 <b>CHAPTER 4: INTRODUCTION TO DECISION-MAKING AND RULE UNCERTAINTY .....</b>	 <b>36</b>
 <b>CHAPTER 5: AN EVENT-RELATED POTENTIAL ANALYSIS OF BRAIN ACTIVITY IN DECISION-MAKING IN CERTAIN VERSUS UNCERTAIN CONDITIONS .....</b>	 <b>41</b>
<b>Background .....</b>	<b>41</b>
<b>Methods.....</b>	<b>43</b>
Participants.....	43
Electroencephalography setup.....	45
Analysis .....	45
<b>Results .....</b>	<b>47</b>
Certain versus Uncertain.....	47
Correct versus Incorrect .....	51
<b>Discussion .....</b>	<b>55</b>

<b>CHAPTER 6: NETWORK-BASED ANALYSIS OF BRAIN ACTIVITY USING FMRI IN DECISION-MAKING UNDER UNCERTAIN CONDITIONS .....</b>	<b>58</b>
<b>Introduction .....</b>	<b>58</b>
<b>Methods.....</b>	<b>61</b>
Subjects .....	61
Paradigm.....	61
MRI Acquisition and Preprocessing .....	62
<b>Results .....</b>	<b>65</b>
FEAT Analysis .....	65
Network Analysis .....	69
<b>Discussion .....</b>	<b>74</b>
 <b>CHAPTER 7: DECISION-MAKING UNDER UNCERTAIN CONDITIONS: A COHERENCE NETWORK ANALYSIS USING EEG .....</b>	 <b>79</b>
<b>Introduction .....</b>	<b>79</b>
<b>Methods.....</b>	<b>82</b>
Analysis .....	82
<b>Results .....</b>	<b>83</b>
<b>Discussion .....</b>	<b>99</b>
 <b>CHAPTER 8: CONCLUSION .....</b>	 <b>103</b>
 <b>BIBLIOGRAPHY .....</b>	 <b>107</b>
 <b>CURRICULUM VITAE.....</b>	 <b>117</b>

## LIST OF TABLES

Table 1. Demographics of subjects selected from the MCI population who were classified as high or low executive functioning.....	11
Table 2. Regions of interest showing significantly different node degree in functional network connectivity between MCI-highEF and MCI-lowEF individuals.....	12
Table 3. Regions of interest showing differences in cluster coefficient comparing functional networks of MCI-highEF versus MCI-lowEF individuals.....	12
Table 4. Global network measures comparing functional networks of MCI-highEF versus MCI-lowEF individuals.....	13
Table 5. Population statistics for DTI EF analysis .....	21
Table 6. Network measures for DTI EF analysis.....	24
Table 7. Binary Clustering Coefficient (threshold of 5 tracts) for the DTI EF analysis...	27
Table 8. Node degree for DTI EF comparison. ....	28
Table 9. Node Strength for DTI EF comparison.....	28
Table 10. Tract comparison of Volume, MCI-highEF > MCI-lowEF.....	28
Table 11. Tract comparison of FA, MCI-highEF > MCI-lowEF .....	29
Table 12. Tract Comparison of RD, MCI-lowEF > MCI-highEF .....	29
Table 13. NBS algorithm edges for DTI analysis. MCI-highEF> MCI-lowEF. ....	32
Table 14. Clusters produced by FEAT analysis, Certain > Uncertain.....	65
Table 15. Clusters produced by FEAT analysis, Uncertain > Certain.....	67
Table 16. Network size of fMRI networks, comparing certain versus uncertain conditions at varying thresholds.....	69

Table 17. Network density of fMRI networks, comparing certain versus uncertain conditions at varying thresholds. ....	70
Table 18. Network assortativity of fMRI networks, comparing certain versus uncertain conditions at varying thresholds. ....	70
Table 19. Weighted Clustering Coefficient: nodes of significant difference between certain and uncertain condition. ....	71
Table 20. Node strength: nodes of significant difference between certain and uncertain condition. ....	73
Table 21. Size of EEG network for certain versus uncertain conditions at varying thresholds and frequency bands. ....	88
Table 22. Certain versus uncertain EEG network density at varying thresholds and frequency bands. ....	89
Table 23. Certain versus uncertain EEG network assortativity at different frequency bands and thresholds. ....	90
Table 24. Correct versus incorrect EEG network size at varying frequency bands and thresholds. ....	91
Table 25. Correct versus incorrect EEG network density at varying thresholds and frequency bands. ....	92
Table 26. Correct versus incorrect EEG network assortativity at varying thresholds and frequencies. ....	93

## LIST OF FIGURES

Figure 1. Network differences between MCI-highEF and MCI-lowEF as calculated by the NBS algorithm. ....	14
Figure 2. Network measures, as reflected in ROIs of significant difference marked by circles, comparing MCI-highEF and MCI-lowEF. a) Binary node degree. b) Node strength. c) Clustering coefficient. ....	24
Figure 3. Results of NBS algorithm for MCI-highEF > MCI-lowEF.....	30
Figure 4. Decision-making card-matching task paradigm. ....	44
Figure 5. ERP Regions of Interest. ....	46
Figure 6. Certain and Uncertain condition averaged potentials from -200 ms to 2000 ms post card presentation. ROIs are grouped as described in Figure 2. ....	48
Figure 7. Scalp maps of 100 ms intervals from 0-2000 ms of the certain – uncertain condition, averaged and plotted at each electrode in the -4 to 4 uV scale. ....	49
Figure 8. Certain versus Uncertain condition. Significance of epoch per electrode. T-tests comparing measure in each 100 ms interval (x-axis) for each electrode (y-axis). p-values < 0.05 represented by red, all others represented by blue. 336 of 2432 (14%) epochs had $p < 0.05$ . a) min value compared for each 100 ms interval. b) Maximum value compared for each 100 ms interval. 352 of 2432 (14%) epochs had $p < 0.05$ . c) mean value compared for each 100 ms interval. 347 of 2432 (14%) epochs had $p < 0.05$ . ....	50
Figure 9. Correct and incorrect condition averaged potentials from -200 ms to 2000 ms post card presentation. ROIs are grouped as described in Figure 2. ....	52

Figure 10. Scalp maps of 100 ms intervals from 0-2000 ms of the correct – incorrect condition, averaged and plotted at each electrode in the -4 to 4 uV scale.....	53
Figure 11. Significance of each epoch per electrode in correct versus incorrect condition. T-tests comparing measure in each 100 ms interval (x-axis) for each electrode (y-axis). p-values < 0.05 represented by red, all others represented by blue. 185 of 2432 (8%) epochs had p < 0.05. a) min value compared for each 100 ms interval. b) max value compared for each 100 ms interval. 352 of 2432 (14%) epochs had p < 0.05. c) mean value compared for each 100 ms interval. 347 of 2432 (14%) epochs had p < 0.05 .....	54
Figure 12. GLM analysis results of fMRI data as completed by FEAT: certain > uncertain, reflected in serial axial slices. ....	66
Figure 13. GLM analysis results of fMRI as completed by FEAT: certain > uncertain, reflected in coronal and sagittal slices. ....	67
Figure 14. GLM analysis results of fMRI data as completed by FEAT: uncertain > certain, reflected in serial axial slices. ....	68
Figure 15. GLM analysis results of fMRI as completed by FEAT: uncertain > certain, reflected in coronal and sagittal slices. ....	69
Figure 16. Node-based comparison of weighted clustering coefficient in fMRI network data, comparing certain and uncertain conditions. 6 nodes greater in certain condition in blue, 20 nodes greater in uncertain in red.....	72

Figure 17. Node-based comparison of node strength in fMRI network data, comparing certain and uncertain conditions. 15 nodes greater in certain condition in blue, 23 nodes greater in uncertain condition in red.....	74
Figure 18. Scalp maps of EEG power spectral values at frequency bands of interest for the certain condition.....	84
Figure 19. Scalp maps of power spectral values at frequency bands of interest for the uncertain condition.....	84
Figure 20. Power spectra in the 1-30 Hz range plotted for each ROI, comparing the certain and uncertain conditions. ....	85
Figure 21. Scalp maps of EEG power spectral values at frequency bands of interest for the correct feedback. ....	86
Figure 22. Scalp maps of power spectral values at frequency bands of interest for the incorrect feedback. ....	86
Figure 23. EEG power spectra in the 1-30 Hz range plotted for each ROI, comparing the correct and incorrect conditions.....	87
Figure 24. Node strength for certain > uncertain condition for the EEG frequency bands of interest. Green areas with unlabeled electrodes represent no significant difference. ....	95
Figure 25. Cluster coefficient for certain > uncertain condition for the EEG frequency bands of interest. Green areas with unlabeled electrodes represent no significant difference. ....	96

Figure 26. Electrodes reflecting increased node strength for the correct condition over the incorrect condition for the EEG network analysis.....	97
Figure 27. Electrodes reflecting increased node strength for the incorrect condition over the correct condition for the EEG network analysis. ....	98
Figure 28. Electrodes reflecting increased cluster coefficient for the incorrect condition over the correct condition for the EEG network analysis. ....	99



## LIST OF ABBREVIATIONS

ACC	Anterior Cingulate Cortex
AD	Alzheimer's Disease
ADF	Axial Diffusivity
ADNI	Alzheimer's Disease Neuroimaging Initiative
BOLD	Blood Oxygen Level Dependent
CDR	Clinical Dementia Rating
DTI	Diffusion Tensor Imaging
dIPFC	Dorsolateral Prefrontal Cortex
EEG	Electroencephalography
EF	Executive Function
EMCI	Early Mild Cognitive Impairment
EPSP	Excitatory Post-Synaptic Potential
ERP	Event-Related Potential
F	Female
FA	Fractional Anisotropy
FRN	Feedback-related negativity
fMRI	Functional Magnetic Resonance Imaging
FEAT	fMRI Expert Analysis Tool
FDR	False Discovery Rate
FFT	Fast Fourier Transformation
GLM	General Linear Model

IU .....	Intolerance of Uncertainty
IPSP.....	Inhibitory Post-Synaptic Potential
LMCI.....	Late Mild Cognitive Impairment
M.....	Male
MCI.....	Mild Cognitive Impairment
MCI-highEF .....	Mild Cognitive Impairment, High Executive Function
MCI-lowEF .....	Mild Cognitive Impairment, Low Executive Function
MD .....	Medial Diffusivity
MMSE.....	Mini Mental Status Exam
MRI.....	Magnetic Resonance Imaging
NBS.....	Network Based Statistic
OFC.....	Orbitofrontal Cortex
PRR.....	Parietal Reach Region
ROI.....	Region of Interest
rs-fMRI .....	Resting State Functional Magnetic Resonance Imaging
RD.....	Radial Diffusivity
vmPFC .....	Ventromedial Prefrontal Cortex

## **CHAPTER ONE: INTRODUCTION TO HIGH VERSUS LOW EXECUTIVE ABILITIES IN MILD COGNITIVE IMPAIRMENT**

This project is an examination of the executive abilities of individuals with mild cognitive impairment (MCI) using a network analysis involving resting state functional magnetic resonance imaging (rs-fMRI) and diffusion tensor imaging (DTI). While MCI is primarily thought of as a disorder of memory, the coincident impact this Alzheimer's disease (AD) dementia precursor has on executive abilities cannot be overlooked. Executive abilities are required for normal functioning, and include decision-making, planning, task-switching and response inhibition. Using data from the Alzheimer's Disease Neuroimaging Initiative (ADNI), we grouped individuals diagnosed with mild cognitive impairment based on their executive abilities. We compared functional connectivity using rs-fMRI and white matter connectivity using DTI. Network measures were performed to quantify the connectivity of the two groups.

A diagnosis of MCI is made when an individual "has mild but measurable changes that are noticeable to the person affected and to family members and friends, but that do not affect the individual's ability to carry out everyday activities." (Alzheimer's Association 2013) Half of all individuals who have been diagnosed with MCI progress to AD dementia within 4 years. While individuals may still be able to carry out day-to-day activities, that does not mean that their functioning is unaffected – merely that they are able to compensate. Diminished executive abilities in conjunction with memory impairment, in particular, may predict a conversion to AD dementia (Gibbons 2012). These executive ability impairments may be subtle enough to escape an MCI-mixed type

diagnosis, but are detectable and may signify greater underlying pathology. Zheng et al (2014) related grey matter atrophy in the right inferior frontal gyrus in individuals with MCI to diminished executive abilities. Ye et al (2013) found bilateral dorsolateral prefrontal, anterior and medial temporal, and temporo-parietal association cortices, and the precuneus had diminished cortical thickness as MCI progressed. AD dementia is correlated with widespread accumulation of tau tangles in the neurons. These changes begin in the brainstem, progress into the entorhinal region and the hippocampus, and then move into the temporal neocortex, insula, subgenual and anterogenua frontal regions, and anterior cingulate areas. Finally, the entire cortex is involved (Braak & Tredici 2014, p11). Although widespread cortical involvement may be found in the terminal stage, because of the many brain regions that are dependent on and connected to those with earlier involvement, the network involving cortical regions may be impaired earlier.

The innovations in MRI over the past 20 years have enabled non-invasive, precise measurements of brain structure and function. The blood oxygen level dependent (BOLD) signal yielded by fMRI depends on the magnetic properties of the hemoglobin molecule. Increases in blood flow to an active brain region will cause a paradoxical drop in deoxygenated hemoglobin, thus forming the basis of the signal (Logothetis 2012). rs-fMRI describes how the brain functions as a network while an individual is not attending to a specific task. Common activation patterns in healthy participants have been described and differences in these patterns have been measured in disease states or in correlation with other factors (Biswal 2012). A voxel is a unit established by the limitations of the technology used and not a natural anatomical unit. Many studies have

used a seed-based network measure, in which all correlating voxels to a voxel seed of interest are discovered. A regions-of-interest (ROI) based approach, in which the average of functional activity for all voxels in a given brain region, gives a more accurate measure of connectivity. This approach allows brain regions that ostensibly work as a unit to be measured and correlated against other brain regions. Also, it limits the network size to a more manageable unit and restricts the number of comparisons. ROI-based analysis provides structural justification to the results. DTI allows for white matter tracts to be examined based on the diffusion properties of fluid in neuronal axons. DTI measurements yield magnitude of diffusion, degree of anisotropy, and anisotropy orientation. From these measurements, calculations of fractional anisotropy (FA), radial diffusivity (RD), and tract volume can describe the structural integrity of the white matter tracts (Alexander et al 2007). FA is the scaled (0-1) value of anisotropy in a given tract. RD is inversely related to fractional anisotropy and increases as diffusion increases about the axonal radius. From the diffusion measurements, estimations of the tract boundaries and volume can be described. The structural network can then be defined as the connections found between the ROIs.

Network analysis is a simple way of describing the complex and large datasets that result from imaging experiments (Rubinov and Sporns 2010) and allows the brain to be treated as a whole. ROIs can be described in context of their interaction with other ROIs. Using DTI, we create edges based on the number of tracts connecting two ROIs. We used a threshold of 5 tracts for binary measures to ignore false positives. In the rs-fMRI experiment, we calculated a Pearson correlation coefficient measuring similarity in

BOLD signal levels between two ROIs. We used binary measures, which require a threshold, and weighted measures, which sum the values of the edges. We then calculated network size, which is the sum of the count of the edges above a threshold. Node degree is the number of suprathreshold edges connected to a node, and node strength refers to the sum of all weighted edges attached to a given node. These measures identify regions with high connectivity to other regions. We calculated clustering coefficient and local efficiency, two related measures that describe how efficient or redundant the system is. The clustering coefficient refers to the tendency of triangles to form around a node, which implies redundancy, and local efficiency is a measure of how efficient the network would be with the node missing. Global efficiency is an average of local efficiency. Assortativity is a measure the tendency of a node to connect to a node of similar degree. Therefore, a high assortativity occurs in sparsely connected nodes connected to similarly sparse nodes, and densely connected nodes connected in dense regions. These relatively simple measures can describe how the network behaves as a whole and the node-based measures describe how each region contributes to the network.

The purpose of this study is to describe the underlying network differences in individuals with high and low executive abilities. Participants are grouped by their executive abilities and both structural and functional networks are examined. By using similar participant criteria and similar network measures to compare the groups, we can describe brain structure and function and how they are interrelated. We believe that these measures can provide insight into diminished executive abilities. Because of the

systematic progression of MCI to Alzheimer's disease dementia, some of the more subtle anatomical changes that occur early in disease progression may be discovered through network analysis. The differences in executive abilities may coincide with how the disease progression affects individuals and how these changes manifest anatomically.

One limitation of this study is lack of control over participant data collection. Because the data were collected at various sites as part of ADNI, we did not examine the participants directly and the number of different researchers involved may have introduced some variability in the data collection procedure. In addition, more information about the cognitive abilities and the educational history of the subjects would have been helpful. Another limitation is small sample size due to the small number of individuals who had a diagnosis of MCI and had either a resting state scan or a diffusion scan in the ADNI dataset. It would have been helpful also to add more executive tasks to the neuropsychological assessment. The current tasks were adequate but relied on subtasks of a largely memory-based battery that had an executive component. Future studies would include more specifically executive tasks, with a larger study population size, and a more detailed educational and intelligence history collected.

## **CHAPTER 2: DIFFERENCES IN EXECUTIVE ABILITIES ARE ACCOUNTED FOR BY ALTERATIONS IN FUNCTIONAL NETWORKS**

### **Background**

MCI is a disorder characterized by diminished cognitive function that has been predominantly associated with memory loss. The domain of executive function is often impacted, even in those diagnosed with the so-called amnesic variety of MCI (Aretouli & Brandt, 2010). Diminished executive function can be particularly detrimental as it often disrupts appropriate decision-making, judgment, and other essential aspects of independent daily living. These executive deficits have been reported in MCI patients across all taxonomies (Aretouli & Brandt, 2010). Decline in executive function has even been shown to predict mortality (Johnson, Lui & Yaffe 2007) therefore it is important to understand more about its neurobiological basis. The Executive Function (EF) score developed by Gibbon's et al (2012) is a composite score of executive subtasks of the neuropsychological battery of tests given to ADNI participants. It includes such tasks as the Trails A and B, Digit Span Backwards, WAIS-R Digit Symbol, Clock Drawing and Category Fluency, and has been validated as predictive of progression to AD.

Prior work has shown that the amnesic form of MCI is related to volumetric loss as measured by MRI in the medial temporal region including the parahippocampal cortex and hippocampal formation (Gold, Johnson, Powell & Smith 2012; Ferreira, Diniz, Forlena, Busatto & Zanetti, 2011). However, the location and type of breakdown in neuronal integrity and circuitry that induces executive system failure in subjects with amnesic MCI is not yet well understood. rs-fMRI has emerged over the past two



decades as a non-invasive means of measuring brain activity and functional connectivity (Biswal 2012). This technique allows examination of the synchronicity of brain regions while they are not actively engaged in a task, and has been used to evaluate functional interactions between regions in both normal and diseased states (Biswal 2012). We used an ROI-based analysis to model the brain as a network of interconnected regions and to evaluate the regions that are functionally connected. Often, voxel-based analysis is used in network analysis, but this has limitations as it is more susceptible to noise and does not take the underlying anatomy in consideration. We applied graph theory measures to constructed networks to evaluate and compare the regions of interest in individuals with MCI and low executive function (MCI-lowEF) as compared to those with MCI and high executive function (MCI-highEF). Prior work has shown that individuals with MCI have increased resting state activation over normal individuals, which is often attributed to vascular compensation as a component of disease progression (Esposito et al 2012). We extend these findings to evaluate the functional connectivity as it pertains to executive function performance in MCI in order to demonstrate that the differences in executive ability are accounted for by functional network differences.

## **Methods**

### *Participants*

Data used in the preparation of this article were obtained from the ADNI database (adni.loni.usc.edu). For up-to-date information, see [www.adni-info.org](http://www.adni-info.org).

The ADNI data archive was accessed on January 15, 2014 and the entire dataset was included in our search. The primary selection criterion were 1) diagnosis of MCI,

(including early or late MCI) and 2) had an rs-fMRI scan. The rs-fMRI scan was added to the ADNI protocol for all Philips Medical Systems scanners in the ADNI-GO phase of the study. This search resulted in 94 eligible subjects. Subjects were organized by their Executive Function (EF) score recorded in the ADNI database (Gibbons et al 2012). The mean EF score of the 94 participants was 0.34 with a standard deviation of 0.83. Subjects that were greater or less than one standard deviation from this population mean score were selected for the study groups, resulting in a group of fifteen subjects for the MCI-lowEF group and eighteen subjects for the MCI-highEF group.

### *Procedure*

Structural scans were acquired on 3T Phillip's Medical Systems scanners using the 3D MPRAGE protocol developed by ADNI (TR/TE 3000/4 ms; flip angle 8–9°; section thickness 1.2 mm; 170 sagittal slices). Functional data were acquired while subjects focused on a dot in the middle of the screen, per the ADNI protocol. The rs-fMRI sequence was composed of functional imaging volumes collected in the same slice position as the preceding T1-weighted data. A seven-minute functional run was acquired using a T2\*-sensitive gradient-recalled, single-shot echo-planar imaging pulse sequence (TR/TE 3000/30 ms, FoV = 212 mm, flip angle 80°, matrix size 64×64, inplane resolution 3.3 mm × 3.3 mm). Each volume consisted of 48 slices parallel to the bicommissural plane (slice thickness 3.3 mm, no gap), and each functional run was comprised of 140 volumes.

Freesurfer software ([surfer.nmr.mgh.harvard.edu](http://surfer.nmr.mgh.harvard.edu) version 5.1) was used to parcel and label the structural MPRAGE scans of each of the subjects (Desikan et al 2006). The

software identified grey matter regions in the cortex and sub-cortex. The results were checked for accuracy manually. Sixty-four grey matter regions of interest (ROIs) from the cortex and sub-cortex were chosen from these labels, excluding those highly susceptible to field distortions. All of the rs-fMRI scans were visually inspected to ensure that they were free from any artifacts (i.e. pencil beam artifact). No scans were excluded due to artifact. The fMRI data were preprocessed with motion correction using MCFLIRT, spatial smoothing with a kernel size of 5 mm, and highpass temporal filtering using a local fit of a straight line. FMRI Expert Analysis Tool (FEAT; Oxford, UK; v6.0 <http://fsl.fmrib.ox.ac.uk/fsl/fslwiki/FSL>) was used for this preprocessing (Smith et al 2004). Each subject was registered to the structural scan generated by Freesurfer and the resulting rs-fMRI sequence was labeled using the generated Freesurfer ROIs. A mean time series for each ROI was calculated by averaging all fMRI voxel values within each ROI over time, resulting in 140 time points calculated for each 7 minute resting state session.

A network consisting of nodes and edges was constructed for each subject. Each node corresponds to the averaged time series of the voxels in each ROI. Edges were calculated using a correlation coefficient between the time series of two nodes. A threshold of 0.4 was applied to determine the presence of an edge. Two ROIs are said to be functionally connected if they have a high degree of similarity between averaged BOLD signal activities over time.

The following network measures were calculated: network size, global efficiency, assortativity, cluster coefficient and node degree. Node degree and cluster coefficient

were calculated for each node, while all other measures were calculated for the entire network. Network size was calculated by counting the number of edges above the threshold per network, and node degree was calculated by counting the number of suprathreshold edges each node was connected to. Assortativity, cluster coefficient and global efficiency were calculated using the Brain Connectivity Toolbox.

A permutation test was performed by calculating a test statistic for each network measure. This was done by taking the mean values for MCI-highEF and subtracting the values of the MCI-lowEF for each measure. Then, ten thousand random permutations were generated by pooling the values of these two groups. The exchangeable values, i.e., the value at each edge, were shuffled between subjects to obtain the new datasets. Then the network measures were calculated for each of the random datasets. Each dataset was separated into two groups, one of size 18 to correspond to the MCI-highEF group and one of size 15 to correspond to the MCI-lowEF group. A statistic was then calculated for the given measure by averaging the measure for the first group, and subtracting the average measure of the second group. The number of values higher and lower than the test statistic were calculated and divided by the number of permutations in order to assess significance. Because node degree and cluster coefficient both resulted in 64 comparisons, one for each ROI, the false discovery rate method was used to control for the multiple comparisons problem.

The Network-Based statistic (NBS) software was used to calculate network differences between the two groups (Zalesky, Fornito & Bullmore 2010). This algorithm uses depth-

first search to discover a significantly different network based on a threshold applied to t-statistic calculations between groups. A t-statistic threshold of 2.5 was set to measure edge difference between conditions.

## Results

The ages, MCI diagnosis, gender and MMSE scores of MCI-highEF and MCI-lowEF groups are listed in Table 1.

	EMCI	LMCI	M	F	MMSE mean	MMSE standard deviation	Age mean	Age standard deviation
MCI-highEF	7	11	8	10	29.2	2.6	67.3	5.6
MCI-lowEF	7	8	9	6	25.3	2.9	73	6.4
p-value					0.0003		0.01	

**Table 1.** Demographics of subjects selected from the MCI population who were classified as high or low executive functioning.

All subjects had a Clinical Dementia Rating (CDR) score of 0.5, which is consistent with MCI diagnosis. A non-parametric permutation test was used for calculations of statistical differences between the two groups. The node degree calculation yielded a statistically significant difference in fifteen of the nodes (Table 2).

<b>Brain Region</b>	<b>MCI-highEF mean</b>	<b>MCI-highEF stdev</b>	<b>MCI-lowEF mean</b>	<b>MCI-lowEF stdev</b>	<b>p-value</b>
Left Inferior Parietal Cortex	6.11	4.04	8.07	4.73	0.001
Left Inferior Temporal Cortex	4.22	2.41	5.93	3.20	0.002
Left Paracentral Cortex	6.94	4.15	10.80	5.31	<0.0001
Left Precuneus	7.28	4.27	9.33	4.39	0.001
Left Superior Frontal Cortex	8.67	5.11	11.00	5.22	0.003

Left Superior Parietal Cortex	6.89	4.24	9.80	6.94	<0.0001
Right Inferior Parietal Cortex	5.67	2.54	8.80	5.44	<0.0001
Right Inferior Temporal Cortex	4.33	3.25	6.20	4.11	0.001
Right Paracentral Cortex	8.72	3.29	11.27	5.69	0.001
Right Pars Orbitalis	8.06	3.92	10.07	2.65	0.003
Right Postcentral Cortex	9.78	4.43	13.33	4.15	<0.0001
Right Posterior Cingulate Cortex	7.06	4.61	10.33	5.98	<0.0001
Right Precentral Cortex	9.33	4.35	11.53	5.63	0.004
Right Precuneus	6.11	3.83	8.07	5.73	0.001
Right Superior Frontal Cortex	4.22	5.19	5.93	5.82	0.002

Table 2. Regions of interest showing significantly different node degree in functional network connectivity between MCI-highEF and MCI-lowEF individuals.

Cluster coefficient, or the measure of the tendency to form a small subnetwork around a given node, was significantly different in two of the brain regions (Table 3).

Brain Region	MCI-highEF mean	MCI-highEF standard deviation	MCI-lowEF mean	MCI-lowEF stdev	p-value
Left Precentral Cortex	0.50	0.15	0.57	0.15	0.0013
Right Parahippocampal Cortex	0.52	0.37	0.67	0.37	0.0019

Table 3. Regions of interest showing differences in cluster coefficient comparing functional networks of MCI-highEF versus MCI-lowEF individuals.

Assortativity, network size and global efficiency all showed statistically significant differences (Table 4).

	<b>MCI-highEF mean</b>	<b>MCI-highEF stdev</b>	<b>MCI-lowEF mean</b>	<b>MCI-lowEF stdev</b>	<b>Corrected p-value</b>
Assortativity	0.370	0.37	0.312	0.13	0.0151
Global efficiency	0.379	0.38	0.400	0.08	<0.0001
Network size	227.94	227.94	251.73	79.39	<0.0001

**Table 4. Global network measures comparing functional networks of MCI-highEF versus MCI-lowEF individuals.**

The NBS algorithm resulted in a network of forty-one edges that were shown to be strengthened (higher correlation coefficient) in those with high versus low executive abilities (Figure 1). This is a nonspecific cortical network with ROIs spread across the frontal, temporal and parietal lobes.

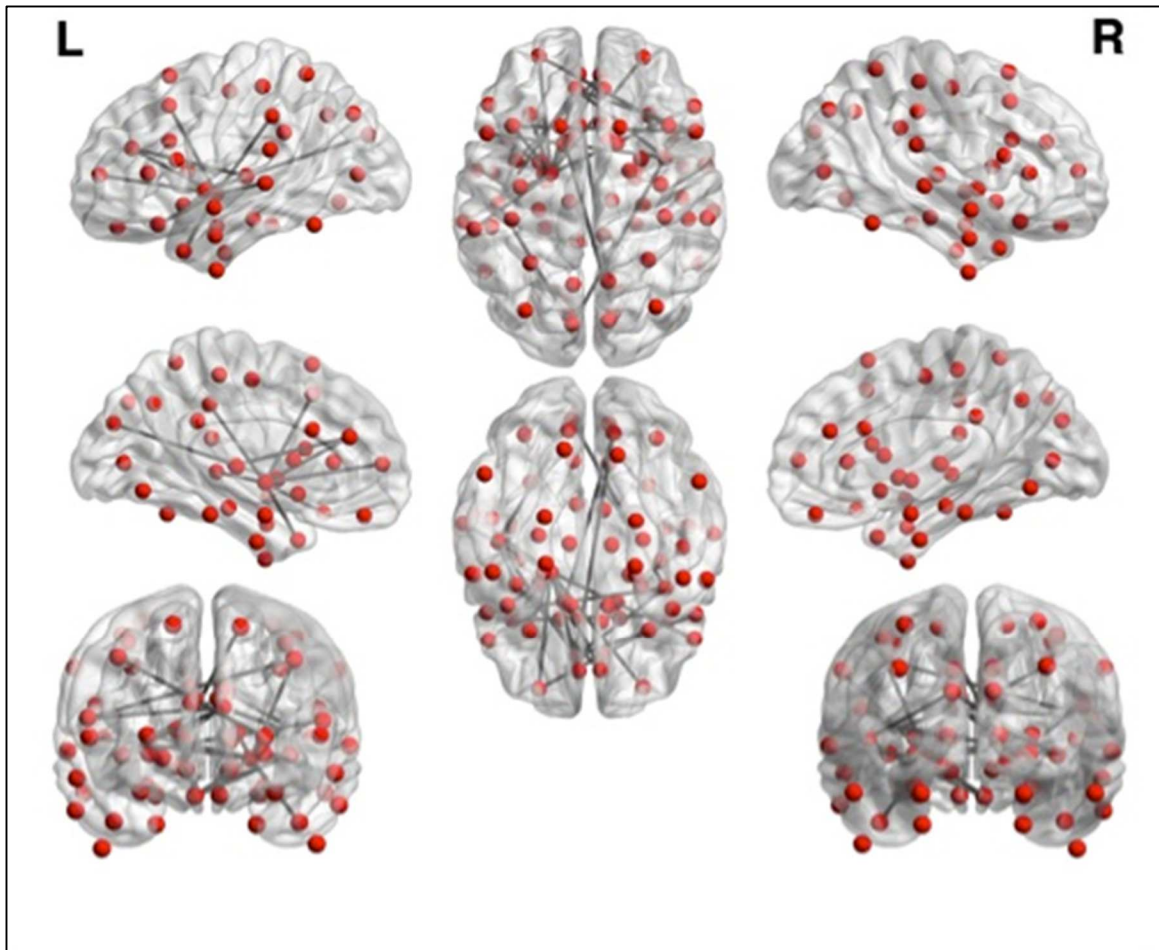


Figure 1. Network differences between MCI-highEF and MCI-lowEF as calculated by the NBS algorithm.

## Discussion

The term MCI defines a group of cognitive states that represents a somewhat broad range of functional abilities (Alzheimer's Association 2013). While it is true that some patients with MCI only exhibit a disorder of memory, many individuals with MCI not only evidence impaired memory, but also exhibit poor executive function abilities that cannot be simply attributed to memory dysfunction (Pereiro, Juncos-Rabadan & Facal 2014; Zheng et al 2014). We found that individuals in the MCI-lowEF group showed more nonspecific connectivity when using a threshold of 0.4 to establish network



size – with a higher network size, and greater global efficiency than the MCI-highEF. The MCI-lowEF group showed a number of nodes that had greater node degree and a higher clustering coefficient. The regions of greater node degree (thus higher connectivity) were largely centered in the bilateral frontal, temporal and parietal cortex. Clustering in some regions was also higher in individuals with low executive functioning. Taken together, these results indicate that individuals in the MCI-lowEF have nonspecific, diffuse connections between regions of the brain responsible for executive functions. Those in the MCI-highEF group showed greater assortativity, or a tendency of nodes with similar degree measure to connect. The NBS algorithm results showed a statistically significant network of regions in the MCI-highEF that was not apparent in the MCI-lowEF group. The NBS algorithm measures differences in edge correlation strength and discovers a network above a t-statistic threshold, which was increased in the network of edges represented in Figure 1. All of these data suggest that although individuals with low executive abilities have more nonspecific connections between brain regions, these connections lead to inefficient interactions that are detrimental to functioning. Individuals with high executive abilities have a more specific, and thus more effective, network that may produce better performance on executive tasks in day-to-day life. This function may represent a pre-existing state for these individuals or it may be a successful compensatory mechanism achieved in those living with MCI, which enables the preservation of executive abilities.

Many of the current findings to date have measured differences in specific regions of the brain, rather than using a network-based approach. For example, structural

alterations in the brains of patients with amnesic MCI include decreased hippocampal volume and thinning of the medial temporal lobe cortices (Franko & Joly 2013). In addition, Zheng et al (2014) correlated measures of executive function to measures of cortical thickness in the right inferior frontal gyrus of amnesic MCI patients with impaired executive function. Decreased functional activity of the anterior cingulate, striatum, and thalamus has also been found to correlate with scores on a test of executive function the Trailmaking-B test (Terada et al 2013). Diffusion Tensor Imaging (DTI) has demonstrated changes in mean diffusivity in the anterior cingulate and in the fornix of patients with MCI over time, which suggests altered structural connectivity in patients with MCI (Nowrangi et al 2013). The network approach that we used provides a means for assessing the combined impact of the underlying etiology on the brain and the interactions between relevant structures involved in cognition. We found differences between the MCI-highEF and MCI-lowEF in the network interactions of the temporal, frontal, parietal, and anterior cingulate cortices. Because of the known predominant impact of Alzheimer's disease on the temporal lobe this result is unsurprising (Ferreira et al. 2011). Our findings of network differences between groups with differing executive abilities is consistent with the known involvement of frontal, parietal and anterior cingulate regions in executive function. We surmise that, in particular, greater numbers of weaker connections between these regions in those individuals with MCI-lowEF is responsible for their diminished performance on tests of executive function.

Our findings suggest that the network connections responsible for efficient brain activity can be compromised early in the progression to Alzheimer's disease dementia

and reminds us that the diagnostic categories that are used to represent distinct stages of disease actually represent a continuum rather than discrete stages. One interesting possibility is that early on in the disease process there are impaired connections between networks either as a direct response to the disease or as a compensatory mechanism. Buckner, Andrews-Hanna & Schacter (2008) found high amyloid accumulation in resting state hubs of individuals with Alzheimer's disease, which correlated with the levels of functional connectivity across the brain. It follows, then, that individuals with MCI due to Alzheimer's disease would begin to show similar pathology in these hubs. Increased functional connectivity in individuals with MCI compared to controls has been shown in the default mode network (Buckner, Andrews-Hanna & Schacter 2008), suggesting the use of a potential compensatory strategy. The default mode network consists of medial temporal lobe, medial prefrontal cortex, posterior cingulate cortex and the precuneus—therefore, this is consistent with our findings in the temporal, frontal and cingulate cortices. Esposito et al (2013) found increased connectivity in resting state networks of individuals with MCI compared to normal aged adults. They have hypothesized that this increased connectivity is due to compensation through recruiting other brain regions more heavily, a concept that is consistent with the findings of task based fMRI. In the present study, when we compared the network connectivity in two subgroups of MCI subjects we found that those with low executive abilities had more isolated functional connections, greater node degree of numerous nodes, a greater clustering coefficient in the brain. However, the greater assortativity and the network resulting from the NBS algorithm in those individuals with MCI-highEF suggest that a more sparse and tightly

connected network allows for more efficient connections and greater executive function performance. As a consequence of functional isolation and noisy interactions, individuals with low executive capacities are less able to compensate as effectively and minimize disease effects in the executive function realm.

Further studies will be needed to better determine the role of weakened network connections on the progression from MCI to Alzheimer's disease dementia and the ability to cope with disease progression. Analysis of functional connectivity in the brain has the potential for increasing our understanding of the impact of disease on the brain as a whole and may provide another means for assessing the efficacy of interventions. Finally, while functional network connectivity gives important information about interactions that take place in the brain, we would benefit from examining the structural network connections in these subjects in order to know if reductions in function are related to structural alterations in the brain.

## **CHAPTER 3: STRUCTURAL DIFFERENCES IN MCI PATIENTS WITH DISPARATE EXECUTIVE ABILITIES**

### **Introduction**

MCI is a disorder that is severe enough to cause cognitive deficits but not to disrupt day-to-day function. The most common complaint of those with MCI is memory loss though it is not uncommon for this impairment to be accompanied by executive deficits, which can have a deleterious impact on day-to-day activities (Aretouli and Brandt 2010).

Gibbons et al (2012) developed an Executive Function (EF) score using a number of neuropsychological tasks in the Alzheimer's Disease Neuroimaging Initiative (ADNI) dataset, and have reported that this EF score is the major predictor of conversion from MCI to AD dementia. Therefore, MCI patients who have better executive abilities may be more resilient to disease progression leading to a conversion to dementia. From a cognitive neuroscience perspective, executive function has been described as the higher order ability that is needed in any task that involves planning, organization, memory, time management and flexible thinking. As such, it requires integrated coordination between a number of brain regions across white matter connections. In this study, we investigated whether alteration in the network of white matter connections in the brain leads to differences in executive abilities found in individuals with MCI. By grouping subjects with MCI who have a high EF score (MCI-highEF) and those who have a low EF score (MCI-lowEF), we used a network-based and tract-based approach to investigate whether structural differences exist between these groups. To date, major findings of differences

of individuals with AD have included widespread decrease in fractional anisotropy, most commonly in the uncinate fasciculus, fornix, and superior longitudinal fasciculus (for review, Gold et al., 2012). In addition, individuals with MCI have also shown changes in DTI measures, including FA in the frontal and parietal regions (Nowrangi et al 2015). Network changes in AD include widespread network disruption (Daiunu et al 2013), and changes in topological organization in a network analysis (Lo et al 2012). Our study not only aims to describe MCI-related changes in white matter morphology in association with executive abilities, but we include both a graph-theory based network analysis in addition to tract-based analysis. Because executive skills require a number of brain regions working in concert, evaluating the structural network connectivity is appropriate and can describe overall system functioning more completely than evaluating regions individually.

We used an ROI-based approach to create networks using grey matter ROIs to represent nodes and the number of tracts between ROIs to represent edges. We performed a series of network measures on these networks, and to assess the group differences between the networks. We calculated global network measures, such as size and density, in addition to local network measures, such as nodal degree and clustering coefficient. We also performed a tract-based analysis using TRACULA to determine if the tract-based differences exist (Yendiki et al 2011). We used permutation testing to assess the significance level between the two groups, and used the false discovery rate (FDR) for measures requiring multiple comparisons. This study is unique because although a few studies have linked executive abilities and MCI using DTI, none that we know of have

used these network measures to describe differences in abilities. These network measures can describe how brain regions function together, and how differences in these measures can illustrate the underlying anatomic differences that may cause diminished functioning.

## Methods

Data used in the preparation of this article were obtained from the ADNI database (adni.loni.usc.edu). For up-to-date information, see [www.adni-info.org](http://www.adni-info.org). The data archive was accessed on July 25, 2014 and the entire dataset was included in our search. The primary selection criteria were 1) diagnosis of MCI (including early or late MCI) and 2) had a DTI scan. The DTI scan was added to the ADNI protocol for GE scanners in the ADNI-GO phase of the study. This search resulted in 128 eligible subjects. The mean EF score of this group was 0.15, with a standard deviation of .76. MCI-highEF subjects were classified as being one standard deviation above the group mean EF score, resulting in 20 subjects with a score above 0.91. MCI-lowEF subjects were classified as being one standard deviation below the group mean, resulting in 18 subjects with a score below -0.61. See Table 1 for demographic information. This study was approved by institutional review boards of all participating institutions and written informed consent was obtained by from all participants or authorized representatives.

	Male	Female	EMCI	LMCI	Age (mean)	MMSE * (mean)
High EF	8	6	16	4	70.9	28.4
Low EF	11	6	9	10	77.45	25.6
				p-value	0.007	6.3E-05
*MMSE: 1 value missing from high EF group, 2 values missing from Low EF group.						

**Table 5. Population statistics for DTI EF analysis**

### *MRI acquisition*

Standard anatomical T1-weighted spoiled gradient echo sequences were collected (256 · 256 matrix; voxel size = 1.2 · 1.0 · 1.0 mm<sup>3</sup>; inversion time [TI] = 400 msec, repetition time [TR] = 6.984 msec; echo time [TE] = 2.848 msec; flip angle = 11°) in the same session as the diffusion-weighted images (DWI; 256 × 256 matrix; voxel size: 2.7 × 2.7 × 2.7 mm<sup>3</sup>; TR = 9000 ms; scan time = 9 min; more imaging details can be found at [http://adni.loni.ucla.edu/wp-content/uploads/2010/05/ADNI2\\_GE\\_3T\\_22.0\\_T2.pdf](http://adni.loni.ucla.edu/wp-content/uploads/2010/05/ADNI2_GE_3T_22.0_T2.pdf)) were collected. 46 separate images were acquired for each DTI scan: 5 T2-weighted images with no diffusion sensitization (b<sub>0</sub> images) and 41 diffusion-weighted images (b = 1000 s/mm<sup>2</sup>).

### *Analysis*

Freesurfer software (surfer.nmr.mgh.harvard.edu version 5.1) was used to parcel and label the structural MPAGE scans of each of the subjects (Desikan et al 2006). The software identified grey matter regions in the cortex and sub-cortex. The results were checked for accuracy manually. Ninety-three grey and white matter regions of interest (ROIs) from the cortex, sub-cortex, brainstem and cerebellum were chosen from these labels. The DTI data were preprocessed using Freesurfer's dt\_recon, which performed eddy/motion correction on the DTI files. Freesurfer's bregister registered the structural data files to the DTI files. Then, diffusion values for each ROI were then extracted from the registered and corrected data. Fiber tracking files were generated from the DTI data using DSI\_Studio and tract data was generated between each ROI using a seed count of 10,000, an FA threshold of 0.0241, a turning angle of 60, and smoothing parameter of



0.3. Tracts of size 20 mm – 140 mm were included. A matrix was generated that included the number of tracts found between each ROI, and values normalized by dividing by seed count (10,000).

Network measures including network size, network density, binary clustering coefficient, node degree, and node strength were calculated on each network, and the MCI-highEF group was compared to the MCI-lowEF group. Permutation testing as described in Chapter 2 was performed in order to assess significance of differences between the two groups. Network based measures were assessed for significance using a p-value threshold of 0.025, with both greater and less than measures calculated. Node-based measures were corrected for multiple comparisons using the false discovery rate.

Freesurfer TRACULA was used to perform tract-based analysis on the dt\_recon processed DTI data. 18 major white matter tracts were reconstructed and calculations of volume, fractional anisotropy (FA), axial diffusivity (ADF), mean diffusivity (MD), and radial diffusivity (RD) were performed. The MCI-highEF and MCI-lowEF groups were compared using t-testing and permutation testing for each measure. The false discovery rate was used to control for multiple comparisons.

## **Results**

A network was constructed by generating number of tracts between ROIs, and then normalizing by the number of seeds (10,000). For binarized network measures, a threshold of 0.0005 (5 tracts) between regions was used to eliminate connections that were incorrectly generated. Permutation testing was done by generating 10,000 random datasets and performing the same calculations on the dataset as on the actual dataset. P-

values were generated by comparing to permuted values and dividing by the number of permuted values. A significance level of 0.025 per tail (high > low, and low > high) was applied to each test, with the False Discovery Rate method used to correct for family-wise errors.

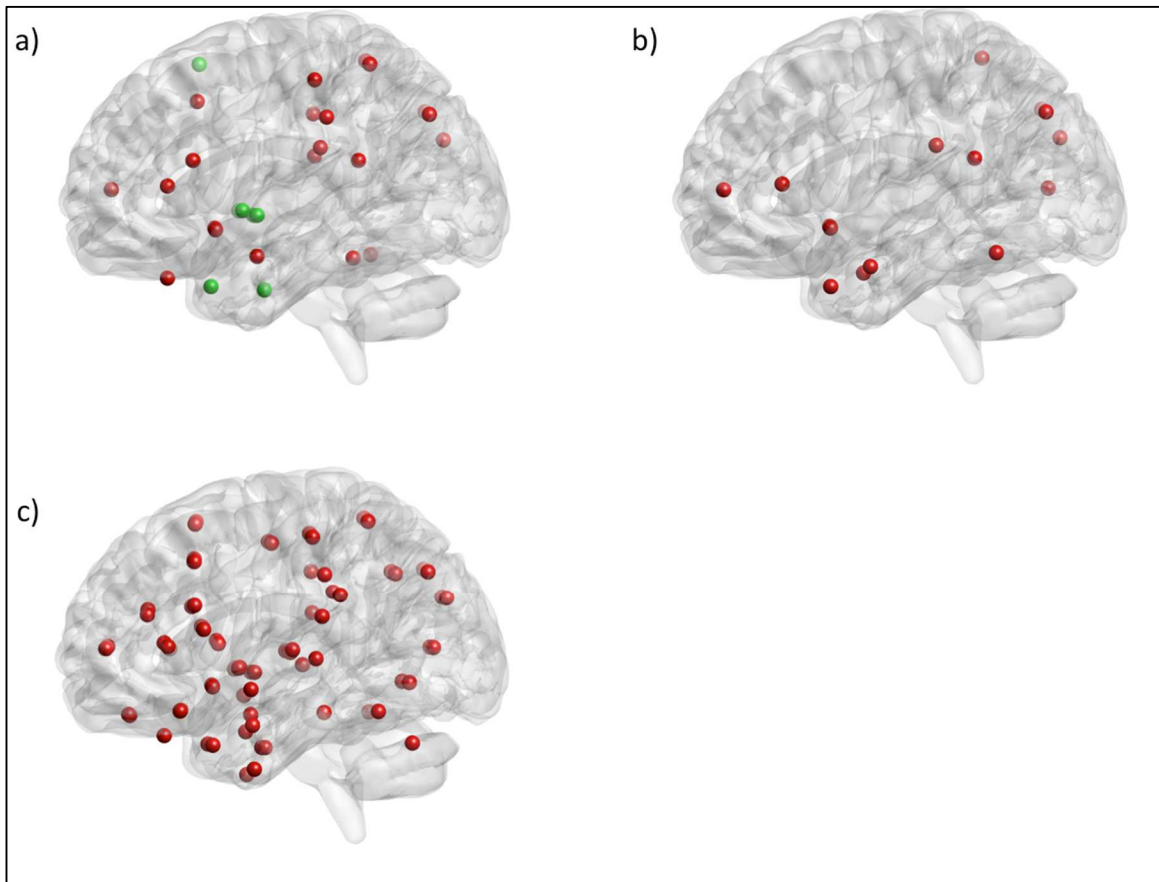


**Figure 2.** Network measures, as reflected in ROIs of significant difference marked by circles, comparing MCI-highEF and MCI-lowEF. a) Binary node degree. b) Node strength. c) Clustering coefficient.

The average network density of the MCI-highEF group and the average network size of the MCI-highEF group were significantly greater than the MCI-lowEF group.

Measure	pval	HighEF	LowEF
Density	<0.0001	0.1345	0.1313
Size	0.0002	1194.60	1164.76

**Table 6.** Network measures for DTI EF analysis

The MCI-highEF group had a higher binary clustering coefficient in 80 out of the 93 ROIs than the MCI-lowEF group.

<b>ROI</b>	<b>pval</b>	<b>HighEF</b>	<b>LowEF</b>
Left Cerebellum White Matter	0.0139	0.0098	0.0078
Left Thalamus Proper	0.0003	0.0066	0.0043
Left Caudate	0.0026	0.0074	0.0052
Left Putamen	<0.0001	0.0053	0.0035
Left Pallidum	0.0001	0.0079	0.0042
Left Accumbens area	<0.0001	0.0082	0.0046
Right Thalamus Proper	<0.0001	0.0070	0.0040
Right Caudate	<0.0001	0.0081	0.0044
Right Putamen	<0.0001	0.0062	0.0041
Right Pallidum	0.0039	0.0085	0.0059
Right Amygdala	0.0004	0.0076	0.0055
Right Accumbens area	<0.0001	0.0097	0.0046
Optic Chiasm	0.0071	0.0224	0.0059
Corpus Callosum Anterior	<0.0001	0.0079	0.0041
Left Banks of the STS	<0.0001	0.0141	0.0061
Left Caudal Anterior Cingulate	0.0022	0.0057	0.0041
Left Caudal Middle Frontal Cortex	0.0001	0.0157	0.0049
Left Cuneus	<0.0001	0.0081	0.0046
Left Entorhinal	0.0003	0.0106	0.0072
Left Fusiform	0.0129	0.0102	0.0082
Left Inferior Parietal	<0.0001	0.0090	0.0044
Left Inferior Temporal	0.0002	0.0134	0.0085
Left Isthmus Cingulate	<0.0001	0.0061	0.0035
Left Lateral Occipital	0.0029	0.0088	0.0065
Left Lateral Orbitofrontal	0.0006	0.0061	0.0044
Left Lingual	<0.0001	0.0075	0.0049
Left Medial Orbitofrontal	<0.0001	0.0069	0.0039
Left Middle Temporal	<0.0001	0.0096	0.0045
Left Parahippocampal	0.0044	0.0094	0.0074
Left Pars Opercularis	0.0005	0.0081	0.0051
Left Pars Orbitalis	0.0021	0.0105	0.0069
Left Pars Triangularis	0.0003	0.0107	0.0063
Left Pericalcarine	<0.0001	0.0095	0.0048
Left Postcentral	<0.0001	0.0097	0.0056

Left Posterior Cingulate	0.0065	0.0047	0.0038
Left Precentral	<0.0001	0.0075	0.0044
Left Precuneus	<0.0001	0.0057	0.0031
Left Rostral Anterior Cingulate	<0.0001	0.0070	0.0040
Left Rostral Middle Frontal	0.0006	0.0075	0.0044
Left Superior Frontal	<0.0001	0.0051	0.0033
Left Superior Parietal	<0.0001	0.0086	0.0038
Left Superior Temporal	<0.0001	0.0053	0.0032
Left Supramarginal	0.003	0.0092	0.0072
Left Frontal Pole	0.0001	0.0079	0.0050
Left Temporal Pole	<0.0001	0.0070	0.0048
Left Transverse Temporal	<0.0001	0.0097	0.0062
Left Insula	<0.0001	0.0043	0.0033
Right Banks of the STS	0.0003	0.0140	0.0079
Right Caudal Anterior Cingulate	<0.0001	0.0067	0.0040
Right Caudal Middle Frontal	<0.0001	0.0130	0.0055
Right Cuneus	<0.0001	0.0078	0.0042
Right Entorhinal	0.0117	0.0099	0.0077
Right Fusiform	0.0212	0.0094	0.0076
Right Inferior Parietal	<0.0001	0.0140	0.0053
Right Inferior Temporal	<0.0001	0.0134	0.0077
Right Isthmus Cingulate	0.0002	0.0055	0.0040
Right Lateral Occipital	<0.0001	0.0117	0.0072
Right Lateral Orbitofrontal	0.0005	0.0069	0.0051
Right Lingual	0.0001	0.0072	0.0053
Right Medial Orbitofrontal	<0.0001	0.0070	0.0048
Right Middle Temporal	<0.0001	0.0101	0.0045
Right Paracentral	0.0094	0.0094	0.0067
Right Pars Opercularis	0.0004	0.0092	0.0055
Right Pars Orbitalis	<0.0001	0.0113	0.0072
Right Pars Triangularis	<0.0001	0.0111	0.0067
Right Pericalcarine	<0.0001	0.0079	0.0050
Right Postcentral	<0.0001	0.0086	0.0057
Right Posterior Cingulate	<0.0001	0.0058	0.0038
Right Precentral	0.0005	0.0075	0.0052
Right Precuneus	<0.0001	0.0059	0.0035
Right Rostral Anterior Cingulate	<0.0001	0.0060	0.0040

Right Rostral Middle Frontal	<0.0001	0.0075	0.0044
Right Superior Frontal	<0.0001	0.0046	0.0032
Right Superior Parietal	<0.0001	0.0074	0.0042
Right Superior Temporal	<0.0001	0.0064	0.0035
Right Supramarginal	<0.0001	0.0117	0.0066
Right Frontal Pole	<0.0001	0.0084	0.0048
Right Temporal Pole	<0.0001	0.0072	0.0050
Right Transverse Temporal	<0.0001	0.0149	0.0078
Right Insula	<0.0001	0.0047	0.0030

Table 7. Binary Clustering Coefficient (threshold of 5 tracts) for the DTI EF analysis.

For the node degree, 7 ROIs were greater for the MCI-lowEF group, and 21 ROIs were greater for the MCI-highEF group (Figure 1a, Table 8).

ROI	pval	HighEF	LowEF	Greater Group
Left Amygdala	<0.0001	11.33	8.41	High
Left Accumbens area	<0.0001	10.47	7.06	High
Right Cerebellum Cortex	0.0021	31.60	28.35	High
Right Accumbens area	0.0001	10.53	7.65	High
Optic Chiasm	<0.0001	12.07	6.65	High
Corpus Callosum Posterior	<0.0001	8.33	3.00	High
Corpus Callosum Mid-posterior	<0.0001	3.93	0.59	High
Corpus Callosum Mid-anterior	<0.0001	2.87	1.35	High
Corpus Callosum Anterior	0.0006	13.00	10.18	High
Left Lateral Occipital	0.0003	19.13	16.35	High
Left Postcentral	0.0022	9.47	7.82	High
Left Superior Parietal	0.0001	19.80	16.29	High
Left Supramarginal	0.0019	8.80	7.53	High
Right Caudal Middle Frontal	0.0008	4.47	3.35	High
Right Cuneus	0.0004	12.13	9.24	High
Right Fusiform	0.0001	19.53	16.18	High
Right Inferior Parietal	0.001	9.80	8.06	High
Right Lateral Occipital	0.0024	15.93	13.82	High
Right Superior Parietal	<0.0001	22.00	17.06	High
Right Supramarginal	0.0015	9.00	7.47	High
Right Frontal Pole	0.0001	11.93	8.94	High
Left Putamen	0.0016	25.53	29.24	Low
Left Pallidum	<0.0001	16.87	23.00	Low

Right Putamen	<0.0001	22.67	27.59	Low
Right Pallidum	0.0001	16.80	21.41	Low
Right Entorhinal	0.0005	8.13	10.35	Low
Right Superior Frontal	0.0016	18.13	21.18	Low
Right Temporal Pole	<0.0001	18.80	21.94	Low

**Table 8. Node degree for DTI EF comparison.**

15 nodes had greater node strength for the high EF group (Figure 1b, Table 9).

ROI	pval	HighEF	LowEF
Left Accumbens area	<0.0001	0.073	0.031
Right Accumbens area	0.0027	0.068	0.041
Corpus Callosum Posterior	<0.0001	3.933	0.010
Corpus Callosum Mid-posterior	<0.0001	0.018	0.001
Corpus Callosum Anterior	<0.0001	0.124	0.054
Left Fusiform	<0.0001	0.310	0.228
Left Lateral Occipital	<0.0001	0.380	0.133
Left Middle Temporal	<0.0001	0.201	0.109
Left Frontal Pole	0.0027	0.065	0.028
Left Temporal Pole	0.0017	0.391	0.252
Right Cuneus	0.0007	0.089	0.057
Right Lateral Occipital	0.0026	0.195	0.116
Right Middle Temporal	<0.0001	0.253	0.169
Right Pericalcarine	0.0014	0.048	0.032
Right Superior Parietal	0.0001	0.140	0.092

**Table 9. Node Strength for DTI EF comparison.**

A number of white matter tracts have greater volume (Table 10) and higher FA (Table

11) average in the high EF group

Tract	Volume - High	Volume - Low	pval_lt
Corpus Callosum - Forceps Major	1094.8	631.3125	0.0042
Left Cingulum - Angular (Infracallosal) bundle	451.6	251.0625	0.0077
Right Cingulum - Angular (Infracallosal) bundle	315.4	182.6	0.0106
Right Inferior Longitudinal Fasciculus	673.4	463	0.001

**Table 10. Tract comparison of Volume, MCI-highEF > MCI-lowEF**

Tract	FA_Avg-High	FA_Avg-Low	pval_lt
Left Inferior Longitudinal Fasciculus	0.48	0.42	0.001
Left Superior Longitudinal Fasciculus - Parietal bundle	0.41	0.38	0.0008
Left Superior Longitudinal Fasciculus - temporal bundle	0.44	0.41	0.0008
Left Uncinate Fasciculus	0.39	0.37	0.021
Right Inferior Longitudinal Fasciculus	0.46	0.42	0.0074
Right Superior Longitudinal Fasciculus - Parietal bundle	0.43	0.4	0.0003
Right Superior Longitudinal Fasciculus - Temporal bundle	0.44	0.41	0.0071

**Table 11. Tract comparison of FA, MCI-highEF > MCI-lowEF**

The low EF group has increased RD measures in a number of the white matter tracts (Table 12).

	RD Avg – MCI-highEF	RD Avg – MCI-lowEF	pvals
Left Inferior Longitudinal Fasciculus	5.8E-4	6.5E-4	0.001
Left Superior Longitudinal Fasciculus - Parietal bundle	5.8E-4	6.4E-4	0.0013
Left Superior Longitudinal Fasciculus - Temporal bundle	5.7E-4	6.2E-4	0.0006
Right Inferior Longitudinal Fasciculus	5.8E-4	6.7E-4	0.0007
Right Superior Longitudinal Fasciculus - Temporal bundle	5.5E-4	6.0E-4	0.0001

**Table 12. Tract Comparison of RD, MCI-lowEF > MCI-highEF**

Using the network based statistic software, a statistically significant network difference (LEF > HEF) was found using a threshold of 1.8, suggesting a greater number of tracts between these specific regions (Figure 2). This resulting network had 84 edges between 63 nodes.

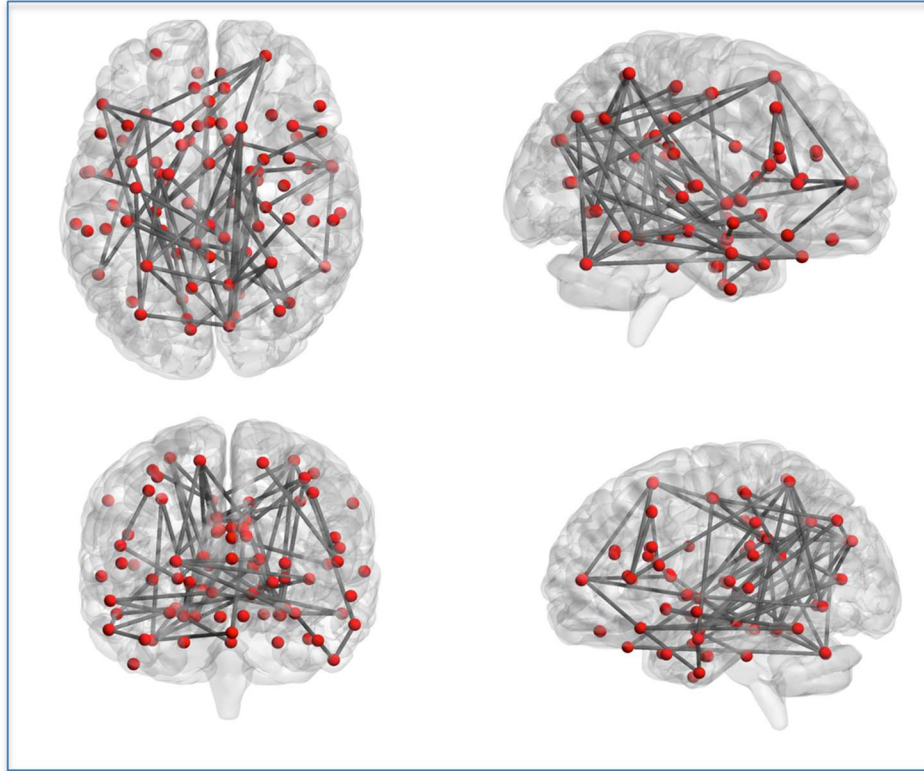


Figure 3. Results of NBS algorithm for MCI-highEF > MCI-lowEF.

ROI 1	ROI 2
Left Hippocampus	Left Accumbens area
Left Thalamus Proper	Right Cerebellum White Matter
Left Pallidum	Right Cerebellum White Matter
Left Hippocampus	Right Caudate
Right Thalamus Proper	Right Putamen
Left Accumbens area	Right Hippocampus
Brainstem	Right Amygdala
Left Hippocampus	Right Accumbens area
Right Cerebellum White Matter	Optic Chiasm
Left Accumbens area	Left Fusiform
Right Cerebellum White Matter	Left Isthmus Cingulate
Right Cerebellum Cortex	Left Isthmus Cingulate



Right Putamen	Left Isthmus Cingulate
Left Amygdala	Left Lateral Occipital
Left Hippocampus	Left Lateral Orbitofrontal
Left Fusiform	Left Lateral Orbitofrontal
Left Inferior Temporal	Left Lateral Orbitofrontal
Left Hippocampus	Left Lingual
Left Inferior Temporal	Left Middle Temporal
Left Isthmus Cingulate	Left Parahippocampal
Left Caudal Middle Frontal Cortex	Left Pars Triangularis
Left Hippocampus	Left Pericalcarine
Left Amygdala	Left Pericalcarine
Corpus Callosum Posterior	Left Postcentral
Left Lateral Occipital	Left Precentral
Left Middle Temporal	Left Precentral
Left Amygdala	Left Precuneus
Right Cerebellum Cortex	Left Precuneus
Optic Chiasm	Left Precuneus
Corpus Callosum Posterior	Left Precuneus
Left Lingual	Left Precuneus
Corpus Callosum Central	Left Rostral Middle Frontal
Left Postcentral	Left Rostral Middle Frontal
Left Isthmus Cingulate	Left Superior Frontal
Left Pars Triangularis	Left Superior Frontal
Right Pallidum	Left Superior Parietal
Left Lingual	Left Superior Parietal
Left Parahippocampal	Left Superior Parietal
Left Pars Triangularis	Left Superior Parietal
Corpus Callosum Posterior	Left Transverse Temporal
Left Isthmus Cingulate	Left Insula
Left Lingual	Left Insula
Right Amygdala	Right Cuneus
Left Isthmus Cingulate	Right Cuneus
Left Lateral Occipital	Right Cuneus
Left Posterior Cingulate	Right Cuneus
Left Precuneus	Right Cuneus
Right Hippocampus	Right Fusiform
Left Isthmus Cingulate	Right Fusiform
Right Cuneus	Right Fusiform

Right Cerebellum White Matter	Right Lateral Occipital
Right Cerebellum Cortex	Right Lateral Occipital
Right Hippocampus	Right Lateral Orbitofrontal
Right Entorhinal	Right Lateral Orbitofrontal
Left Cuneus	Right Lingual
Right Hippocampus	Right Middle Temporal
Right Fusiform	Right Middle Temporal
Right Lingual	Right Middle Temporal
Right Pallidum	Right Parahippocampal
Left Isthmus Cingulate	Right Paracentral
Right Cuneus	Right Paracentral
Right Isthmus Cingulate	Right Paracentral
Right Putamen	Right Pars Opercularis
Right Caudal Middle Frontal	Right Pars Opercularis
Right Amygdala	Right Pericalcarine
Right Isthmus Cingulate	Right Pericalcarine
Right Paracentral	Right Pericalcarine
Left Precentral	Right Posterior Cingulate
Right Amygdala	Right Precuneus
Left Superior Parietal	Right Precuneus
Right Postcentral	Right Precuneus
Left Isthmus Cingulate	Right Rostral Anterior Cingulate
Corpus Callosum Central	Right Rostral Middle Frontal
Right Thalamus Proper	Right Superior Parietal
Left Precuneus	Right Superior Parietal
Right Lingual	Right Superior Parietal
Right Precuneus	Right Superior Parietal
Right Amygdala	Right Superior Temporal
Right Accumbens area	Right Superior Temporal
Left Caudate	Right Frontal Pole
Left Lateral Orbitofrontal	Right Frontal Pole
Left Insula	Right Frontal Pole
Right Superior Frontal	Right Frontal Pole
Right Middle Temporal	Right Temporal Pole

Table 13. NBS algorithm edges for DTI analysis. MCI-highEF > MCI-lowEF.

## Discussion

We found greater white matter integrity and a larger nonspecific network in the MCI-highEF group. Notably, the corpus callosum had a higher node degree, clustering coefficient in many of its corresponding ROIs, and higher FA in the forceps major. The parietal and temporal regions had greater clustering coefficient and node degree, and the parietal and temporal components of the superior longitudinal fasciculus had higher FA. Because the temporal lobe is affected in MCI and AD dementia (Ferreira et al 2011), this result is unsurprising. The higher node degree and strength of many regions of the MCI-highEF group and the greater clustering coefficient of most regions in comparison to the MCI-lowEF group suggests that a more “small-world” structure of the MCI-highEF group – or, the ability to traverse from one region to another in a smaller number of steps. Small-world networks are more efficient in transferring information, and it follows that the group with higher executive abilities may have a more efficient network. While a higher node degree was found for a number of regions in the MCI-lowEF group, the corresponding node strength (or weight based on number of fibers leaving the region) was not higher, which suggests that perhaps the MCI-lowEF group has more sparse connections in a few regions. Application of the NBS algorithm resulted in a nonspecific suprathreshold network involving many regions, including the prefrontal, orbitofrontal, parietal and temporal regions of interest. In the MCI-lowEF group, we found a higher RD in the superior and inferior longitudinal fasciculus, which corresponds to findings of greater increases in RD in a pre-AD state (Gold et al., 2012). Because of the

requirements of the prefrontal, parietal and temporal regions in executive tasks (Gibbons et al 2012; Zheng et al 2014), the greater network connectivity of these regions suggests that the white matter integrity is instrumental in retaining these abilities.

The findings of this study reflect that the MCI-lowEF group shows more similarities in pathology to those with AD dementia than does the MCI-highEF group. These similarities include widespread network disruptions in AD dementia (Daianu et al 2013), and disrupted topological organization (Lo et al 2010). Decreased FA in a number of tracts has been shown to be a marker of AD dementia, including the uncinate fasciculus, the superior longitudinal fasciculus, and the corpus callosum (for review, Goveas et al 2015). FA has been shown to be less sensitive to early changes (Acosta-Cabronero 2014); however, it appears that earlier FA changes may accompany diminished EF abilities in individuals with MCI (Nowrangi et al 2015). Our findings suggest underlying white matter abnormalities that correspond to decreased EF score, which Gibbons et al. (2012) describes as predictive of progression to AD. These network measures and the differences in the white matter tracts is likely contributing to the EF dysfunction and may reflect the changes of those who will actually progress to AD. Our previous findings demonstrated a high functional connectivity in an MCI-lowEF group, which may be compensation for the diminished structural integrity described in this study.

Limitations of this study include a lack of correction for age, educational level, and pre-MCI intelligence level. It is possible that the differences observed here may be due to age (Table 1). It may also be that higher educational level induces a stronger white matter network but this needs further investigation. Similarly, higher pre-morbid IQ may

be the result of better network connections, another notion that needs further investigation. Because non-impaired individuals with greater intelligence tend to have better executive abilities, it is unclear if prior abilities confer a protection against the impairment of executive abilities associated with MCI, or if the disease progression is responsible for the diminished abilities. A study tracking subject educational level and intelligence prior to MCI onset could help resolve this. Also, tracking these individuals to assess who did, in fact, progress to AD dementia or another disorder would be instrumental in determining the significance of the white matter abnormalities and structural differences.

## **CHAPTER 4: INTRODUCTION TO DECISION-MAKING AND RULE UNCERTAINTY**

Decision-making is a ubiquitous executive ability required by humans and animals alike. Many decisions require that a rule be applied. For example, in picking a route to a destination, the desired outcome (reaching the destination) is known, but a few rules may be chosen from, such as optimizing for time, or optimizing for distance, or avoiding tolls. Overcoming this uncertainty is required for intelligent behavior. This project used both electroencephalography (EEG) and fMRI to describe the brain regions involved in applying rules under uncertain and certain conditions. Using network analysis, we describe how the regions of the brain work together to complete a decision-making task with rule uncertainty.

Pouget, Drugowitsch, and Kepecs (2016) have defined confidence as the probability a participant assigns to their perceived success. They define uncertainty as involving the external factors that come into play in arriving at that confidence. We compare conditions with high levels of certainty and uncertainty during rule application. Participants were given a task in which they could be certain or uncertain of the rule to apply in a set of trials.

Many studies measure responses to outcome uncertainty or risk, and use a small component of study payment dependent on task performance or food rewards for animals to simulate risk. Fewer tasks look at rule uncertainty specifically. In our study, we used a task in which a subject receives feedback (correct or incorrect) that thus carries a small but inherent risk. However, the gains or losses are minimal, as they are neither being

compensated nor punished for their performance. Risk requires that the individual have something to gain or lose (Anselme 2014; Zhang 2014). Primate studies have found that subjects will work to avoid uncertainty, even to their detriment. This avoidance corresponds to activation in the ventral midbrain, which includes the substantia nigra pars compacta (Bromberg-martin and Hikosaka 2010; Fiorillo 2003). In addition, Kiani and Shadlen (2009) described primates opting out of an uncertain condition even when it meant a smaller reward. This suggests that certainty is inherently rewarding and that uncertainty is aversive (for review, see Bach 2010). Humans show slowing in response time in uncertain conditions, which corresponds to ventral striatum activity (Buzzell et al 2016). Studies using the intolerance of uncertainty (IU) task found a connection between uncertainty aversion and higher levels of anxiety and increase of worry (de Bruin, Rassin, Muris 2006; Rosen and Knauper 2009). The anterior insula is found to be engaged in situations of increased certainty (Bhanji et al 2010), yet is also thought to be involved in prediction of risk (Bossaerts 2010, review), and modulated by rule complexity (Bhanji et al 2010).

Areas associated with reward are the orbitofrontal cortex and amygdala (Baxter et al 200; Kepecs 2008; Klein-Flugge 2013) as well as the hippocampus (Labreton 2013). Because of the minimization of reward in this task, we would expect to see less of this regional involvement. However, because we are using a rule application paradigm, we would expect to see frontal cortex involvement (Badre et al; Badre and D'Esposito 2009). The dorsolateral prefrontal cortex, dorsal anterior cingulate cortex, and bilateral anterior insula increase in activation with increasing rule complexity (Bhanji et al 2010). The

anterior cingulate cortex is involved in conflict monitoring, outcome evaluation, and decision-making (Botvinick 2007). A model of reinforcement learning and optimal decision-making developed by Bogacz and Larsen (2011) requires basal ganglia participation, most specifically communication between the striatum, subthalamic nucleus, and globus pallidus. These regions interact with the cortex and thalamus to accomplish learning during decision-making. The lateral intraparietal sulcus has been found to encode choice accumulation in primate saccadic choice task (Churchland et al 2011; Ganguli et al 2008; Beck et al 2008), and the parietal reach region (PRR) corresponds to expected reward coding (Anderson and Cui 2009).

The purpose of this study is to describe the brain regions involved in a novel uncertainty task, in which the risk is minimal but there is inherent certainty or uncertainty, allowing comparison of these two conditions in relative isolation from variations in reward and certainty levels. The use of the methods described here as well as the novel task will help to describe the physiological mechanism involved in the brain applying rules under uncertain conditions. This study will add information to the growing body of literature about brain regions involved in these states and their network interactions.

EEG measures the summed potential of millions of parallel neurons firing synchronously. An excitatory post-synaptic potential (EPSP) or an inhibitory post-synaptic potential (IPSP) will be generated at a neuron's apical dendrites. Summation to threshold of an EPSP will generate an action potential; however, the action potential is transient and not likely to contribute much to the EEG signal (Speckmann, Elger, and



Gorji 2010). The EEG signal is thought to be generated by EPSP and IPSP summed and detected at the cortical surface. The orientation of cortical neurons in parallel allows for a summation of these potentials. Subcortical regions are oriented in a less organized fashion and thus are a less likely generator for EEG signal (Pizzagalli 2006). EEG allows for detection of neural events at the millisecond time scale. Averaging post-stimulus epochs in order to find potential differences that occur is a means of examining focused, non-rhythmic events in the brain that are transient in nature. Event-related potential (ERP) analysis is a means of capturing non-oscillatory signal (Rosler 2005). We are looking at the signal time locked to intervals of interest, and then comparing them. This allows us to examine narrow (~100 ms) time intervals to look for differences in neural activity between conditions. fMRI network analysis was performed in the same manner as described in Chapter 2. In addition, we used a General Linear Model (GLM) in order to assess the components of the BOLD signal that are attributable to the task.

We recruited 30 participants for EEG and 25 participants for fMRI. Three EEG subjects and 2 fMRI subjects were excluded on the basis of excessive artifact. We used a card-matching task in which subjects were instructed to match a card to one of five other cards based on similarity in exactly one of five attributes. The subjects were not given any information on matching criteria. In the certain condition, the subjects' first choice of rule to apply was the choice for the remainder of the run. In the uncertain condition, the rule to match changed at every interval. The subjects were categorized in either the EEG or fMRI condition. The fMRI paradigm had fixation blocks interspersed between tasks within each run, otherwise the timing for the conditions was identical.

Limitations include not jittering the fMRI sequence, in order to allow for performing event-related analysis on the BOLD signal data to separate the feedback from task performance. However, this would have sacrificed the simplicity of the GLM analysis and introduced some task confounding variables. In addition, running the protocol on each participant for both the EEG and fMRI component would have been ideal in order to be able to compare the brain regions involved more directly. However, this would have had some practice effect on the participant as they performed the task twice. Educational history and intelligence level were not assessed for the participants. These may have been useful variables to control for in the analysis.

Future variations of this study would include a jittered component to the fMRI task, in order to allow for an event-related analysis of the fMRI data. This would allow for the resolution of the subcomponents of the task, and for us to determine when and where BOLD signal activation is responding to either feedback or card presentation. Also, a counterbalanced dual-modality approach for each subject. This would allow for more specific study of in different events in the fMRI time frame, and for the union of the EEG and fMRI results. Then, we could examine how these networks are affected in pathological states in which decision-making is affected, such as MCI. In addition, we did not gather information about intelligence, educational level, or general psychological traits of the participants. In future studies, this would be a helpful means of better describing neurologic response to the task.

## **CHAPTER 5: AN EVENT-RELATED POTENTIAL ANALYSIS OF BRAIN ACTIVITY IN DECISION-MAKING IN CERTAIN VERSUS UNCERTAIN CONDITIONS**

### **Background**

Decision-making is essential to human functioning, and encompasses such varied abilities as choosing a correct answer on a test, selecting a food to eat, making an investment, or selecting a life partner. Resolving uncertainty is arguably the most difficult component of decision-making. Uncertainty can arise when the desired outcome is known but the means to achieve that outcome is not. In this case, an individual is uncertain of which rule to apply (rule uncertainty). We created a card-matching task that alternated a condition in which the subject was certain of the rule to apply with a condition in which the subject was uncertain of the rule to apply. The aim of this study was to compare brain activity in the certain condition to the uncertain condition using EEG and ERP analysis. 128-lead high-density EEG and ERP can localize cortical activity and provide insight into early (0-2 second) brain activation. In this study, we analyze the brain activity evoked by rule uncertainty using EEG and ERP. EEG measures electrical brain activity with millisecond precision, and the use ERP allows for localization and timing of stimulus-locked responses. Of the decision-making studies to date, some have focused on the potentials corresponding to feedback (Cui et al 2013; Trujillo 2007) and have found greater feedback-related negativity (FRN) potentials. These are reflected as an 80-100 ms negativity when subjects are presented with negative feedback. Philastides et al (2010) describes a 220 ms post stimulus potential correlated

with decision difficulty, and advantageous and disadvantageous choices in an Iowa Gambling task corresponded with a left and right hemisphere p300, respectively (Cui et al 2013).

Decision-making is an executive function, and thus generally thought to require the frontal lobe. However, complex tasks generally require many components of the cortex and the basal ganglia. The importance of the basal ganglia in decision-making is becoming more apparent; the basal ganglia, in both the executive and limbic loops, contains many reciprocal connections with the cortex (Nieuwenhuys; Bogacz and Tobias). In addition, the anterior cingulate cortex engages the prefrontal cortex in times of uncertainty (Nieuwenhuys; Botvinick 2007).

A complex network of brain regions is required in the resolution of uncertainty. This study helps describe the brain activity involved in this function, and the task performed neatly separates the certain and uncertain conditions – which allows for future study of gradations between these two conditions. Decision-making is impaired in many pathological conditions, including schizophrenia, mild cognitive impairment, and obsessive-compulsive disorder (Triebel 2009; Matsuzawa 2014; Zhang 2015). The effects of this impairment provide daily challenges to those afflicted, and in providing a baseline for normal functioning we may begin to examine the changes that occur in pathological states. In addition, we introduce a decision-making novel task for the examination of this function in both pathological and normal states.

Many studies use traditional neuropsychological tasks that have gradations of reward and levels of uncertainty to study decision-making. We used a card-matching

task in which the level of uncertainty was controlled in order to compare the two extremes of certainty and uncertainty. We alternated a condition in which the first rule the subject used became the correct rule for the duration of the run with one in which the rule changed at every interval. We examine the event-related potentials that occur after the card-matching stimulus is presented, while the subject is making the decision, as well as the potentials after the feedback occurs. We measure peak amplitudes as well as plot scalp maps to describe the changes that occur in the brain in the certain and uncertain conditions.

## **Methods**

### *Participants*

Thirty-one young right-handed individuals (11 males, ages 18-40) with no neurologic disease participated in the task. Four female subjects were excluded based on heavy artifact in the data collected. Subjects signed a consent form approved by the institutional review board. The entire session lasted approximately 90 minutes, with 60 minutes of EEG setup and 30 minutes of task.

### *Task*

Subjects sat in front of an 18 inch computer monitor, 18 inches from the screen in a dark, quiet room with a 5-button keyboard to allow for selection of numbers 1-5 using the right hand. Subjects were presented with a series of five cards in a row on the top half of the computer monitor, and one card in the bottom middle of the computer monitor (Figure 4). Subjects were instructed to choose one of the five cards from the top of the screen that they believed matched the bottom card, and to press the corresponding button.

They were not given any information about the correct rule to apply. Subjects were given four seconds to respond and were given feedback of “Correct”, “Incorrect”, or “Skipped” for two seconds. Brief instructions were presented at the beginning of each run; there were six runs with 30 card presentations per run. At the end of the run, the instructions would reappear, and subjects would be allowed to adjust slightly and rest before beginning the next run with a key press.

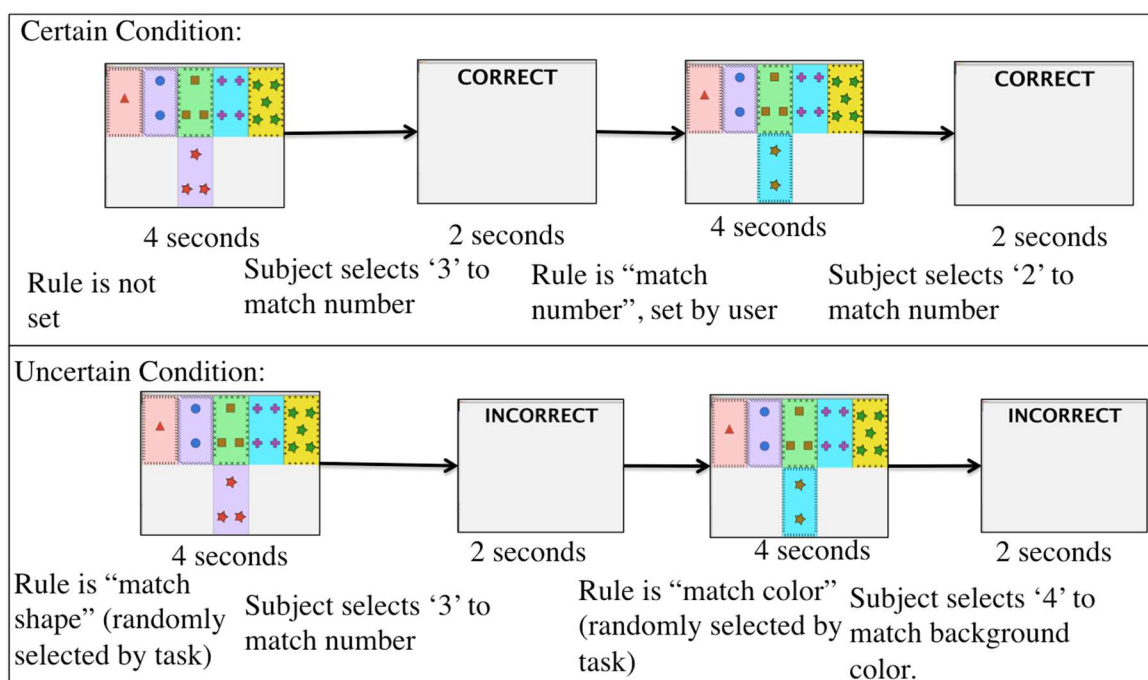


**Figure 4. Decision-making card-matching task paradigm.**

The cards had five attributes: background color, shape, shape color, number of shapes, and border. Each of the top cards matched the bottom card in exactly one attribute. In the certain condition, the rule was set by the match condition the subject first used and the rule did not change until the end of the run. In the uncertain condition, the rule changed randomly at every card presentation. Therefore, there was a correct rule at each match but there was no way for the subject to be sure of it. The certain runs were

alternated with uncertain runs. Half of the subjects began with the certain condition and the other half began with the uncertain condition.

### *Electroencephalography setup*

We used a BioSemi Active 2 system with 128-channel Biosemi Active-headcap. Four sets of 32 Pin-Type Active Electrodes were connected to the ActiveTwo AD-box, which transmitted amplified EEG signal to a personal computer using ActiveView (Version 7.06) software on the Windows XP platform. Stimuli were presented on a separate personal computer using a Java graphical user interface application, which sent triggers through a parallel port to the ActiveView software. Impedance was adjusted to <20 kOhms. A sampling rate of 1024 Hz was used, and later each output file was decimated to 256 Hz for processing ease.

### *Analysis*

Output EEG files were preprocessed using EMSE software for detrending, baseline correction, band-pass filtering (0.03 to 30 Hz), and blink reduction. Data were exported and the remainder of the analysis was performed using MATLAB software. Epochs were extracted for the first two seconds of the post-card presentation, as well as the first two seconds of post-feedback activity. For the certain condition, intervals in which the subject was not certain (i.e., had just started the task or had incorrectly selected a match previously) were discarded. For the uncertain condition, intervals in which the subject had randomly selected the correct match in the previous match were discarded.

Epochs were averaged and baseline corrected to the average 200 ms prestimulus interval. An average for each epoch type was constructed for each electrode. In addition, regions of interest (ROIs, shown in Figure 5) were averaged and calculated. Scalp maps were generated using averages of time intervals and by plotting the values of these averages at each electrode. Maximum, minimum and mean values for intervals of interest were extracted, and paired t-tests were used to assess significance. The values at electrodes and ROIs are not independent because the same sources of EEG signal will impact many electrodes to varying degrees, so we will report the values uncorrected. Although this does increase the risk for Type I error, our results are above the rate at which one would expect this error to occur.

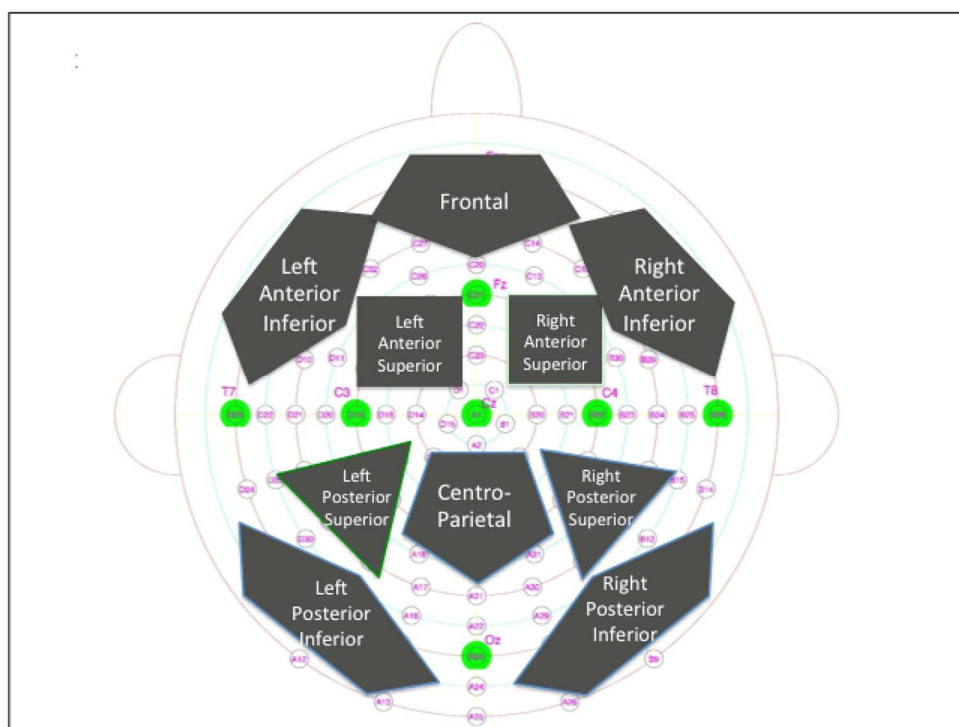


**Figure 5. ERP Regions of Interest.**



## Results

### *Certain versus Uncertain*

In the certain versus uncertain conditions, there are small differences between the condition's potentials, in the first 500 ms post-stimulus. Differences include small increases in the uncertain over the certain condition in the left anterior superior region, reflected in the ROI plot (Figure 6) and in the scalp map (Figure 7) between 300 – 500 ms. After this interval, the differences are more pronounced, including a large increased positivity in the certain over the uncertain condition moves from the posterior scalp to the front of the brain. From 500 – 1200 ms, this increase in the certain over the uncertain potential is reflected in the occipital and parietal regions. This is reinforced by the ROI plots (Figure 3), which show the increase in certain over uncertain in the left posterior inferior, left posterior superior, centro-parietal, right posterior inferior, and right posterior superior ROIs. After this interval, from 1000-2000 ms post-stimulus, the difference between certain and uncertain becomes smaller in the previously described ROIs, and becomes larger in the left anterior inferior region, the right anterior inferior region, and the centro-frontal region.

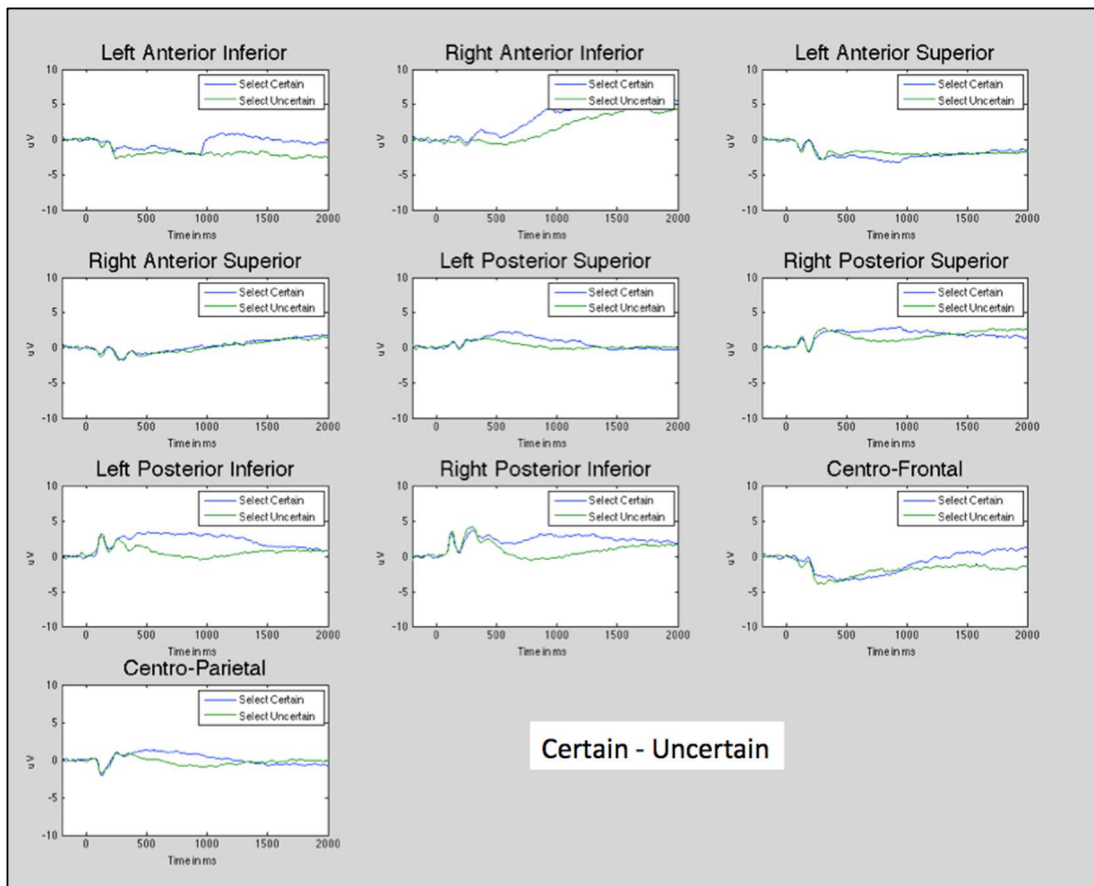


Figure 6. Certain and Uncertain condition averaged potentials from -200 ms to 2000 ms post card presentation. ROIs are grouped as described in Figure 2.

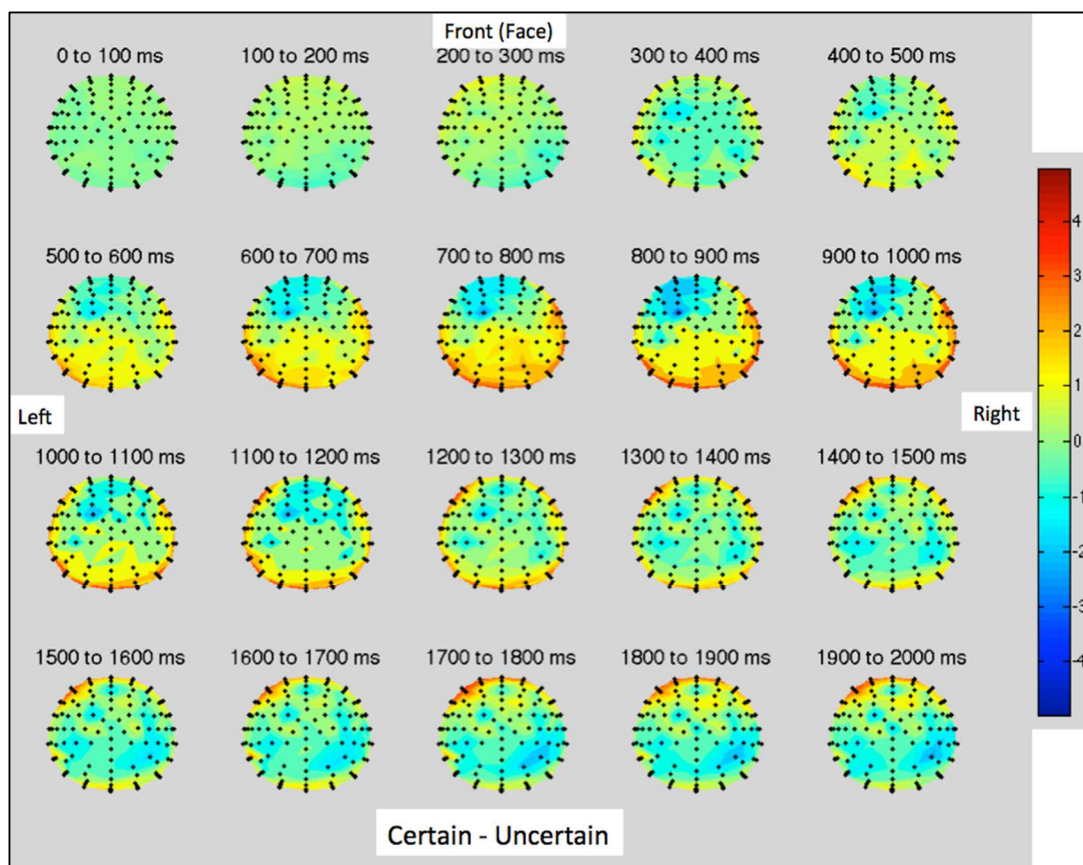
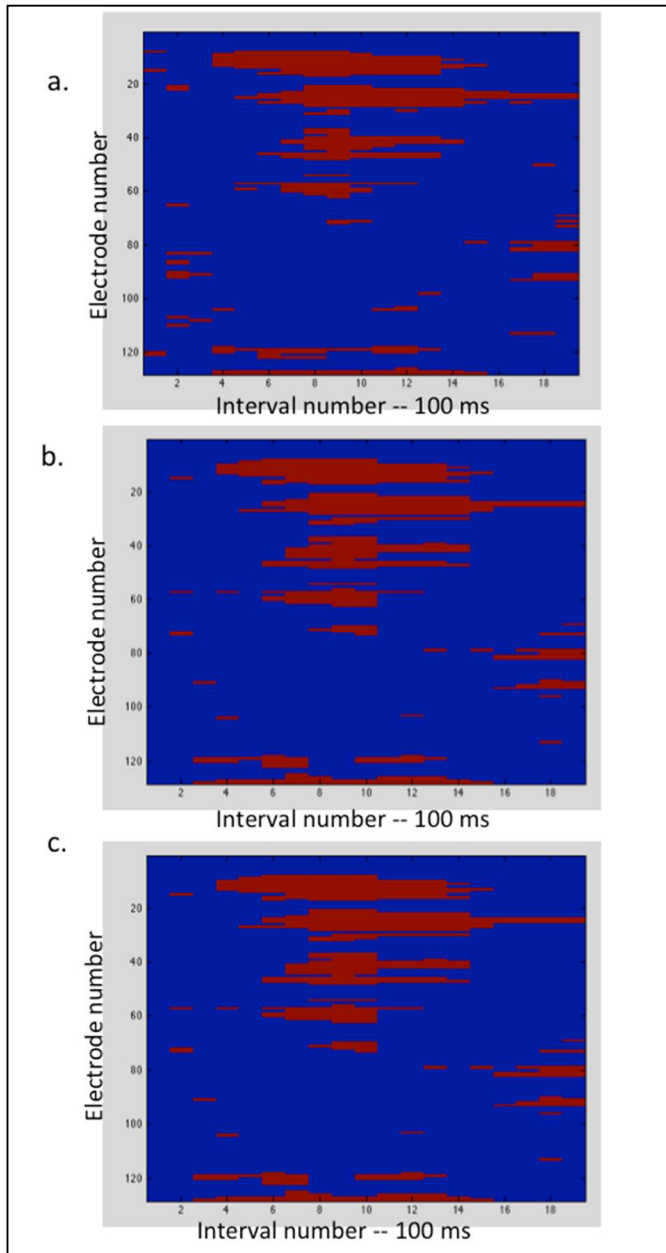


Figure 7. Scalp maps of 100 ms intervals from 0-2000 ms of the certain – uncertain condition, averaged and plotted at each electrode in the -4 to 4 uV scale.

In the 500 to 1000 ms time frame, a central fronto-parietal region remained elevated in the uncertain condition, as demonstrated by the left anterior superior and the centro-frontal region. In the post-1000 ms timeframe, the centro-parietal region and the right posterior superior region showed elevations in the certain over the uncertain condition. The right anterior superior region showed very little difference between the two conditions. Significance testing of the minimum, maximum and mean in each 100 ms epoch revealed very similar values. In all three cases 14% of the epochs tested yielded a p-value < 0.05, which is more than the 5% false positive rate one would expect

from multiple comparisons. The greatest numbers of significant differences are reflected in the 500-1400 ms time frame, most in the parietal and occipital regions (Figure 8).



**Figure 8. Certain versus Uncertain condition. Significance of epoch per electrode. T-tests comparing measure in each 100 ms interval (x-axis) for each electrode (y-axis). p-values < 0.05 represented by red, all others represented by blue. 336 of 2432 (14%) epochs had  $p < 0.05$ . a) min value compared for each 100 ms interval. b) Maximum value compared for each 100 ms interval. 352 of 2432 (14%) epochs had  $p < 0.05$ . c) mean value compared for each 100 ms interval. 347 of 2432 (14%) epochs had  $p < 0.05$**

*Correct versus Incorrect*

An increase in the incorrect feedback condition over the correct feedback condition is reflected in the 300 to 600 ms post-stimulus timeframe in the left frontal region, which is shown in the scalp maps of that period and is reflected in the left anterior superior, left anterior inferior, and centro-frontal region (Figure 9 and Figure 10). This increase is diminished between 600 to 1400 ms. Between 1400 to 2000 ms another increase in the incorrect feedback over the correct feedback is reflected in the right and left posterior inferior, and the right and left anterior superior regions. Increased positivity in the correct over the incorrect condition is reflected in the 300 to 600 ms time frame in the right anterior inferior, and the right and left posterior inferior regions. Also of note is the strong negative deviation in both conditions in the right anterior inferior, with a much stronger negative deflection in the incorrect condition. Significance testing of the maximum, minimum, and mean in each interval reflected the greatest number of differences with  $p < 0.05$  in the 300-600 ms interval (Figure 11). There were 14%, 8%, and 14% with p-values  $< 0.05$ .

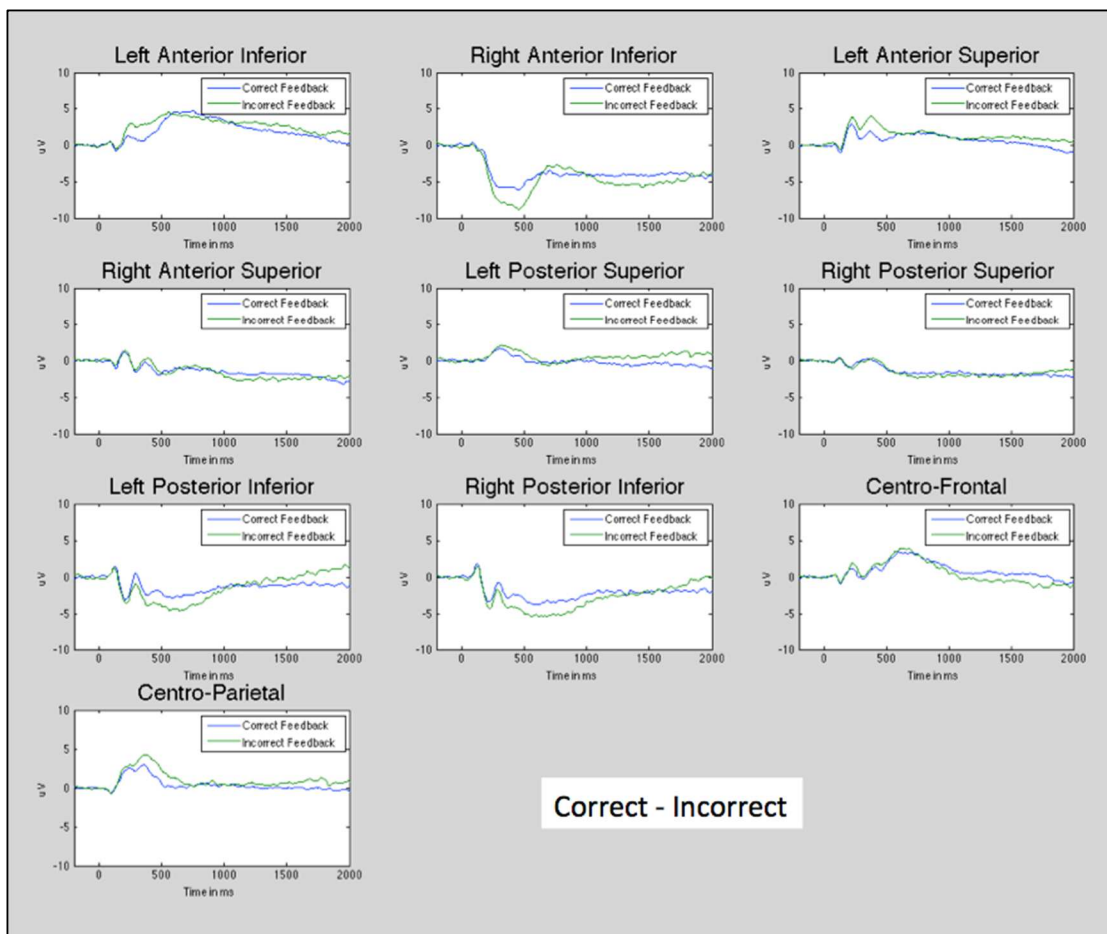


Figure 9. Correct and incorrect condition averaged potentials from -200 ms to 2000 ms post card presentation. ROIs are grouped as described in Figure 2.

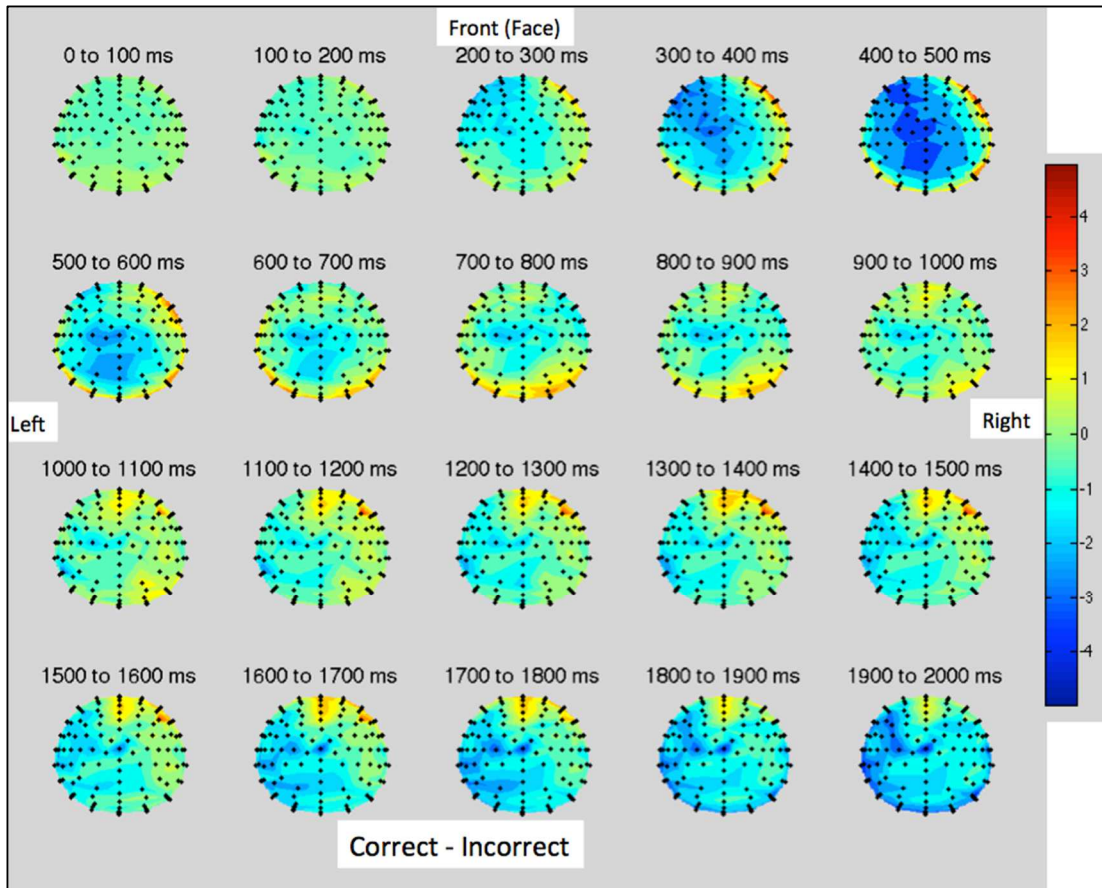
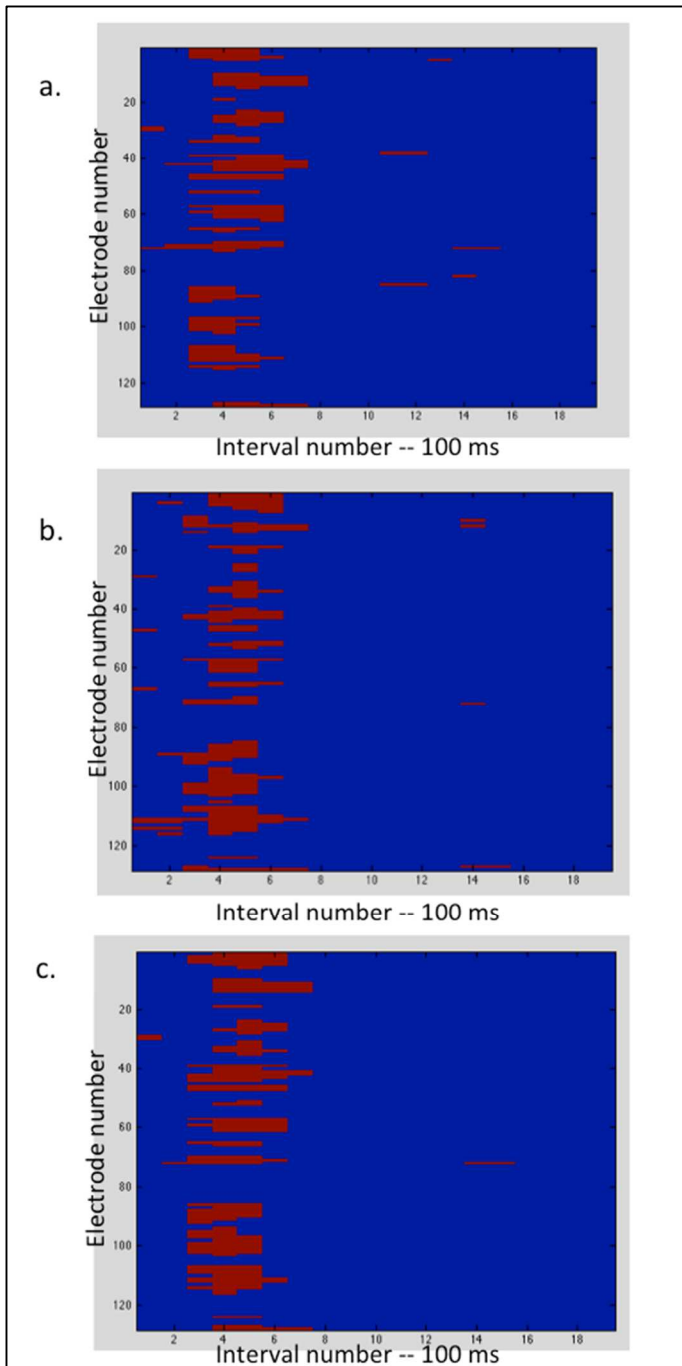


Figure 10. Scalp maps of 100 ms intervals from 0-2000 ms of the correct – incorrect condition, averaged and plotted at each electrode in the -4 to 4 uV scale.



**Figure 11. Significance of each epoch per electrode in correct versus incorrect condition. T-tests comparing measure in each 100 ms interval (x-axis) for each electrode (y-axis). p-values < 0.05 represented by red, all others represented by blue. 185 of 2432 (8%) epochs had  $p < 0.05$ . a) min value compared for each 100 ms interval. b) max value compared for each 100 ms interval. 352 of 2432 (14%) epochs had  $p < 0.05$ . c) mean value compared for each 100 ms interval. 347 of 2432 (14%) epochs had  $p < 0.05$**



## Discussion

Although the task introduced in this paper is novel, some studies have described ERP correlates of decision-making under uncertain conditions. This has been examined in the context of gambling and risky decision-making, such as a study of advantageous choice and nonadvantageous choice in the Iowa Gambling task, which demonstrated an increased p300 in the right hemisphere during the advantageous choice and an increased p300 in the left hemisphere during the nonadvantageous choice (Cui et al 2013). We confirmed an increased potential in the 300 ms time frame, but found opposite laterality from those in the Iowa Gambling Task results: higher potential in the uncertain condition in the left hemisphere, and higher potential in the right hemisphere in the certain condition. Because the authors suggest the magnitude of the reward is the modulating effect on this potential, the uniformity of the reward/punishment in our task may contribute to the differences. The effect that we found may be the p3a described by Polich (2007). The p3a is generally associated with stimulus-driven frontal mechanisms and correlates to the location and task difficulty that we are describing. However, the potential differences found in the 300-500 ms time frame were not as pronounced as those in the later interval. The results from the 500-1000 ms time frame reflected a decreased potential in the parietal and occipital regions in the uncertain condition. Bland and Schaefer (2011) describe task volatility, which was similar in quality to the task uncertainty defined in our study, as producing a N2/N400 complex. Bland's results are similar to the diminished potentials we saw in the uncertain condition in the 400-800 ms interval in most of the examined ROIs. Conflict monitoring during a Go/NoGo task

produced an n400-like response that Brunner et al (2015) suggests is likely the work of the anterior cingulate cortex. The later potentials (post 500 ms) show a greater positivity in the parietal/occipital regions in the certain condition. This is similar to the late positive component (LPC), a phenomenon that arises during memory tasks and is associated with decision accuracy and confidence (Finnigan et al 2002; Chen et al 2014). While the LPC is generally associated with recognition of previously seen items, in this case recognition and reinforcement of the rule is occurring in the certain condition.

Decision-making studies often focus on feedback-related negativity. We found a negative right frontal deflection in the incorrect/uncertain condition that may correspond to the feedback related negativity. This negativity is also present in the correct condition, but is not as pronounced. Because the FRN is thought to be an early reflection of updating context or rules based on feedback (Cohen, Elger, and Ranganath 2007), the frontal presence of the FRN-like wave is consistent with expectations. Because the anterior cingulate cortex is thought to be engaged in conflict anticipation (Botvinick 2007), it follows that this signal may be resulting from prefrontal engagement by the anterior cingulate cortex.

A widespread increase in amplitude in the left frontal and parietal regions is evidenced in the 300-500 ms timeframe. This is consistent with both a p3a and p3b effect, which are associated with task processing and memory updating, respectively (Polich 2007). It follows then that feedback may trigger rule updating or changing of the mental conception of the rule that is evidenced during the rule uncertain condition.

The results of this study reinforce current understanding of rule application, rule updating, and ERPs seen during times of uncertainty. The increased potential in the frontal region in the 500-1000 ms time frame in the uncertain condition reflects increased cognitive processing, and the increased positivity in the certain condition in the posterior may reflect memory updating. The feedback related negativity seen in the uncertain condition is consistent with what might be expected from the literature; however, the evidence of p3a and p3b suggests cognitive processing that occurs immediately after the subject realizes that they are not certain of the rule. The results reinforce that the novel task developed is a good means of measuring cognitive response to uncertainty. The markers described are a good baseline. Further study could include post-response processing, measures looking for specific ERPs – including fractional area analysis and timing and peak value in the intervals of interest.

## **CHAPTER 6: NETWORK-BASED ANALYSIS OF BRAIN ACTIVITY USING FMRI IN DECISION-MAKING UNDER UNCERTAIN CONDITIONS**

### **Introduction**

Individuals are faced with decisions daily that require that a rule be applied, such as selecting a route to reach a destination or choosing an investment strategy to optimize profit. Uncertainty regarding the optimal rule to apply to reach the desired outcome is often inherent in these decision-making processes. Resolving this uncertainty is the most challenging component of the decision-making process. However, being able to make decisions under conditions of rule uncertainty is vital to human function, and the impairment of this process in diseases such as MCI, schizophrenia and obsessive-compulsive disorder is particularly harmful (Triebel et al 2009; Matsuzawa 2015; Zhang et al 2015). The aim of this study is to describe the brain regions involved in decision-making under conditions of rule uncertainty using fMRI, and to describe the interactions of these brain regions using network analysis. The current analysis of decision-making during rule uncertainty is incomplete, therefore healthy young individuals are examined in this study in order to provide a baseline measurement of rule uncertainty activity. This will allow for future comparison against pathological states to determine the neural regions that are particularly impaired in these conditions. FMRI is a non-invasive means of measuring the neuroanatomical activity correlating with the task conditions. The BOLD signal is a measurement of the cerebral blood flow to a brain region, which

increases coincident with brain region activation (Logothetis 2002). A decision-making task in which the correct rule to apply is either completely certain (known from first trial) or completely uncertain (changes at every trial) is used and an examination of BOLD signal differences between these two states yields information about the brain regions involved in decision-making in uncertain conditions.

Much of the cortex is implicated in decision-making in conditions of uncertainty. Prior fMRI studies have suggested involvement of the orbitofrontal cortex (OFC), the dorsolateral prefrontal cortex (dlPFC) and the anterior cingulate cortex (ACC) (Esslinger 2013; White et al 2014) in making decisions in uncertain conditions. Other implicated regions include the insula, the posterior parietal, the inferior parietal, and inferior temporal areas (White 2014; Krug 2013). Studies have suggested that information about the correct decision is stored in the ventral temporal cortex and posterior parietal cortex (Philastides 2010; Hutchinson 2015), whereas the ventromedial prefrontal cortex (vmPFC) has been implicated in computing expected value and reward outcome in processing decisions (Daw and Doya, 2006). The vmPFC works with the hippocampus during mismatch detection (Garrido et al 2014). In addition, the role of the basal ganglia in decision-making, particularly as rules are learned, is becoming increasingly evident. The striatum is involved with reward learning and habitual actions, and activation may correlate with prediction of punishment (Daw and Doya 2006; Stalnaker et al 2012; Samejima et al 2005). A computational model of decision-making as performed by the basal ganglia, developed by Bogacz and Tobias (2011), involves a circuit that includes the cortex, striatum, subthalamic nucleus, and globus pallidus. This corresponds to the

dorsolateral prefrontal(executive) loop of the basal ganglia (Nieuwenhuys 2008 p 439). The ACC engages the prefrontal cortex and is implicated in conflict monitoring and outcome evaluation (Botvinick 2007).

The interactions between the brain regions involved in decision-making under uncertain conditions are complex and we would expect to see many areas of activation. By using the GLM to estimate the contribution of each task condition to BOLD signal over time, we can identify regions with increased blood flow and draw some conclusions about regional activity. However, because so many regions are likely involved, functional network connectivity can describe similar activity between ROIs. Network analysis has emerged as an instructive method for describing the brain – as brain regions rarely act in isolation – so we can learn much about how the brain regions interact. ROI-based analysis allows for each region to be treated as a node of the network, and for the level of connectivity between ROIs to be established by BOLD signal correlation. Graph theory measures such as network size, density, node degree, clustering coefficient, and assortativity describe the networks and the differences between them.

The comparison of BOLD signal response in the certain and uncertain states in a task that is otherwise matched in requirements allows for the comparison of the effect of certainty and uncertainty on various brain regions. Other studies that measure responses to uncertainty have used the Iowa Gambling Tasks or tasks that manipulated the levels of uncertainty. The task used in this study allows for a binary difference to be measured. The network analysis allows for a description of the functional connection between

participating regions of the brain, and various properties that these functional networks demonstrate.

## **Methods**

### *Subjects*

Twenty-three healthy subjects ages 18-37 were selected (9 males) from the greater Boston community. Subjects signed a consent form approved by the institutional review board. Four subjects were excluded based on excessive artifact, leaving nineteen subjects (7 males). The entire session lasted approximately 90 minutes, with 60 minutes in the MRI scanner.

### *Paradigm*

The task was projected from a personal computer onto a high-resolution screen, which was reflected in a mirror above the subject's face as he or she lay in the MRI. The screen showed a row of five cards on the top, and a row at the bottom with a single card (Figure 4). The subjects were instructed to match the bottom card to a card in the top row to the best of their ability, with no further instruction about matching criteria. Each card had five different properties: shape, shape color, background color, number of shapes, and border. Each of the top cards matched the bottom card in exactly one attribute. The card-matching screen was presented for four seconds, and subjects were instructed to match within those four seconds. Card presentation feedback was shown for two seconds. Feedback was "Correct", "Incorrect", or "Skipped". There were thirty card

presentations per run; fixation periods of 30 seconds were alternated with task periods of 30 seconds that contained five cycles of card presentation and feedback. The top row remained the same throughout each run, and the bottom card changed. The fixation was a “#” symbol in the middle of the screen, and subjects were asked to watch the fixation mark while relaxed, attentive, and awake.

There were two conditions, one in which the rule was certain, and one in which the rule was uncertain. In the certain condition, the matching criteria were locked to the first matching rule the subject applied. In the uncertain condition, the matching criteria changed at every single interval. A run of thirty card matches would be entirely either the certain or uncertain condition, and the six runs alternated between certain and uncertain conditions. The sequence of cards shown was identical for pairs of uncertain and certain conditions – for example, the same top row and same series of bottom cards would be shown for runs 1 and 2. However, the matching rules would be set as described previously. The start condition was varied between subjects. Some had the certain condition in runs 1, 3, and 5; some had the certain condition in runs 2, 4, and 6. Subjects were instructed to hold a five-fingered button box in their right hand and to select the button corresponding to their choice. Choices aligned with the finger position (1 left to 5 right).

### *MRI Acquisition and Preprocessing*

Data were collected using a Phillips T3 Scanner and a 32-channel head coil. The scan began with localization and a reference scan, followed by six functional runs of a single shot echo-planar imaging sequence (TR = 2 s, TE = 35 ms, 30 slices, 3 mm slice



thickness, inplane resolution 3 mm × 3 mm) and finally a T1-weighted structural image (1 mm<sup>3</sup> voxel size).

Freesurfer software ([surfer.nmr.mgh.harvard.edu](http://surfer.nmr.mgh.harvard.edu) version 5.1) was used to parcel and label the structural scans of each of the subjects (Desikan et al 2006). The software identified grey and white matter regions in the cortex and sub-cortex. Eighty-two gray matter regions were selected from this set for network analysis. The fMRI data were preprocessed with motion correction using MCFLIRT (Jenkinson et al 2001), spatial smoothing, and temporal filtering using fMRI Expert Analysis Tool (FEAT; Oxford, UK; v6.0 <http://fsl.fmrib.ox.ac.uk/fsl/fslwiki/FSL>). Filtering using FEAT applies a linear high pass filter to remove low frequency artifacts (Smith et al 2004). Using FEAT, the fMRI data were registered to both the T1-weighted structural image of the brain, extracted from Freesurfer, and the MNI152 average. The preprocessed fMRI data were labeled using the generated Freesurfer ROIs. A mean time series for each ROI was calculated by averaging all fMRI voxel values within each ROI over time, resulting in 90 time points calculated for each of the six six-minute runs. The portions of the time course associated with fixation were removed in order to only correlate task performance.

Networks were constructed with the ROI time series as the nodes, and the Pearson correlation coefficients between each pair of nodes as the edges. Network measures were calculated on these constructed networks. Binary measures were calculated on networks constructed by using threshold values ranging from 0.4-0.9 of the correlation coefficient. Weighted measures were calculated using the Fisher transformation of the correlation coefficient of the matrix. The measures calculated included: network size (the number of

suprathreshold edges present in the network), node strength (the sum of the edge weights for each node), cluster coefficient (the tendency of clusters of three node cycles to form around each node), network density (the average connectivity of the nodes in the network), and assortativity (the tendency of nodes with similar degree to connect to each other). All of these measures except for size were calculated using the Brain Connectivity Toolbox (Rubinov and Sporns 2010).

In order to assess significance, permutation testing was used. 10,000 random datasets were constructed by shuffling the edges between subjects. Then, the network measures were calculated on each of these generated datasets, and the placement on the distribution of these network measures was assessed in order to calculate the p-value.

Data were also analyzed by FEAT (Oxford, UK; v6.0 <http://fsl.fmrib.ox.ac.uk/fsl/fslwiki/FSL>) and performed statistical analysis using the GLM to calculate task contribution to the BOLD signal. For each subject and in each run, a GLM was constructed of the blood flow in each voxel in comparing the task condition to the fixation condition. Higher-order FEAT stats were calculated by averaging within each subject for each condition. A paired comparison of a subject's averaged uncertain versus certain condition was calculated using the GLM. Z-statistic images were thresholded with clusters in which  $Z > 2.3$  and the corrected cluster significance was  $p < 0.05$ .

## Results

### *FEAT Analysis*

The GLM analysis determining the contributions of the task to each signal yielded significant differences between the two conditions. In comparing certain > uncertain BOLD signal, the analysis yielded bilateral clusters in the insula that extend into the boundary of the parietal and temporal lobe, as well as a medial frontal cluster (Figure 2 and 3, Table 14). The uncertain > certain comparison yielded 3 large clusters – a midline cluster that extended through midbrain, the thalamus, bilateral prefrontal cortex, the striatum, then bilateral clusters that extended through the parietal cortex and occipital cortex (Figure 4 and 5, Table 15).

Cluster Index	Voxels	p-value
1	858	0.000138
2	1286	2.3e-6
3	2074	3.5e-9

**Table 14. Clusters produced by FEAT analysis, Certain > Uncertain**

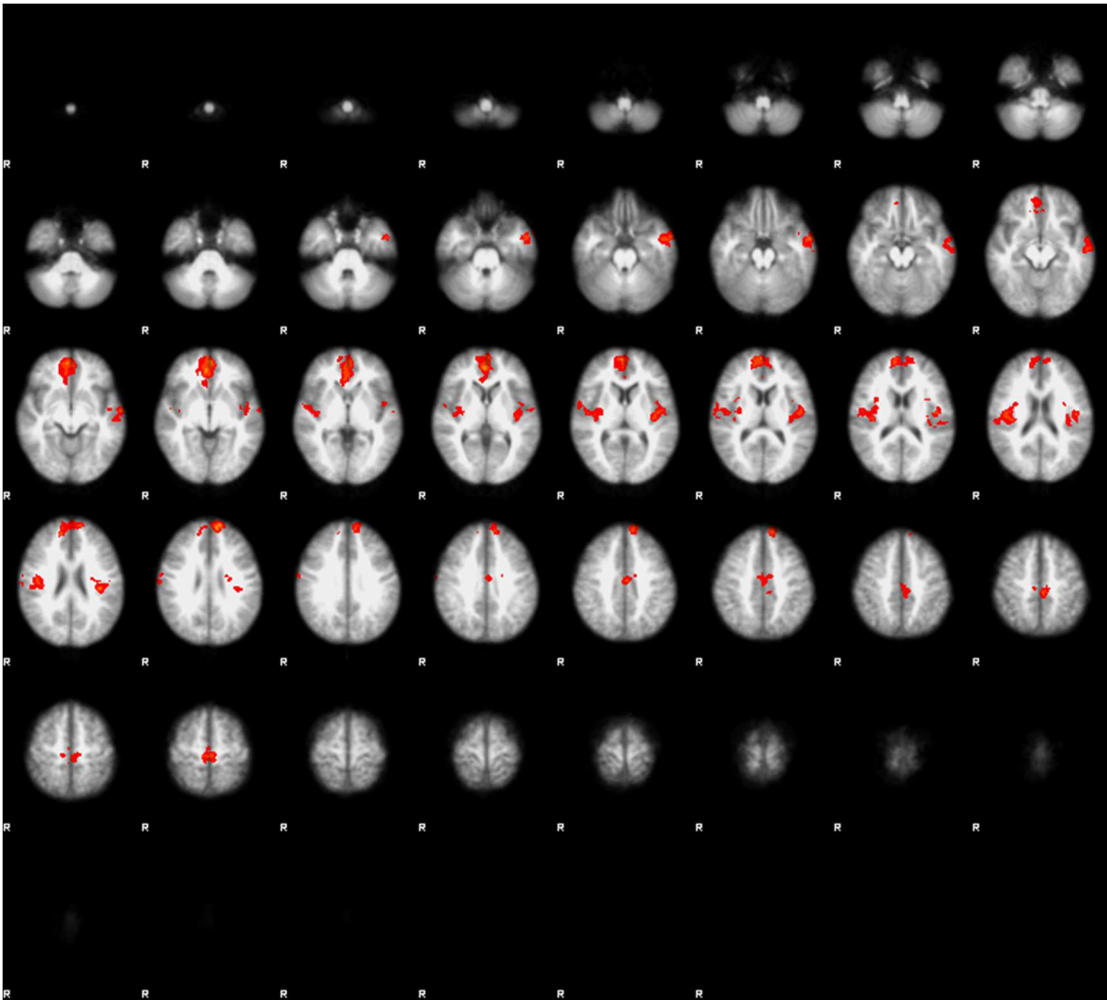


Figure 12. GLM analysis results of fMRI data as completed by FEAT: certain > uncertain, reflected in serial axial slices.

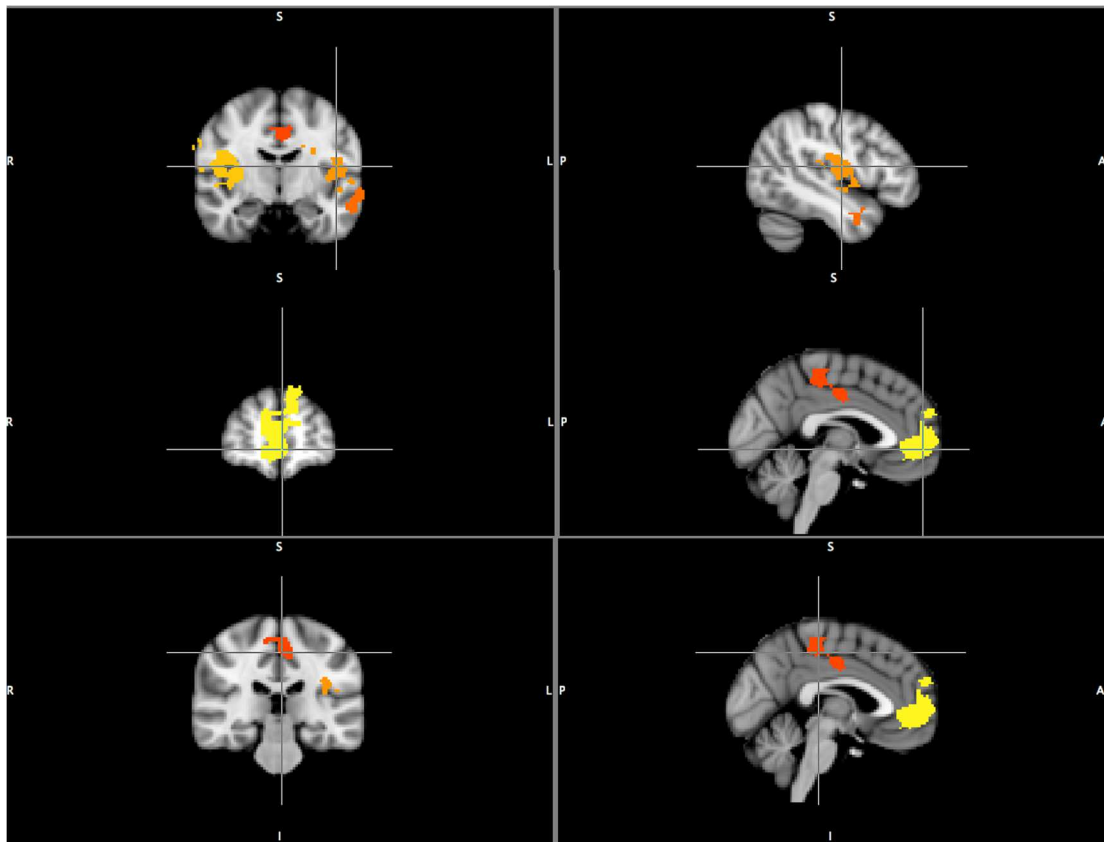


Figure 13. GLM analysis results of fMRI as completed by FEAT: certain > uncertain, reflected in coronal and sagittal slices.

Cluster Index	Voxels	p-value
1	1809	2.81e-8
2	13002	6.05e-43
3	16777	1.92e-40

Table 15. Clusters produced by FEAT analysis, Uncertain > Certain

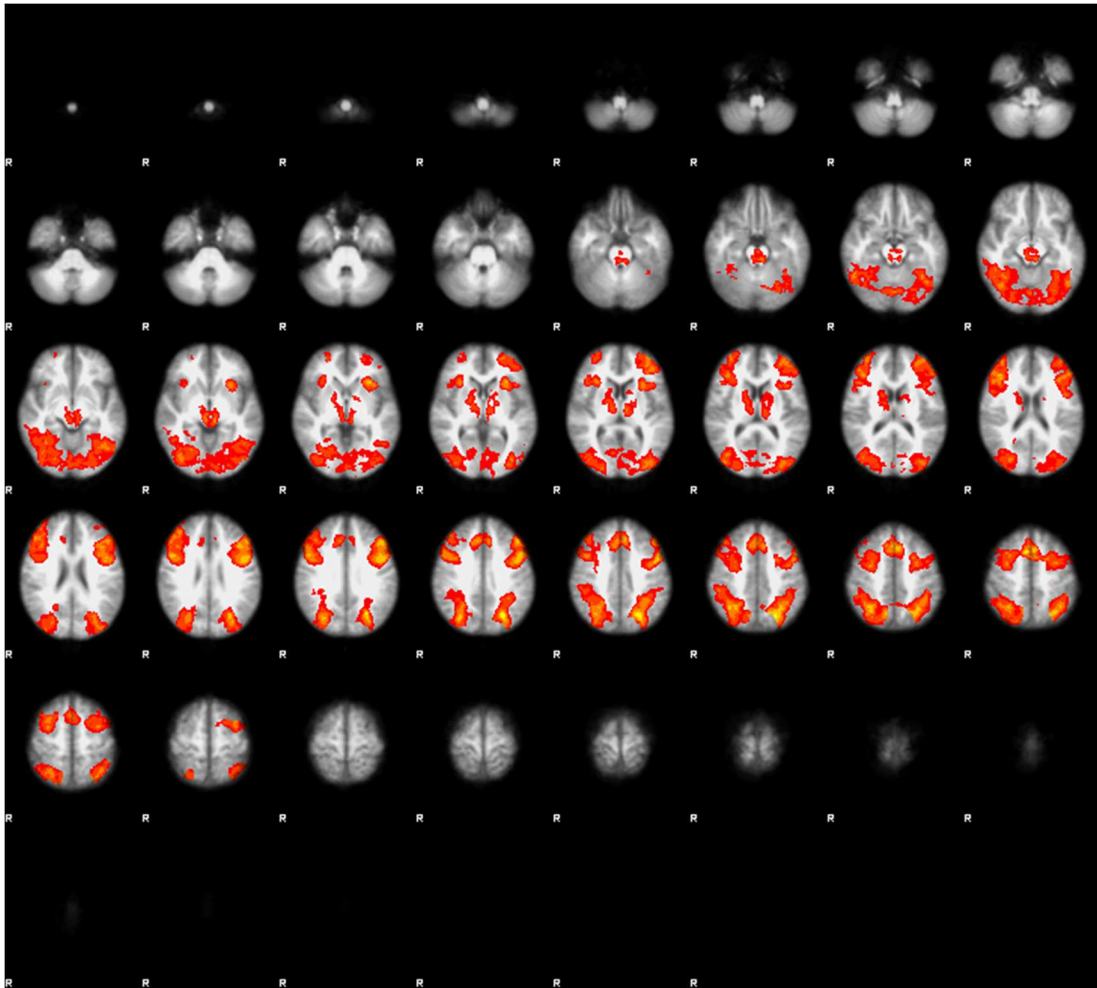


Figure 14. GLM analysis results of fMRI data as completed by FEAT: uncertain > certain, reflected in serial axial slices.

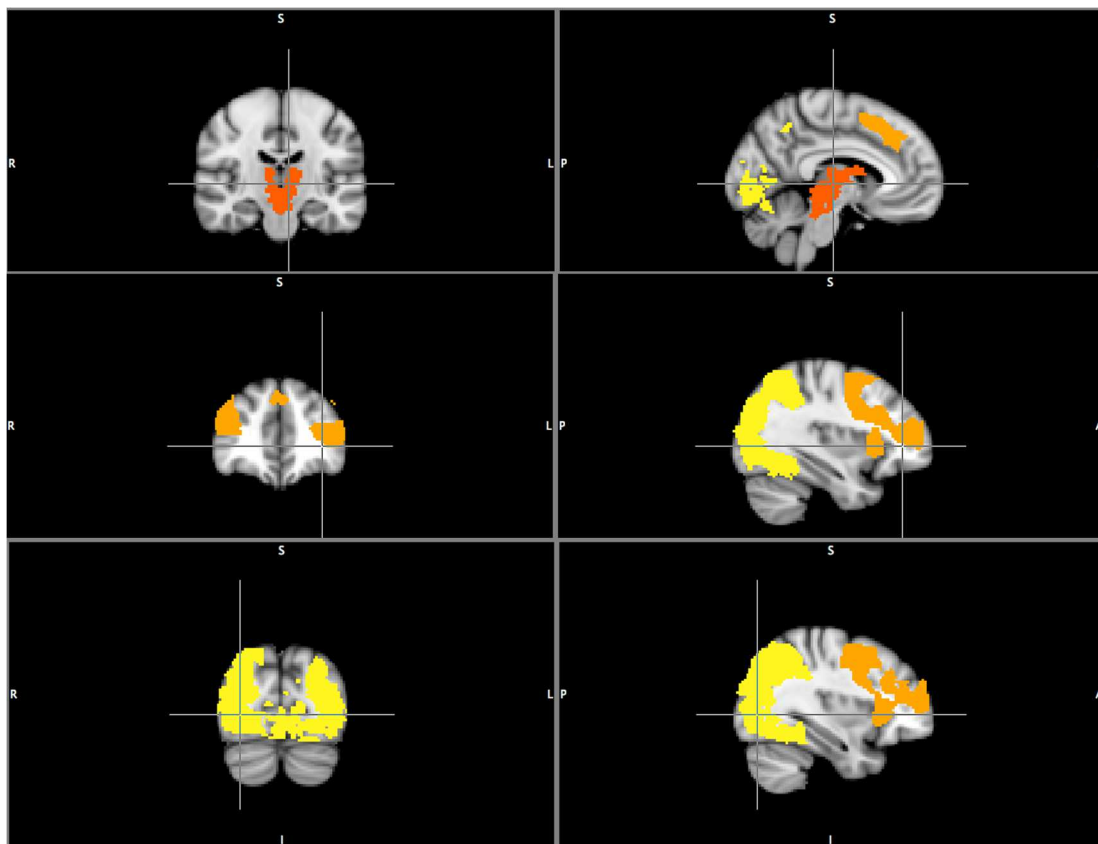


Figure 15. GLM analysis results of fMRI as completed by FEAT: uncertain > certain, reflected in coronal and sagittal slices.

### *Network Analysis*

Using a threshold of 0.4-0.9 for binary network measures, we found a number of differences that were consistent across thresholds. Network size was significant at all values with correction for multiple comparisons using the FDR method, except that at threshold 0.8 the network was larger for the certain condition (Table 16).

Threshold	Certain Mean	Uncertain Mean	P value
0.4	3335	3915	<0.0001
0.5	2279	2363	<0.0001
0.6	1367	1429	<0.0001
0.7	692	704	0.0052
0.8	281	269	0.0001

Table 16. Network size of fMRI networks, comparing certain versus uncertain conditions at varying thresholds.

Network density was significant for all p-values except 0.7 (Table 17), and assortativity was only significant at threshold 0.7 (Table 18).

Threshold	Certain Mean	Uncertain Mean	P value
0.4	0.56	0.57	0.0002
0.5	0.38	0.4	<0.0001
0.6	0.23	0.24	<0.0001
0.7	0.12	0.12	0.24
0.8	0.056	0.054	<0.0001

Table 17. Network density of fMRI networks, comparing certain versus uncertain conditions at varying thresholds.

Threshold	Certain Mean	Uncertain Mean	P value
0.4	0.0817	0.0728	0.14
0.5	0.15	0.15	0.27
0.6	0.23	0.22	0.18
<b>0.7</b>	<b>0.28</b>	<b>0.32</b>	<b>0.0031</b>
0.8	0.08	0.07	0.14

Table 18. Network assortativity of fMRI networks, comparing certain versus uncertain conditions at varying thresholds.

Weighted clustering coefficient showed significant difference for 15 ROIs where certain > uncertain, and 23 ROIs for uncertain > certain (Figure 16; Table 19).

ROI	Mean Certain	Mean Uncertain	p-value
Right Pallidum	0.41	0.40	0.0007
Left Caudal Middle Frontal	0.47	0.45	<0.0001
Left Frontal Pole	0.30	0.26	<0.0001
Left Fusiform	0.49	0.47	0.0001
Left Inferior Temporal	0.49	0.48	0.0021
Left Lateral Occipital	0.46	0.44	<0.0001
Left Lingual	0.48	0.47	0.0015
Left Medial Orbital Frontal	0.39	0.37	<0.0001
Left Rostral Anterior Cingulate	0.44	0.42	<0.0001
Left Transverse Temporal	0.45	0.44	0.0002
Right Entorhinal	0.31	0.29	0.003
Right Frontal Pole	0.33	0.29	<0.0001
Right Lateral Occipital	0.46	0.43	<0.0001
Right Lateral Orbitofrontal	0.41	0.39	<0.0001
Right Temporal Pole	0.31	0.27	<0.0001



Left Accumbens Area	0.36	0.38	0.001
Left Amygdala	0.37	0.39	<0.0001
Left Pallidum	0.38	0.39	<0.0001
Right Accumbens	0.30	0.31	<0.0001
Right Amygdala	0.28	0.30	<0.0001
Right Hippocampus	0.41	0.42	0.0005
Right Thalamus	0.51	0.53	0.0007
Left Cuneus	0.49	0.51	<0.0001
Left Inferior Parietal	0.50	0.52	<0.0001
Left Insula	0.48	0.50	<0.0001
Left Middle Temporal	0.48	0.49	0.0012
Left Parahippocampal	0.30	0.33	<0.0001
Left Pars Triangularis	0.45	0.46	0.0013
Left Precuneus	0.52	0.54	<0.0001
Left Superior Frontal	0.56	0.57	<0.0001
Left Supramarginal	0.53	0.54	0.0021
Left Temporal Pole	0.31	0.33	0.001
Right Caudal Anterior Cingulate	0.50	0.51	<0.0001
Right Isthmus Cingulate	0.48	0.50	0.0001
Right Parahippocampal	0.39	0.40	<0.0001
Right Precentral	0.53	0.54	0.0025
Right Precuneus	0.53	0.55	0.0001
Right Supramarginal	0.51	0.52	0.0002

**Table 19. Weighted Clustering Coefficient: nodes of significant difference between certain and uncertain condition.**

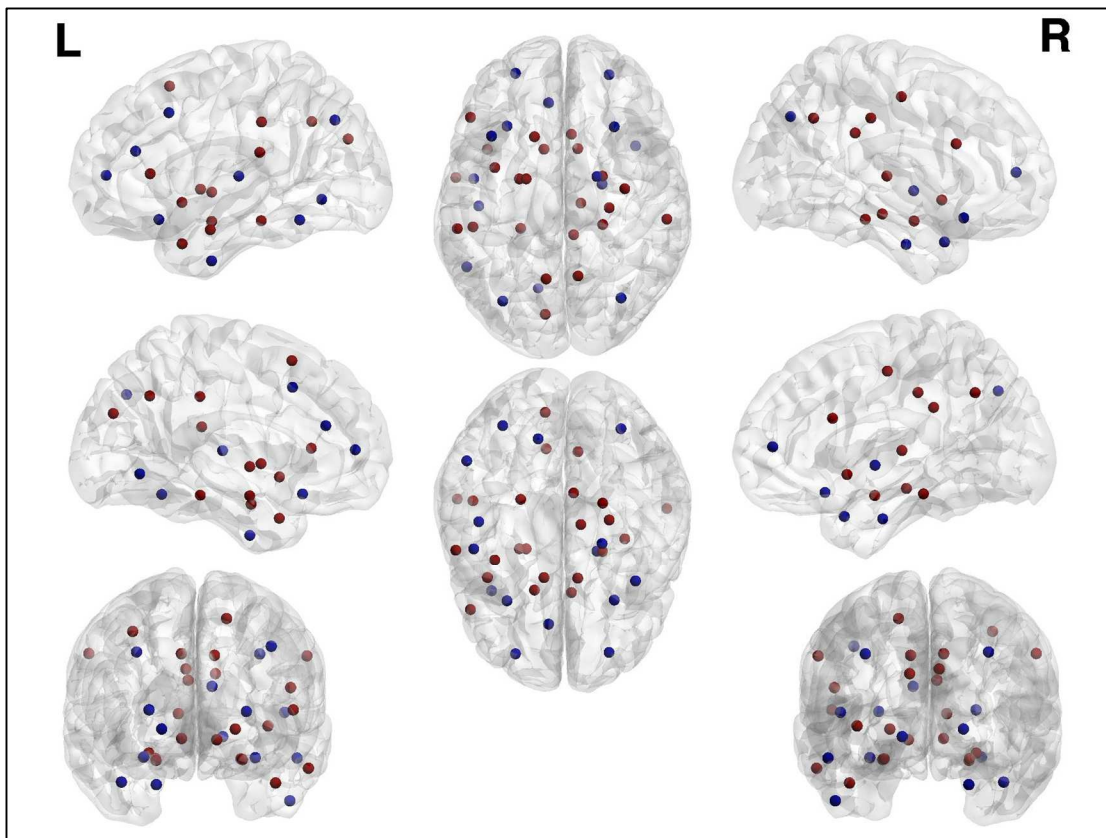


Figure 16. Node-based comparison of weighted clustering coefficient in fMRI network data, comparing certain and uncertain conditions. 6 nodes greater in certain condition in blue, 20 nodes greater in uncertain in red.

Node strength had 6 nodes significantly greater in the certain condition and 20 nodes significantly greater in the uncertain condition (Figure 17; Table 20).

ROI	Certain Mean	Uncertain Mean	P value
Right Pallidum	33.90	32.27	0.001
Left Frontal Pole	21.89	18.78	<0.0001
Left Lateral Occipital	40.74	39.06	0.0016
Left Medial Orbital Frontal	32.06	30.37	0.0015
Left Rostral Anterior Cingulate	37.54	35.49	0.0003
Left Transverse Temporal	38.23	36.63	0.0013
Right Frontal Pole	25.37	22.40	<0.0001
Right Lateral Occipital	40.48	38.71	0.0011
Right Lateral Orbitofrontal	33.61	31.87	0.0003
Right Temporal Pole	23.10	19.75	<0.0001
Left Amygdala	29.13	31.63	<0.0001

Left Pallidum	30.24	31.65	0.0044
Right Accumbens	22.76	24.23	0.0028
Right Amygdala	20.82	22.77	<0.0001
Right Hippocampus	33.89	35.54	0.0015
Left Cuneus	43.48	45.94	0.0002
Left Inferior Parietal	44.69	47.38	<0.0001
Left Insula	42.78	44.36	0.0032
Left Parahippocampal	22.15	24.91	<0.0001
Left Precuneus	47.76	50.39	<0.0001
Left Superior Frontal	52.10	54.23	0.0004
Left Temporal Pole	23.65	25.02	0.0018
Right Caudal Anterior Cingulate	44.54	46.45	0.001
Right Isthmus Cingulate	42.73	44.38	0.0021
Right Parahippocampal	30.92	32.48	0.0008
Right Precuneus	49.37	51.22	0.0016

**Table 20. Node strength: nodes of significant difference between certain and uncertain condition.**

The brain networks were visualized with the BrainNet Viewer

(<http://www.nitrc.org/projects/bnv/>; Xia et al., 2013).

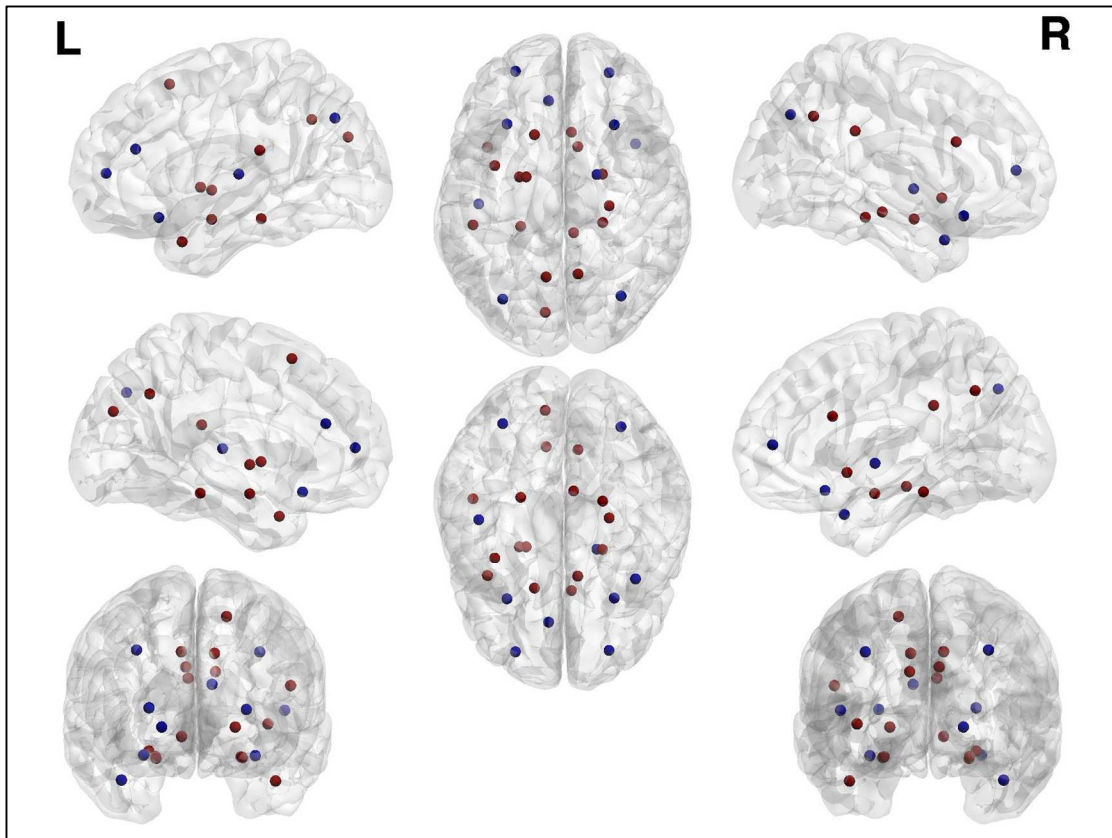


Figure 17. Node-based comparison of node strength in fMRI network data, comparing certain and uncertain conditions. 15 nodes greater in certain condition in blue, 23 nodes greater in uncertain condition in red.

## Discussion

The increased activity demonstrated in the uncertain condition when compared with the certain condition yielded by the GLM analysis corresponded to a larger network and many ROIs with greater connectivity, as indicated by clustering coefficient and node strength. However, a number of nodes showed greater clustering coefficients and node strengths in the certain condition, and some regional increases resulted from the GLM analysis.

Certainty is inherently desirable and uncertainty inherently aversive (Bach 2010; Reuman et al 2015; Zhang et al 2014). Therefore, even in our task with only the small gain or loss that coincides with feedback, we see activation in the reward circuits. During

the certain condition, we saw greater activation in some areas associated with reward, including the vmPFC and the OFC. The vmPFC has been found to be active in valuating reward (Daw and Doya 2006; Bengtson 2009). OFC activity has also been found to correlate with reward expectation (Kepecs 2008; Klein-Flugge 2013). We also found increased insula activation, which has been shown to be more active in a decision-making task with a certainty component (Bhanji et al 2010). We found ROI-based network measures that showed increased connectivity in the OFC, frontal ROIs, and temporal ROIs.

A meta-analysis conducted by White et al (2014) described that greater activation was observed in ACC, insula, and dlPFC and posterior parietal cortices in decision-making under uncertain conditions. We found some confirmation of the expected activation of brain regions under uncertain conditions, including activation of the ACC, the dlPFC, and the striatum. We expected to see ACC activation based on the research describing its role in conflict monitoring and anticipation (Botvinick 2007; Nieuwenhuys 2008 p390). The ACC is known to engage the dlPFC and contains many reciprocal connections; therefore we would expect to see increased activity of the dlPFC. Likewise, the executive loop of the basal ganglia involves the dlPFC (Nieuwenhuys 2008 p249). The striatum is involved with reward-based learning, although activation may correlate with punishment (Daw and Doya 2006; Stalnaker et al 2012; Samejima et al 2005). The computational model of decision-making developed by Bogacz and Tobias (2011) incorporates the cortex, the striatum, the subthalamic nucleus, and the thalamus.

A large increased parietal and occipital cluster of activation was shown in the uncertain condition. Activation of the posterior parietal cortex has been shown to vary as a function of uncertainty (Hutchinson 2015). In addition, the lateral intraparietal area has been shown to encode value for saccadic choices in primates (Kiani and Shadlen 2009; Beck et al 2008; Anderson and Cui 2009). This area corresponds to the ventral intraparietal area in humans (Nieuwenhuys 2008 p607). Therefore the activation may correlate with encoding the value of the choice involved.

Unexpectedly, strong midbrain activation was found in the uncertain condition. The midbrain has generally been found to be active in reward (Reuman et al 2015; Zhang et al 2014); however, there are substantial connections in the direct circuit of the basal ganglia, which involves the substantia nigra and the striatum (Nieuwenhuys 2008 p249). The direct circuit is a motor circuit, and it could be that greater motor control is required in this task because of the increased uncertainty. In addition, the increased activation of the occipital cortex in the uncertain condition was unexpected, given the equally visual nature of the certain and uncertain conditions. However, because of the increased attention likely involved in the uncertain component of the task, this may correspond to increased occipital activation.

ROIs reflecting greater network connectivity in the uncertain condition include the amygdala and hippocampus, as well as frontal and parietal regions that were discussed previously. The amygdala is thought to encode emotional valence (Berntson et al 2009; Styliadis et al 2013), and because uncertainty correlates to increased anxiety and worry (de Bruin, Rassin, Muris 2006; Rosen and Knauper 2009), this may correspond to

the negative emotions that occur during uncertainty. The hippocampus is generally active during memory tasks, and is also thought to help in valuating outcomes (Lebreton 2013). While this suggests a reward encoding, there are also substantial connections between the hippocampus and the amygdala (Nieuwenhuys 2008 p408), so it logically follows that if one is highly connected, the other will also be highly connected. In addition, because of the memory capabilities required to discard and update the rule choices in the uncertain condition, the coincident activation of the hippocampus is expected.

Taken together, these results reinforce many studies of decision-making under conditions of rule uncertainty versus rule certainty as well as include new information about the brain's behavior between these two conditions. The involvement of the insula, parietal cortex, temporal cortex, ventromedial cortex, and orbitofrontal cortex of the certain condition are generally associated with rule certainty and reward. The activation of areas related to reward reinforces the notion that certainty is inherently rewarding. The widespread activation in the uncertain condition included the prefrontal cortex, the striatum, the thalamus, the midbrain, the amygdala, the hippocampus, and the parietal cortex and occipital cortex. While the prefrontal cortex, parietal cortex, striatum, thalamus, amygdala and hippocampal involvement were expected, the occipital cortical involvement and the midbrain involvement were less expected. The increased involvement of these regions may be attributed to increased visual attention and increased motor control. Because the task involved in this study contains a binary condition with minimized outcome risk, this may explain these unexpected results.

Because we used a block design for our task, we could not separate the components of the task (i.e., performing the task and receiving feedback). Had we jittered the intervals at which our stimuli were presented, the separate analyses would have been possible. However, this would introduce an irregularity to the timing of our task that may have been disconcerting to subjects and introduced confounding variables. Therefore, this was the appropriate first experiment to complete. An event-related fMRI paradigm based on the current task would be an interesting next step and would allow us to resolve the task components even further.



## **CHAPTER 7: DECISION-MAKING UNDER UNCERTAIN CONDITIONS: A COHERENCE NETWORK ANALYSIS USING EEG**

### **Introduction**

As described in Chapters 4 and 5, many brain regions are involved in decision-making during rule uncertainty. Having already described the correlates of decision-making measured by fMRI using both GLM BOLD signal analysis and network analysis, as well as ERP analysis using EEG, we can now enhance the previous body of work with a network analysis of EEG data. Frequency based analyses can reveal much about brain function. This study builds on previous results by providing a description of frequencies, power, and network analysis of EEG electrodes in decision-making under uncertain conditions.

Starting with Berger's discovery in 1948 of EEG and a 10 Hz rhythm corresponding to relaxed wakefulness, activity at frequencies of interest are used to describe brain function (Gloor 1994). The EEG waveform is thought to contain superimposed waves at various frequencies that arise from cortical and subcortical neural generators (Pizzagalli 2006). The contribution of each frequency to the given waveform can be determined using a fast Fourier transformation (FFT) (Kramer 2013). Power is a measure that represents the square of the FFT. The most common frequency bands subject to EEG analysis include: delta (1:3 Hz), theta (4:7 Hz), alpha (8-12 Hz), and beta (13-30 Hz) (Pizzagalli 2006). Gamma analysis (> 30 Hz) is useful but difficult to detect from outside of the scalp; however, some researchers place the gamma band at > 20 Hz, which would include this experiment's high frequency beta band activity (Basar et al

2001; Logothetis 2008). The frequency bands of interest have emerged as rhythms that occur in common states. In this study, we examine low frequency alpha (8-10 Hz) and high frequency alpha (11-12 Hz) separately, as well as low frequency beta (13-17 Hz) and high frequency beta (18-30 Hz), as these bands can show differences in behavior from each other (Pizzagalli et al 2006).

Delta oscillations are associated with inhibition of activity, pathological states, or infancy (Pizzagalli 2006; Pizzagalli 2004). A diffuse increase in delta power has been associated with oddball responses in a p300 task (Basar Eroglu et al 1992). Beta oscillations are associated with greater cognitive effort, and diminish after task rehearsal (Vecchiato et al 2013) and in value-based decision-making (Polania et al 2014). Theta oscillations have been found to be involved in memory encoding in some studies (see Ward 2003), but has also been found to diminish in tasks with increased cognitive demand (Pandey et al 2015). Pizzagalli et al (2004) found correlation between theta rhythm and increased glucose uptake by the rostral anterior cingulate cortex; similarly, Cavanagh (2015) describes an increased midline theta oscillations associated with rostral anterior cingulate cortex activation in cognitive control. Cortical rhythms are thought to occur by cycles of neuronal activation from subcortical structures and cortical structures. A major contribution of the thalamus to the cortex is involved in theta rhythms for encoding of memory tasks and alpha rhythms for retrieval (Ward 2003; Klimesch 1999). Increased alpha power is generally associated with diminished signal in event related tasks (Pandey et al 2015; Pizzagalli 2006) and correlates with decreased activation in the superior temporal, inferior frontal, and cingulate cortices (Goldman et al 2002). This

suggests a diminished engagement of the uncertainty-related brain structures. However, some studies have shown increased alpha power during internally focused attention (Cooper et al 2003; Klimesch, Sauseng, Hanslmeyer 2007; Palva and Palva 2007).

Because the studies to date reflect disparate results, we expect to see differences between the conditions (certain versus uncertain, correct versus incorrect). We looked the two seconds post-stimulus in both conditions in order to capture the widespread effects of the stimuli and to represent the associated cognitive processes.

We not only used power analysis to look at power differences between the electrodes in the certain versus uncertain and correct versus incorrect states but we also established networks based on coherence between each pair of electrodes for the frequency bands of interest. Coherence can be a good approximation of connectivity between regions, as regions that oscillate in the same frequency likely have the same neural generators (Srinivasan et al 2007; Pizzagalli 2006; Gorisek et al 2015). We generated a network for each participant, within each frequency band of interest, and applied network measures on each of these networks. These measures describe the network, including how big it is, how efficiently it operates, and how each electrode behaves within the network.

## Methods

### *Analysis*

For task and electrophysiological setup, see chapter 5. Data were preprocessed using EMSE as described in chapter 5. Filtered data were exported and all subsequent analysis was conducted with MATLAB.

Analyses were grouped into certain versus uncertain conditions and correct versus incorrect conditions. Coherence between the two conditions and power spectral data for each condition were calculated using the Chronux 2.10 package ([chronux.org](http://chronux.org); Mitra and Bokil 2008). Power spectra data were averaged across trials for each participant within each condition. Taper calculations were set with a time-bandwidth product of 3 and a leading number of 5 tapers, in order to minimize rectangular windowing effects on the frequency data. Coherence matrices were generated between each pair of electrodes, for each frequency from 1-30 Hz, for each participant.

The 1-30 Hz frequency dataset was broken up into frequency bands of interest, and averaged within each band as follows: delta: 1-3 Hz, theta: 4-7 Hz, alpha1 (low frequency alpha): 8-9 Hz, alpha2 (high frequency alpha): 10-12 Hz, beta1 (low frequency beta): 13-17 Hz, beta2 (high frequency beta): 18-30 Hz. A matrix for each participant corresponding to each frequency band was used to represent a network. The edges between each pair of electrodes were represented by coherence measurements within each frequency band.

Network measures were calculated on each matrix. These were averaged across participants within a given condition for each frequency band. Network measures

included size, density (weighted and binary), cluster coefficient (weighted and binary), assortativity (weighted and binary), node degree, and node strength. For binary measures, thresholds were varied between 0.4 and 0.9. For weighted measures, a Fisher z-transformation was applied to the matrix to normalize the coherence values. Then, the measures were applied. The Brain Connectivity Toolbox (<https://sites.google.com/site/bctnet/>; Rubinov and Sporns 2011) was used to calculate all previous values except for matrix size, which was calculated using MATLAB functions.

Significance for network values was assessed using permutation testing. 10,000 random networks datasets (of 27 participants, two conditions) were generated by shuffling edges of coherence values for each frequency band. The network values were calculated on each generated dataset, and the false discovery rate method was used to correct for multiple-comparisons on node-based measures.

## **Results**

Power spectra values were increased in the certain versus uncertain conditions for all frequency bands, for most electrodes. Power spectra values for the certain condition are plotted in Figure 18, and values for the uncertain condition are plotted in Figure 19. ROIs of grouped electrodes (Figure 5) are used to compare the power spectra and are plotted in Figure 20.

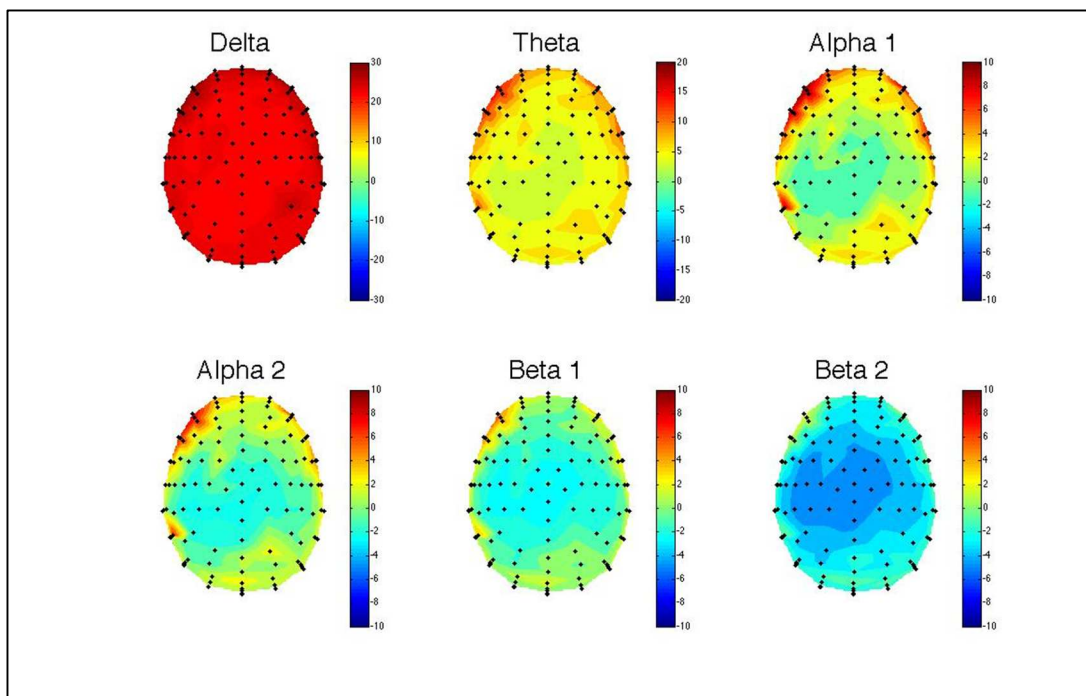


Figure 18. Scalp maps of EEG power spectral values at frequency bands of interest for the certain condition.

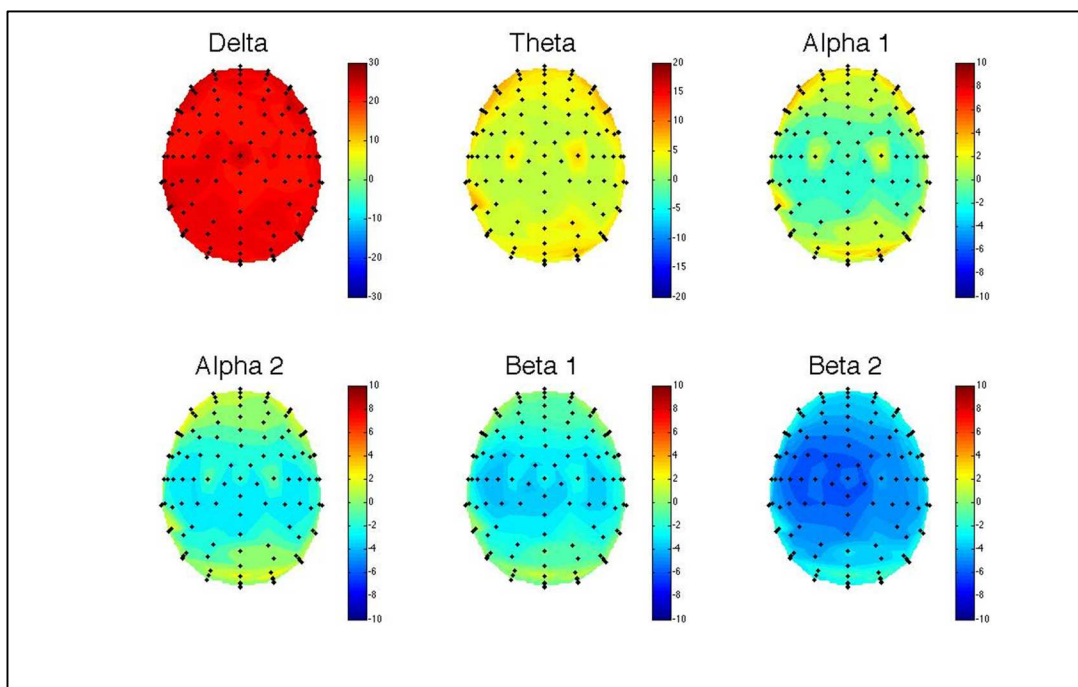


Figure 19. Scalp maps of power spectral values at frequency bands of interest for the uncertain condition.

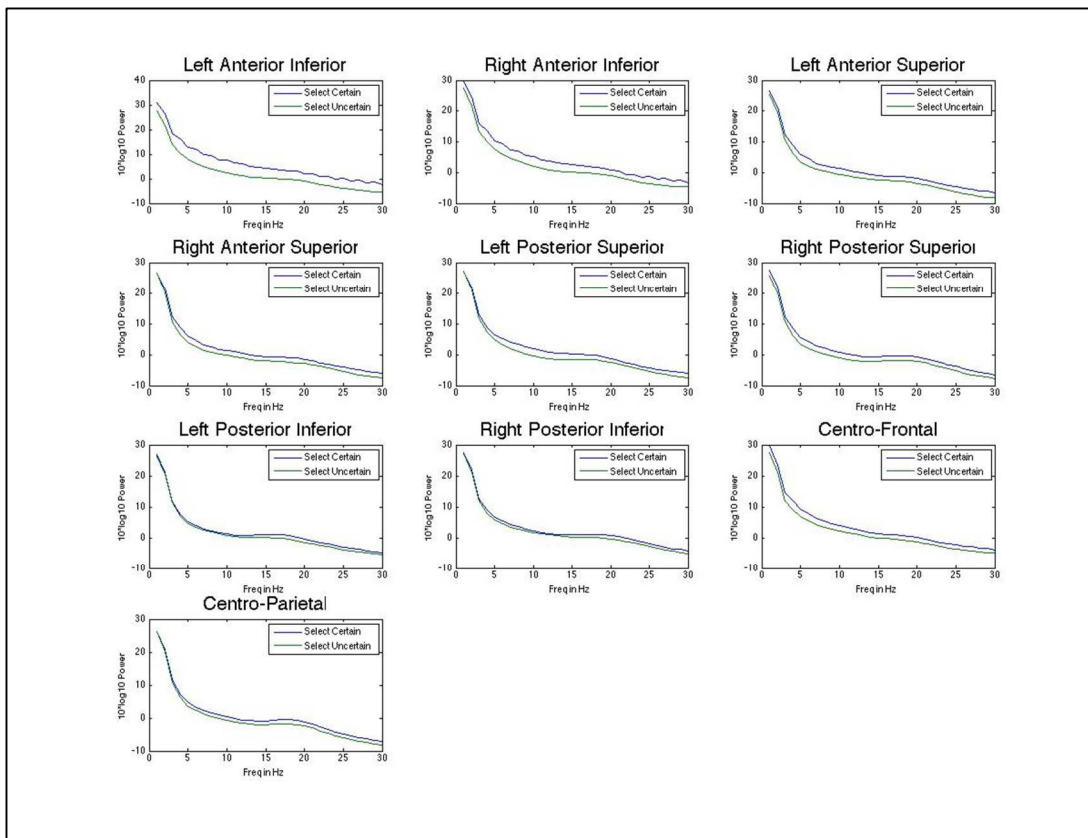


Figure 20. Power spectra in the 1-30 Hz range plotted for each ROI, comparing the certain and uncertain conditions.

Power spectra values are plotted for correct condition (Figure 21) versus incorrect condition (Figure 22).

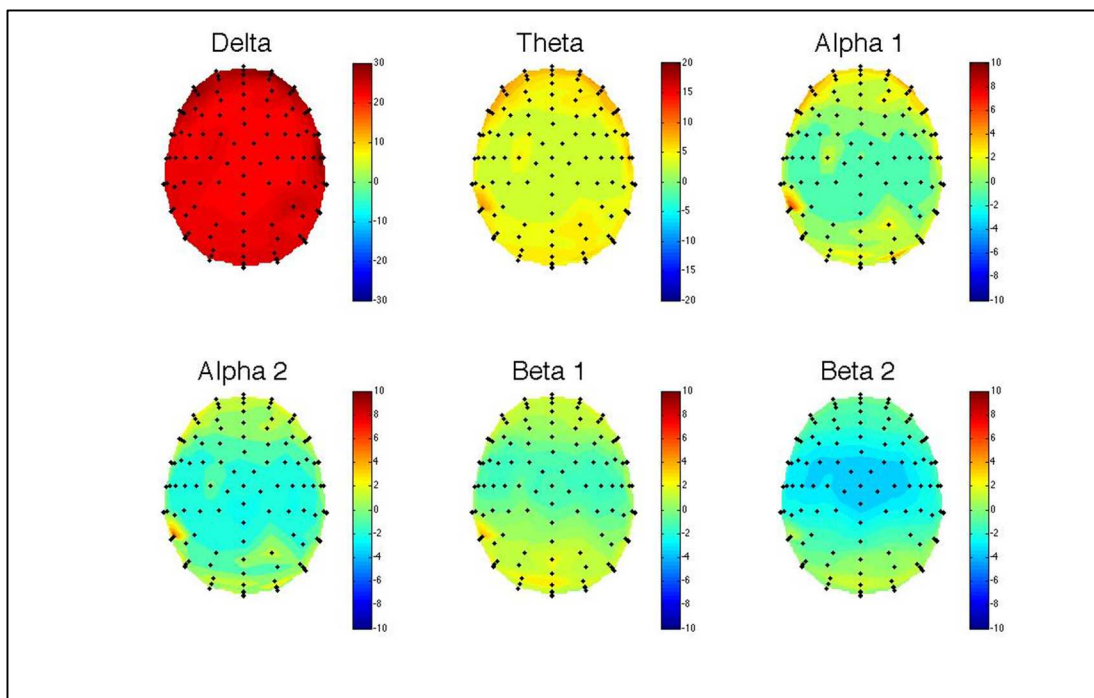


Figure 21. Scalp maps of EEG power spectral values at frequency bands of interest for the correct feedback.

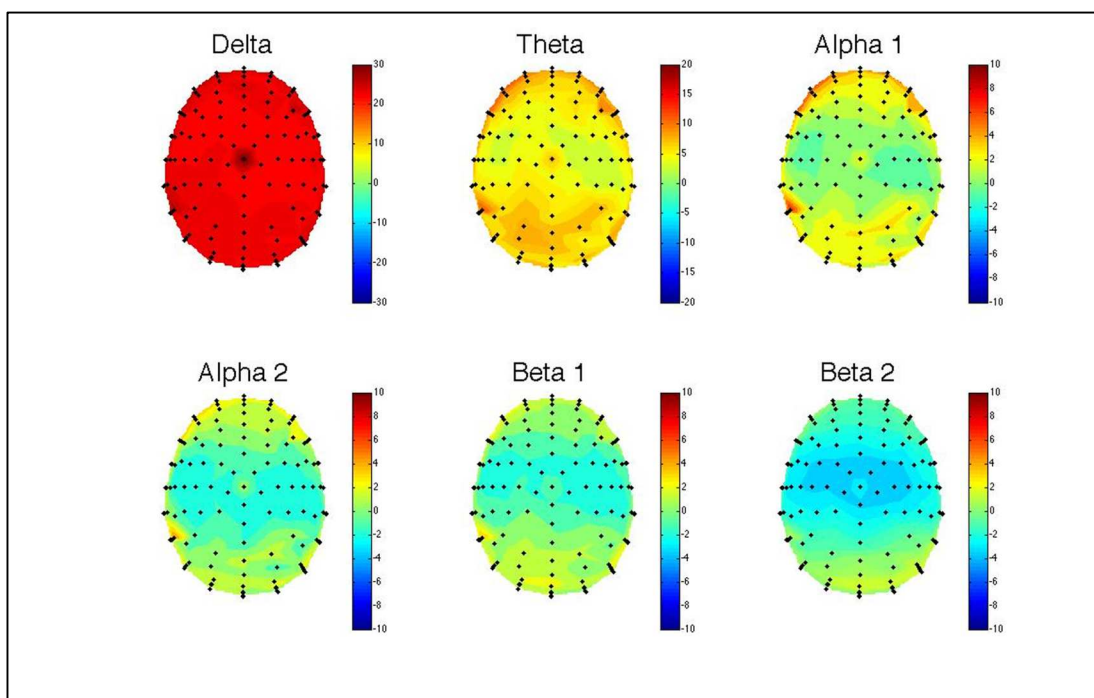
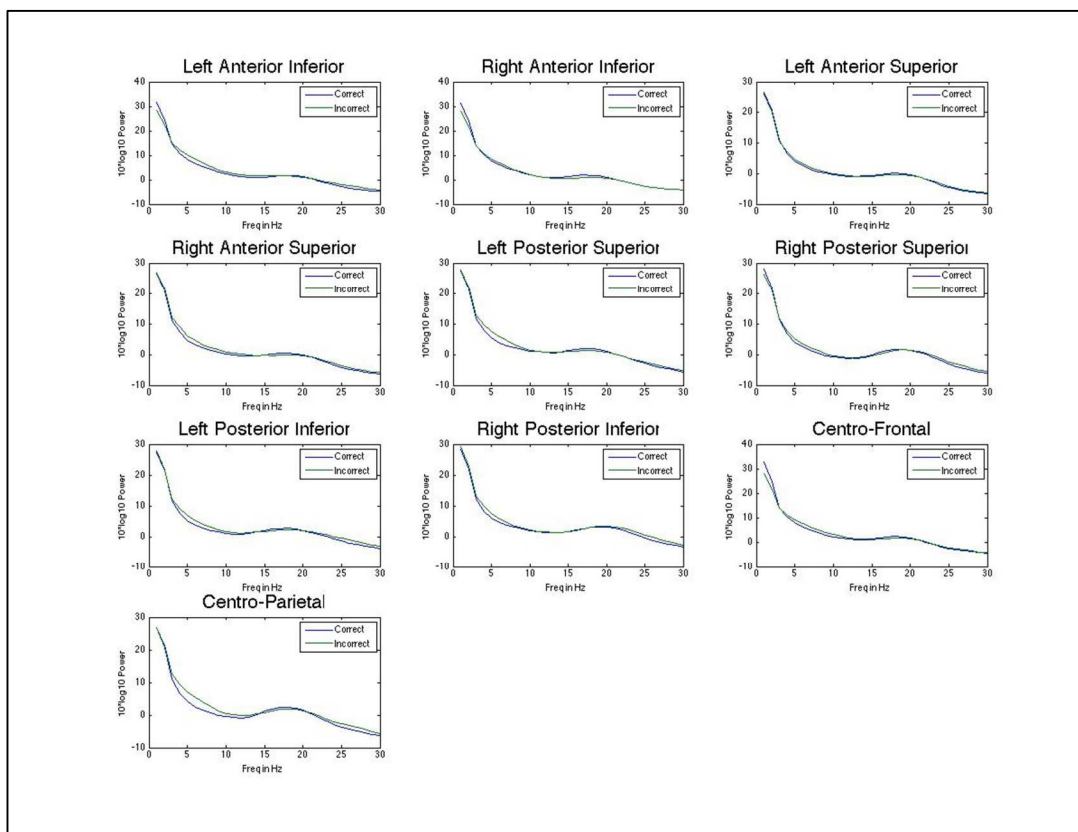


Figure 22. Scalp maps of power spectral values at frequency bands of interest for the incorrect feedback.



The power values associated with correct feedback are greater than those associated with incorrect feedback for the delta frequency (1-3) Hz, and incorrect power values are greater than correct power values for 4-12 Hz (theta, low and high frequency alpha bands) and for > 20 Hz (high frequency beta band) (see Figure 23).



**Figure 23.** EEG power spectra in the 1-30 Hz range plotted for each ROI, comparing the correct and incorrect conditions.

For the constructed coherence networks, the size of the network in certain versus uncertain conditions is displayed in Table 21. The networks show a greater number of connections reflecting higher coherence at every threshold 0.4 – 0.9 and in every frequency band.

Frequency band	Thresholds	Mean Size, Certain	Mean Size, Uncertain	p-value
Delta	0.4	7198.74	6806.59	<0.001
	0.5	5763.30	5295.11	<0.001
	0.6	4618.85	4053.22	<0.001
	0.7	3654.22	3037.52	<0.001
	0.8	2780.00	2118.74	<0.001
	0.9	1818.15	1252.44	<0.001
Theta	0.4	7683.15	7046.56	<0.001
	0.5	6054.78	5270.37	<0.001
	0.6	4454.22	3663.37	<0.001
	0.7	3092.74	2354.89	<0.001
	0.8	2000.07	1377.07	<0.001
	0.9	1009.78	626.89	<0.001
Alpha1	0.4	7398.19	6924.48	<0.001
	0.5	5659.52	5103.78	<0.001
	0.6	4043.96	3431.85	<0.001
	0.7	2624.56	2068.15	<0.001
	0.8	1625.81	1209.96	<0.001
	0.9	806.63	562.41	<0.001
Alpha2	0.4	7441.11	6932.11	<0.001
	0.5	5635.44	5121.37	<0.001
	0.6	3960.52	3424.48	<0.001
	0.7	2550.56	2075.89	<0.001
	0.8	1550.22	1196.00	<0.001
	0.9	742.41	548.44	<0.001
Beta1	0.4	7210.56	6827.26	<0.001
	0.5	5317.93	4959.04	<0.001
	0.6	3628.37	3283.93	<0.001
	0.7	2306.63	1985.67	<0.001
	0.8	1379.37	1129.70	<0.001
	0.9	649.44	526.59	<0.001
Beta2	0.4	6873.89	6371.15	<0.001
	0.5	4894.11	4420.07	<0.001
	0.6	3208.44	2817.19	<0.001
	0.7	2021.26	1750.41	<0.001
	0.8	1229.41	1048.15	<0.001
	0.9	545.11	471.70	<0.001

**Table 21.** Size of EEG network for certain versus uncertain conditions at varying thresholds and frequency bands.

Frequency Band	Threshold	Certain density mean	Uncertain density mean	p-value
Delta	0.4	0.5001	0.4754	<0.001
	0.5	0.4027	0.3723	<0.001
	0.6	0.3245	0.2883	<0.001
	0.7	0.2583	0.2191	<0.001
	0.8	0.1981	0.1539	<0.001
	0.9	0.1303	0.0930	<0.001
Theta	0.4	0.5284	0.4844	<0.001
	0.5	0.4182	0.3650	<0.001
	0.6	0.3103	0.2570	<0.001
	0.7	0.2175	0.1683	<0.001
	0.8	0.1426	0.1018	<0.001
	0.9	0.0746	0.0503	<0.001
Alpha1	0.4	0.5103	0.4783	<0.001
	0.5	0.3928	0.3555	<0.001
	0.6	0.2832	0.2426	<0.001
	0.7	0.1867	0.1497	<0.001
	0.8	0.1177	0.0909	<0.001
	0.9	0.0612	0.0462	<0.001
Alpha2	0.4	0.5142	0.4802	<0.001
	0.5	0.3918	0.3580	<0.001
	0.6	0.2782	0.2432	<0.001
	0.7	0.1823	0.1507	<0.001
	0.8	0.1127	0.0902	<0.001
	0.9	0.0573	0.0455	<0.001
Beta1	0.4	0.4972	0.4721	<0.001
	0.5	0.3687	0.3460	<0.001
	0.6	0.2540	0.2326	<0.001
	0.7	0.1642	0.1442	<0.001
	0.8	0.1007	0.0849	<0.001
	0.9	0.0513	0.0439	<0.001
Beta2	0.4	0.4735	0.4403	<0.001
	0.5	0.3398	0.3091	<0.001
	0.6	0.2255	0.2009	<0.001
	0.7	0.1445	0.1279	<0.001
	0.8	0.0909	0.0796	<0.001

**Table 22. Certain versus uncertain EEG network density at varying thresholds and frequency bands.**

Frequency band	Threshold	Mean Certain Assortativity	Mean Uncertain Assortativity	p-value
Delta	0.4	0.2372	0.2189	<0.001
	0.5	0.3310	0.3028	<0.001
	0.6	0.3796	0.3530	<0.001
	0.7	0.4144	0.4283	.092
	0.8	0.5363	0.5713	<0.001
	0.9	NaN	NaN	<0.001
Theta	0.4	0.2270	0.2212	0.066
	0.5	0.3194	0.3214	0.523
	0.6	0.4165	0.4245	0.794
	0.7	0.4947	0.5080	0.838
	0.8	0.5828	0.5961	0.753
	0.9	0.6660	0.7109	.008
Alpha1	0.4	0.2589	0.2703	.01
	0.5	0.3576	0.3701	0.986
	0.6	0.4619	0.4470	0.003
	0.7	0.4951	0.5203	.016
	0.8	0.5928	0.6112	0.795
	0.9	0.6965	0.7484	.007
Alpha2	0.4	0.2778	0.2949	0.001
	0.5	0.3721	0.3879	0.001
	0.6	0.4725	0.4789	0.701
	0.7	0.5098	0.5357	0.008
	0.8	0.5996	0.6015	0.381
	0.9	0.7153	0.7391	0.848
Beta1	0.4	0.2809	0.3018	<0.001
	0.5	0.3835	0.4032	0.001
	0.6	0.4781	0.4775	0.331
	0.7	0.5290	0.5171	0.07
	0.8	0.5972	0.5935	0.267
	0.9	0.7070	0.7398	0.073
Beta2	0.4	0.2788	0.2757	0.113
	0.5	0.3657	0.3679	0.471
	0.6	0.4557	0.4330	0
	0.7	0.5310	0.5043	0.003
	0.8	0.5732	0.5998	0.048
	0.9	0.7685	0.7976	0.013

Table 23. Certain versus uncertain EEG network assortativity at different frequency bands and thresholds.

Frequency band	Threshold	Correct Mean Size	Incorrect Mean Size	p-value
Delta	0.4	6868.44	7095.44	<0.001
	0.5	5450.44	5484.22	0.002
	0.6	4356.96	4222.89	<0.001
	0.7	3442.11	3174.85	<0.001
	0.8	2663.59	2160.52	<0.001
	0.9	1845.22	1203.74	<0.001
Theta	0.4	7599.56	7714.00	<0.001
	0.5	5923.07	6083.74	<0.001
	0.6	4337.44	4513.59	<0.001
	0.7	2922.74	3073.33	<0.001
	0.8	1812.30	1856.00	<0.001
	0.9	826.74	871.48	<0.001
Alpha1	0.4	7515.70	7574.70	<0.001
	0.5	5712.78	5829.52	<0.001
	0.6	3990.52	4163.19	<0.001
	0.7	2526.00	2670.56	<0.001
	0.8	1461.33	1551.74	<0.001
	0.9	660.44	694.11	<0.001
Alpha2	0.4	7488.41	7515.85	0.006
	0.5	5643.00	5721.26	<0.001
	0.6	3887.48	3981.81	<0.001
	0.7	2396.78	2503.33	<0.001
	0.8	1334.26	1397.33	<0.001
	0.9	610.96	632.22	<0.001
Beta1	0.4	7255.59	7214.41	<0.001
	0.5	5421.52	5417.67	0.354
	0.6	3772.30	3755.48	0.021
	0.7	2321.59	2337.78	0.989
	0.8	1310.26	1308.56	0.376
	0.9	606.59	588.78	<0.001
Beta2	0.4	7189.19	7301.85	<0.001
	0.5	5227.30	5339.85	<0.001
	0.6	3493.44	3614.26	<0.001
	0.7	2126.04	2204.41	<0.001
	0.8	1214.37	1238.44	<0.001
	0.9	538.26	537.22	0.402

Table 24. Correct versus incorrect EEG network size at varying frequency bands and thresholds

Frequency band	Threshold	Density	Density	P-value
Delta	0.4	0.4778	0.4957	0
	0.5	0.3818	0.3864	0.744
	0.6	0.3073	0.3003	0
	0.7	0.2444	0.2283	0
	0.8	0.1903	0.1578	0
	0.9	0.1325	0.0910	0
Theta	0.4	0.5231	0.5314	0.002
	0.5	0.4095	0.4215	0
	0.6	0.3035	0.3156	0
	0.7	0.2073	0.2186	0
	0.8	0.1318	0.1355	0.753
	0.9	0.0637	0.0682	0
Alpha1	0.4	0.5188	0.5230	0.351
	0.5	0.3970	0.4054	0
	0.6	0.2806	0.2931	0
	0.7	0.1810	0.1914	0
	0.8	0.1077	0.1147	0
	0.9	0.0525	0.0558	0.002
Alpha2	0.4	0.5177	0.5198	0.016
	0.5	0.3929	0.3989	0.841
	0.6	0.2744	0.2820	0.003
	0.7	0.1731	0.1809	1
	0.8	0.0993	0.1044	0.001
	0.9	0.0495	0.0517	0.833
Beta1	0.4	0.5007	0.4985	0
	0.5	0.3762	0.3769	0
	0.6	0.2642	0.2646	0
	0.7	0.1657	0.1682	0.037
	0.8	0.0968	0.0976	0
	0.9	0.0489	0.0485	0
Beta2	0.4	0.4939	0.5031	0
	0.5	0.3611	0.3700	0
	0.6	0.2444	0.2534	0
	0.7	0.1514	0.1574	0.005
	0.8	0.0894	0.0910	0.025
	0.9	0.0443	0.0445	0

Table 25. Correct versus incorrect EEG network density at varying thresholds and frequency bands

Frequency Band	Threshold	Mean Assortativity Correct	Mean Assortativity Incorrect	p-value
Delta	0.4	0.2284	0.2162	0
	0.5	0.3137	0.2594	0
	0.6	0.3805	0.3362	0
	0.7	0.4349	0.4346	0.225
	0.8	0.5691	0.5305	0
	0.9	NaN	NaN	0
Theta	0.4	0.2275	0.2473	0
	0.5	0.3230	0.3370	0.008
	0.6	0.4075	0.4311	0.001
	0.7	0.4853	0.4755	0.082
	0.8	0.5806	0.5541	0.006
	0.9	0.7273	0.7184	0.215
Alpha1	0.4	0.2565	0.2917	0
	0.5	0.3498	0.3658	0.001
	0.6	0.4525	0.4483	0.108
	0.7	0.5140	0.4923	0.003
	0.8	0.6338	0.5995	0.001
	0.9	0.7298	0.7395	0.553
Alpha2	0.4	0.2767	0.2977	0
	0.5	0.3788	0.3878	0.926
	0.6	0.4712	0.4700	0.185
	0.7	0.5218	0.5362	0.87
	0.8	0.6196	0.6244	0.422
	0.9	0.7102	0.7343	0.806
Beta1	0.4	0.2751	0.3034	0
	0.5	0.3809	0.4117	0
	0.6	0.4674	0.4924	0
	0.7	0.5323	0.5529	0.024
	0.8	0.6147	0.6168	0.396
	0.9	0.7262	0.7234	0.33
Beta2	0.4	0.2707	0.2585	0
	0.5	0.3661	0.3624	0.037
	0.6	0.4572	0.4529	0.061
	0.7	0.5376	0.5307	0.062
	0.8	0.5969	0.6053	0.626
	0.9	0.7134	0.7097	0.314

**Table 26. Correct versus incorrect EEG network assortativity at varying thresholds and frequencies.**

Similarly, network density shows a significantly higher value in the certain versus uncertain condition at every threshold 0.4-0.9 and in every frequency band (Table 23). In the delta band, the certain assortativity is significantly greater than the uncertain assortativity, but the other frequency bands reflect inconsistent differences and significance (Table 24). The size of the network in the correct versus incorrect varies by frequency band (Table 25). At thresholds 0.4 and 0.5, it is larger for the incorrect condition and from thresholds 0.6-0.9 it is larger for the correct condition. All p-values for these comparisons are significant. For the theta, low frequency alpha and high frequency alpha bands, the incorrect network size is significantly larger. The correct condition is significantly larger in the low frequency beta band except for at threshold 0.7. The incorrect condition is significantly larger for the low beta frequency band for all thresholds except 0.9. Network density follows this trend but there is less consistency across the thresholds (Table 26). Density is higher in the correct condition for the delta and beta1 frequencies for most thresholds, and density is higher in the incorrect condition for the theta, alpha 1, alpha 2, and beta 2 frequency bands.

Assortativity is higher for the correct condition in the delta frequency band, and higher for the incorrect condition in the beta frequency band thresholds 0.4-0.7.

For node-based weighted measures, such as strength and cluster coefficient, the certain condition shows significantly greater means in a number of nodes (Figures 24 and 25).



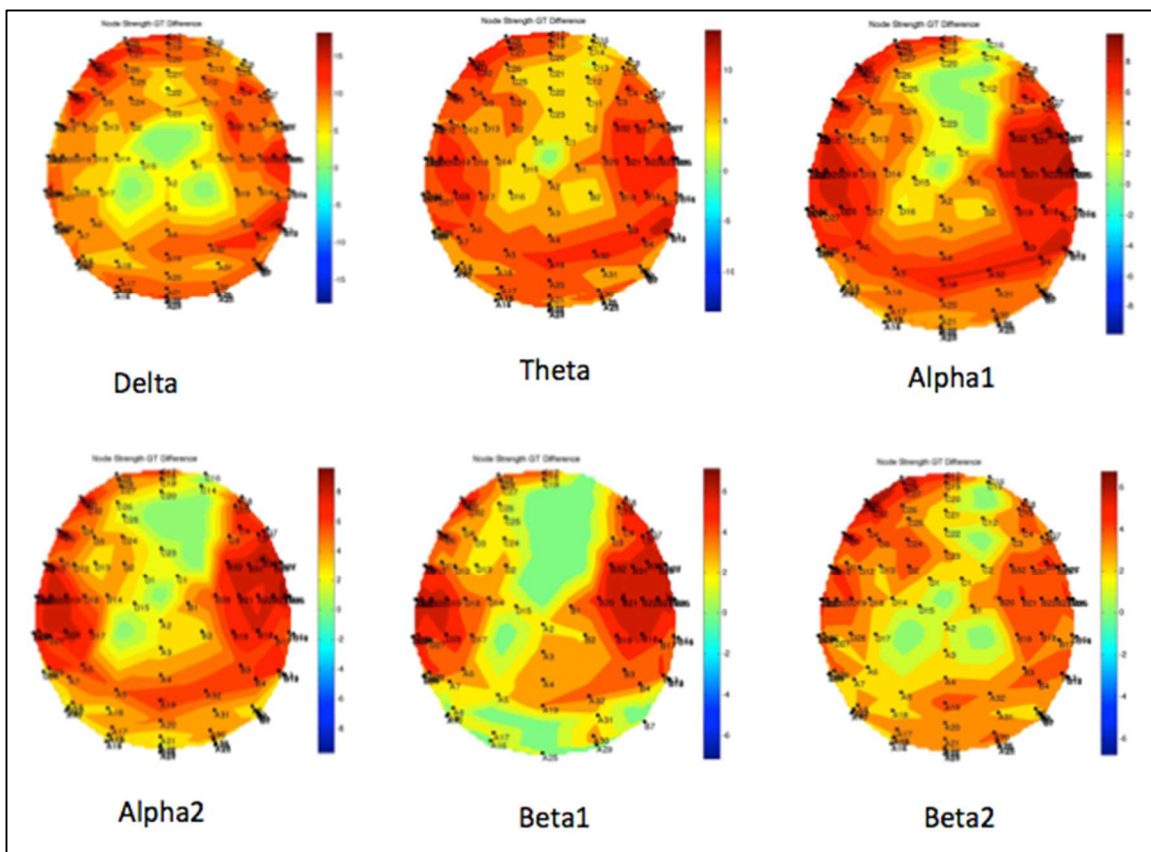
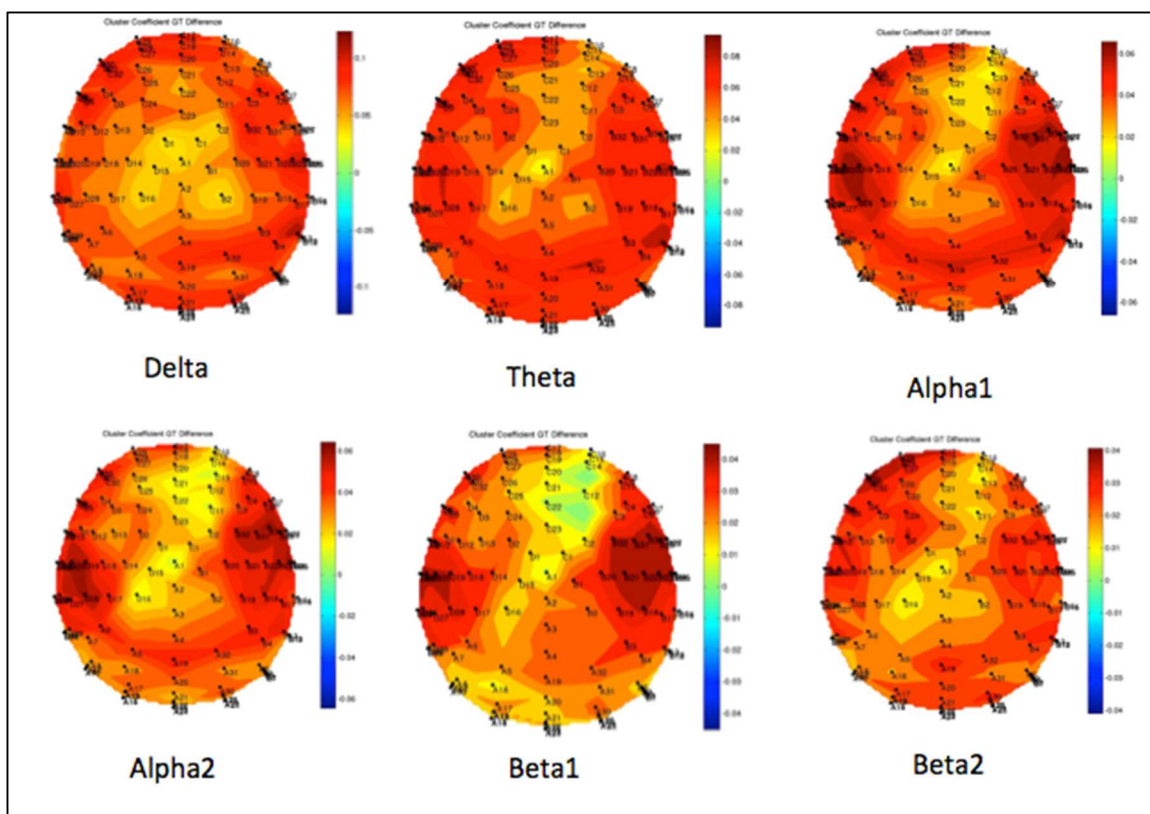


Figure 24. Node strength for certain > uncertain condition for the EEG frequency bands of interest. Green areas with unlabeled electrodes represent no significant difference.



**Figure 25.** Cluster coefficient for certain > uncertain condition for the EEG frequency bands of interest. Green areas with unlabeled electrodes represent no significant difference.

Most of the significance is lost in all frequency bands in the central region; in low frequency alpha, high frequency alpha, and low frequency beta, this lack of significant difference extends to the frontal region (Figure 24). The certain condition network has stronger cluster coefficient at most nodes in all frequencies bands (Figure 25).

Comparing the correct feedback network versus the incorrect feedback network shows limited increased strength in a few states (Figure 26). Delta coherence strength around the periphery of the scalp reflects a prominent difference, with little significant difference in the midline/center of the scalp. This suggests frontal, temporal, and occipital cortical differences are occurring in the delta frequency band. The incorrect network node strength is increased over the correct network node strength in a collection

of central electrodes (Figure 27). These differences are most pronounced in the central/parietal region, with some temporal involvement. There is greater involvement on the left than the right. The cluster coefficient is increased in the delta frequency band of the correct coherence network, with very few differences in the rest of the frequency bands (Figure 28). The cluster coefficient of the incorrect coherence network is increased in numerous electrodes of the theta, low and high frequency alpha, and low and high frequency beta networks. These differences are most prominently seen over the central midline of the scalp, but they are more posterior than the corresponding node strength differences.

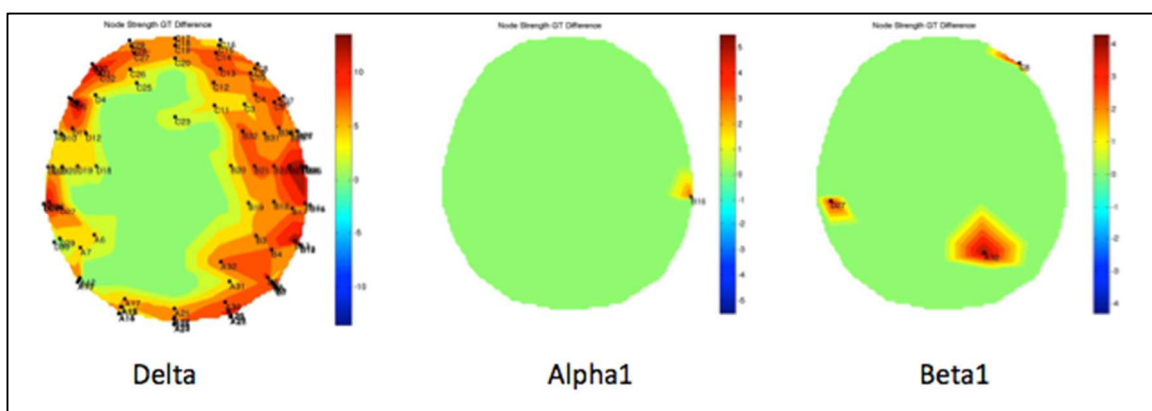


**Figure 26.** Electrodes reflecting increased node strength for the correct condition over the incorrect condition for the EEG network analysis.

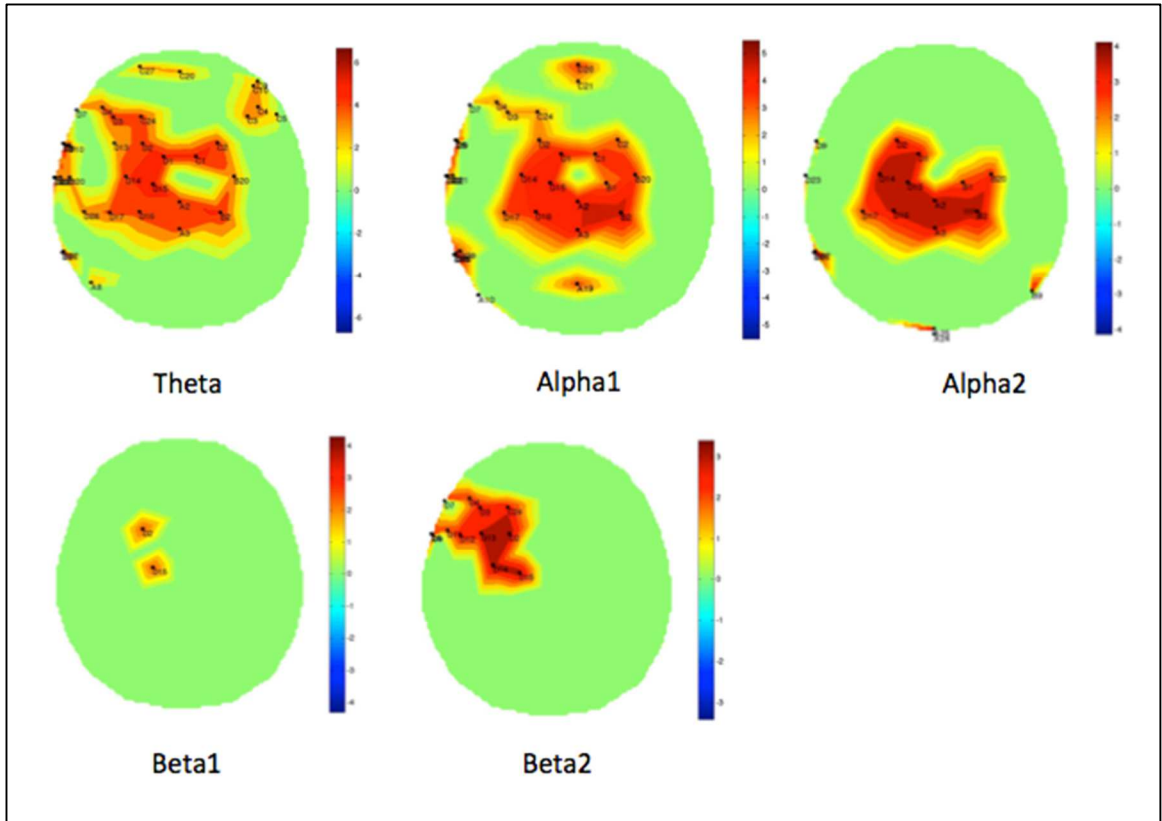


Figure 27. Electrodes reflecting increased node strength for the incorrect condition over the correct condition for the EEG network analysis.

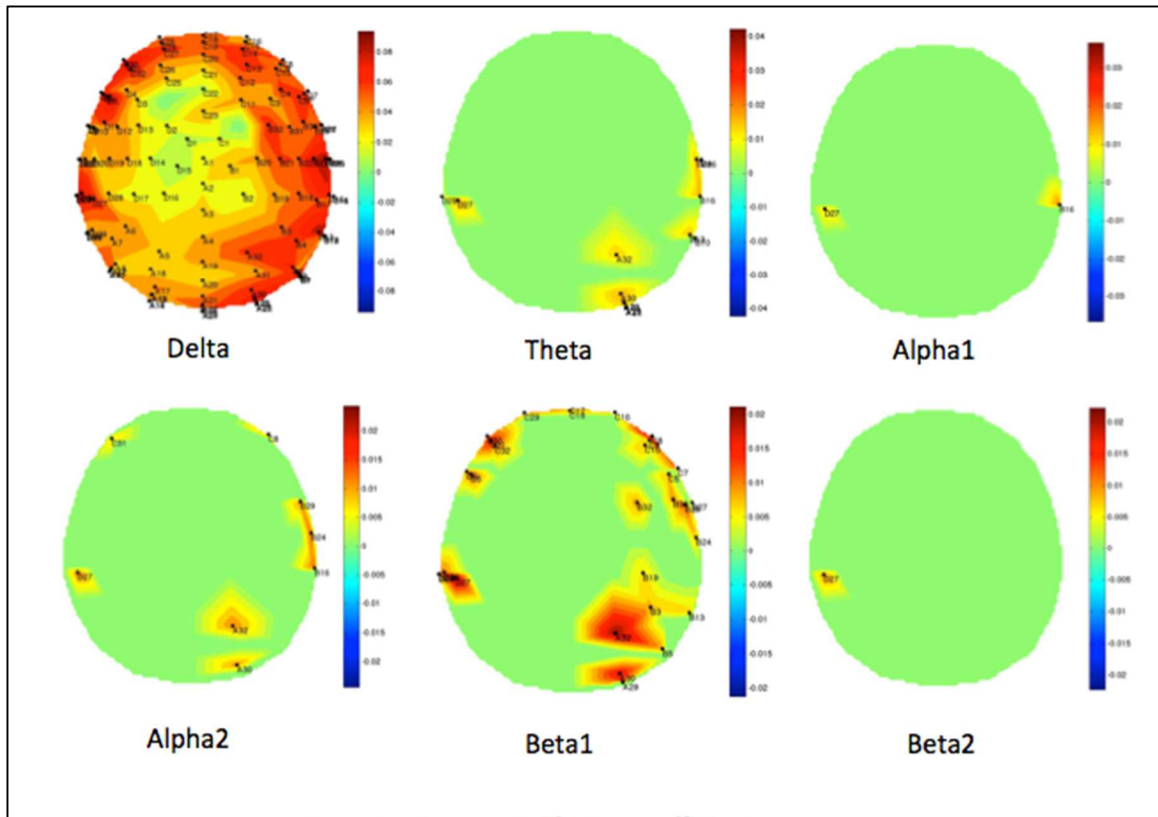


Figure 28. Electrodes reflecting increased cluster coefficient for the incorrect condition over the correct condition for the EEG network analysis.

## Discussion

Our results reflect an overall greater power in all frequency bands in the certain over the uncertain condition, and a greater measure of all network coherence values. This suggests that the level of connectivity is high in the certain condition, and that desynchronization is occurring in the uncertain condition. Given that results reflected in chapter six suggest desynchronization in the uncertain condition in the fMRI network, and temporally focused increases in potentials in the uncertain condition at various intervals post stimulus in chapter five, this is unsurprising. The increased theta power in

the incorrect feedback interval is similar to that found in other uncertainty studies (Cavanagh 2014; Cohen 2007). Increased theta power has been attributed to encoding in memory (Ward 2003) and has been found to correlate with increased activation in the superior frontal gyrus, the inferior frontal gyrus, the inferior parietal lobule, and the inferior temporal gyrus (O’Gorman et al 2013). These regions are associated with memory and executive behavior that aligns with the memory-updating theory. It follows that when receiving incorrect feedback, this causes the individual to update a mental schema that held the potential rule. Increased theta activity in the incorrect condition is found not only in absolute increase but also in network size, cluster coefficient, and node strength of many nodes. The electrodes of significance of the theta band are mostly in the frontal midline with some left frontal involvement. This supports the notion of mental updating in midline frontal cortical structures.

Differences in delta networks in the correct versus incorrect state are minimal. The network size is bigger in the incorrect state at low thresholds, and bigger in the correct state at higher thresholds. This suggests an inconsistency in this measure across thresholds, which diminishes the significance of the results and makes them more difficult to interpret. Node-based measures of node strength show many electrodes that are strengthened in the correct condition. Because delta oscillations correspond to a slow-wave process thought to be inhibitory (Pizzagalli 2006), this may be related to inhibition of cognitive processes in the prevention of updating the mental schema associated with rule updating. Brain regional activation that correlates negatively with increased delta activity includes the cingulate cortex, the middle frontal gyrus, and the

superior temporal gyrus (O’Gorman 2013). The cingulate cortex is involved in error anticipation (Botvinick 2007) and the middle frontal and superior temporal gyri are involved in memory updating, so it follows that the suppression of activation of these structures may be occurring with the increased delta oscillations in specific regions of the brain during the correct feedback.

Interestingly, there was significant difference in both alpha bands in the incorrect > correct condition. Alpha is typically thought of as a frequency band predominant at rest (Pizzagalli 2006), however, during the incorrect feedback, other results point to the brain being more active and involved with updating. Some studies have postulated that it is not a lack of attention, but rather a lack of externally directed attention that increases alpha power (Cooper et al 2003; Klimesch, Sauseng, Hanslmeyer 2007; Palva and Palva 2007). Ward (2003) suggests that alpha activity is associated with memory retrieval. During this task, it makes sense that individuals would be internally focused while updating the mental representation of the rule state. Increased alpha signal is correlated with activation in the insula and thalamus (Goldman et al 2002). The midline central (posterior frontal/anterior parietal) electrodes showed differences in cluster coefficient and node strength, whereas alpha activity typically is a more posterior, occipital finding. This suggests that the alpha oscillations are a function of thalamic input, coordinating attention in these regions to allow for updating of the mental representation of the rule state.

In the incorrect condition, the high frequency beta band showed notable differences in size and density, and notably in cluster coefficient in many frontal, midline,

and posterior electrodes. A small mid-left region of electrodes demonstrated greater node strength. Beta activity is generally associated with greater attention and increased activity (Pizzagalli 2006). However, the frequency band we are referring to is sometimes classified as gamma activity, which some researchers have defined as starting as low as 20 Hz (Logothetis 2008 supplement). Beta activity has been found to be diminished in a rehearsed task (Vecchiato et al 2013). Beta activity increases correlate with middle frontal activation, superior parietal, and inferior temporal gyrus activation (O’Gorman 2013). This adds more evidence that these structures are used in context updating during the incorrect feedback epochs. Beta activity shows a transient increase associated with the cessation of activity during a decision-making motor task (Wade and Brown 2016).

Our findings comparing the certain and uncertain card-matching component of the task found global measures describing greater connectivity and a larger network in the certain condition, suggesting that desynchronization at all frequency bands is occurring in the uncertain card-application condition. However, the correct versus incorrect network comparisons yielded some interesting differences. After incorrect feedback, the increased midline theta, midline alpha, and midline beta activities are consistent with a memory updating phenomena associated with adjusting the rule.



## CHAPTER 8: CONCLUSION

This project used multiple imaging modalities and analyses to evaluate executive brain function and decision-making, both in healthy individuals and in those with MCI. These analyses included not only traditional methods such as GLM analysis of fMRI and ERP analysis of EEG, but also less-used network methods. This project highlighted brain network differences between an MCI-highEF group and an MCI-lowEF group, as well as between conditions of rule certainty and uncertainty during decision-making. This project sought to answer to two main questions:

- What are the brain differences that exist between those with impaired executive abilities and those with intact executive abilities in MCI?
- What are the underlying brain activation differences that occur in individuals when making decisions under uncertain conditions?

These two topics, while seemingly disparate, are importantly linked by the question of what causes impairment in decision-making in disorders such as MCI. Individuals with pathological conditions may be faced with medical care decisions and they may be uncertain of the best way to select a course of action to yield the best effect on their life. This project started with a preliminary study on network differences in individuals with MCI grouped by high versus low executive abilities. Next, we provided an analysis of the brain regions involved in decision-making under conditions of rule certainty compared to rule uncertainty. The results of this study will allow for future studies of decision-making under uncertain conditions in pathological states such as MCI.

Chapter 2 provided an analysis of differences of rs-fMRI networks in an MCI-lowEF group versus an MCI-highEF group. The MCI-highEF group had a larger, nonspecific network. This network involved regions such as the frontal and parietal cortices, regions that are necessary for performing executive tasks and decision-making. The network results suggested functional compensation in those with low executive abilities. Chapter 3 provided an analysis of differences of structural networks in an MCI-lowEF group compared with an MCI-highEF group. The results showed a more connected network and greater white matter structural integrity in the MCI-highEF group. This suggests that those with higher white matter integrity are able to perform better on executive tasks, and that perhaps the greater functional connectivity in those with low executive abilities is compensating for this diminished white matter integrity. Chapter 5 described greater network connectivity in rule uncertain decision-making, as indicated by a number of measures such as network size, strength, and clustering coefficient of many ROIs. This coincided with increased BOLD signal activation in a number of the brain regions in the uncertain condition, particularly in the frontal, parietal, and occipital cortices and in regions of the basal ganglia. Combined with the decreased structural connectivity in MCI-lowEF individuals, this suggests that the decreased white matter connections that coincide with low executive ability may correspond with diminished ability to overcome uncertainty in decision-making. Chapter 6 reflected the ERPs associated with decision-making under uncertain conditions. The ERP analysis allowed for the study of the brain regions involved in making an uncertain decisions compared to a certain decisions, as well as a study of the brain regions involved in receiving feedback

during the two conditions. An n400-like effect was noted during the uncertain condition, and then a long (500-1000 ms) interval of increased potential of the certain condition over the uncertain condition was observed. We surmise that this could arise from the late positive component phenomenon, which is often associated with memory-reinforcing tasks. During feedback, a positive component in the 300 ms post-stimulus timeframe was notable for a large positive amplitude when receiving incorrect feedback. This may be a p300-like effect corresponding to memory updating when incorrect feedback was given. Chapter 7 illustrated that there is overall greater network connectivity in the certain condition during task performance than in the uncertain condition. These networks measures reflected greater frequency coherence in frequency bands of interest: delta, theta, low and high alpha, and low and high theta. The synchronization of these regions doesn't necessarily reflect greater cognitive effort, as our fMRI BOLD signal results indicates. This suggests diminished effort as brain regions synchronize, and desynchronization when effort is made to resolve rule uncertainty. However, during incorrect feedback there was some increased synchronization after incorrect feedback when compared to after correct feedback. This increased power during incorrect feedback occurred in the theta, high and low frequency alpha, and the high frequency beta bands. Taken together, these results suggest internally focused attention corresponding to rule updating, which is followed next by desynchronization as the effort is put forth to search for a new rule.

The results of this study suggest that an increased resting functional network and a decreased structural network, particularly in frontal and parietal regions, reflect

diminished executive abilities in MCI. Because a number of these regions are involved in uncertain decision-making, it follows that in these networks decreased structural integrity may lead to decreased decision-making abilities. In addition, ERP such as a late positive component-like wave arises from uncertainty, and a p300-like component arises from incorrect feedback during an uncertain condition. These findings are markers of uncertainty that can be measured in pathological conditions in which decision-making is impaired, such as MCI. The diminished white matter integrity in MCI may be keeping individuals from creating the focused brain activity necessary for executive abilities, which is paradoxically reflected as increased functional connectivity.

The limitations of this study have been discussed in detail in previous chapters. This study has provided some good initial baseline measures of networks involved in executive ability and decision-making. Future studies that involve measuring the card-matching task in pathological states would provide for greater understanding of the brain regions involved in decision-making and for understanding the pathological implications of impaired decision-making. This would facilitate therapeutic interventions to target improvement of specific brain region interactions.

## BIBLIOGRAPHY

- Acosta-Cabronero, J., & Nestor, P. J. (2014). Diffusion tensor imaging in Alzheimer's disease: Insights into the limbic-diencephalic network and methodological considerations. *Frontiers in Aging Neuroscience*, *6*(241), 143. doi:10.1016/j.media.2006.06.004
- Alexander, A. L., Lee, J. E., Lazar, M., & Field, A. S. (2007). Diffusion tensor imaging of the brain. *Neurotherapeutics*, *4*(3), 316-329.
- Alvarez, J. A., & Emory, E. (2006). Executive function and the frontal lobes: A meta-analytic review. *Neuropsychology Review*, *16*(1), 17-42. doi:10.1007/s11065-006-9002-x
- Alzheimer's Association. (2013). 2013 alzheimer's disease facts and figures. *Alzheimer's & Dementia*, *9*(2), 208-245. doi:10.1016/j.jalz.2013.02.003
- Andersen, R. A., & Cui, H. (2009). Intention, action planning, and decision making in parietal-frontal circuits. *Neuron*, *63*(5), 568-583. doi:10.1016/j.neuron.2009.08.028
- Anselme, P. (2015). Does reward unpredictability reflect risk? *Behavioural Brain Research*, *280*, 119-127. doi:10.1016/j.bbr.2014.12.003
- Aretouli, E., & Brandt, J. (2010). Everyday functioning in mild cognitive impairment and its relationship with executive cognition. *International Journal of Geriatric Psychiatry*, *25*(3), 224-233. doi:10.1002/gps.2325
- Bach, D. R., Pryce, C. R., & Seifritz, E. (2010). The experimental manipulation of uncertainty. *Animal Models of Behavioral Analysis*, *50*, 193-216. doi:10.1007/978-1-60761-883-6\_8
- Badre, D., & D'Esposito, M. (2009). Is the rostro-caudal axis of the frontal lobe hierarchical? *Nature Reviews Neuroscience*, *10*(9), 659-669. doi:10.1038/nrn2667
- Badre, D., Kayser, A. S., & D'Esposito, M. (2010). Frontal cortex and the discovery of abstract action rules. *Neuron*, *66*(2), 315-326. doi:10.1016/j.neuron.2010.03.025
- Basar, E., Basar-Eroglu, C., Karakas, S., & Schurmann, M. (2001). Gamma, alpha, delta, and theta oscillations govern cognitive processes. *International Journal of Psychophysiology*, *39*, 241-248.

- Baxter, M. G., Parker, A., Lindner, C. C. C., Izquierdo, A. D., & Murray, E. A. (2000). Control of response selection by reinforcer value requires interaction of amygdala and orbital prefrontal cortex. *Journal of Neuroscience*, *20*(11), 4311-4319.
- Beck, J. M., Ma, W. J., Kiani, R., Hanks, T., Churchland, A. K., Roitman, J., . . . Pouget, A. (2008). Probabilistic population codes for bayesian decision making. *Neuron*, *60*(6), 1142-1152. doi:10.1016/j.neuron.2008.09.021
- Bengtsson, S. L., Haynes, J. D., Sakai, K., Buckley, M. J., & Passingham, R. E. (2009). The representation of abstract task rules in the human prefrontal cortex. *Cerebral Cortex*, *19*(8), 1929-1936. doi:10.1093/cercor/bhn222
- Berntson, G. G., Bechara, A., Damasio, H., Tranel, D., & Cacioppo, J. T. (2007). Amygdala contribution to selective dimensions of emotion. *Social Cognitive and Affective Neuroscience*, *2*(2), 123-129. doi:10.1093/scan/nsm008
- Bhanji, J. P., Beer, J. S., & Bunge, S. A. (2010). Taking a gamble or playing by the rules: Dissociable prefrontal systems implicated in probabilistic versus deterministic rule-based decisions. *Neuroimage*, *49*(2), 1810-1819. doi:10.1016/j.neuroimage.2009.09.030
- Biswal, B. B. (2012). Resting state fMRI: A personal history. *Neuroimage*, *62*(2), 938-944. doi:10.1016/j.neuroimage.2012.01.090
- Bland, A. R., & Schaefer, A. (2011). Electrophysiological correlates of decision making under varying levels of uncertainty. *Brain Research*, *1417*(C), 55-66. doi:10.1016/j.brainres.2011.08.031
- Bogacz, R., & Larsen, T. (2011). Integration of reinforcement learning and optimal decision-making theories of the basal ganglia. *Neural Computation*, *23*, 817-851.
- Bossaerts, P. (2010). Risk and risk prediction error signals in anterior insula. *Brain Structure and Function*, *214*(5-6), 645-653. doi:10.1007/s00429-010-0253-1
- Botvinick, M. M. (2007). Conflict monitoring and decision making: Reconciling two perspectives on anterior cingulate function. *Cognitive, Affective, & Behavioral Neuroscience*, *7*(4), 356-366.
- Braak, H., & Tredici, K. D. (2014). In Korf H. -. (Ed.), *Neuroanatomy and pathology of sporadic alzheimer's disease*. Frankfurt, Germany: Springer.
- Bromberg-Martin, E. S., & Hikosaka, O. (2009). Midbrain dopamine neurons signal preference for advance information about upcoming rewards. *Neuron*, *63*(1), 119-126. doi:10.1016/j.neuron.2009.06.009

- Bruin, G. O. d., Rassin, E., & Muris, P. (2006). Worrying in the lab: Does intolerance of uncertainty have predictive value? *Behavior Change*, *23*(2), 138-147.
- Brunner, J. F., Olsen, A., Aasen, I. E., Lohaugen, G. C., Haaberg, A. K., & Kropotov, J. (2015). Neuropsychological parameters indexing executive processes are associated with independent components of ERPs. *Neuropsychologia*, *66*, 144-156. doi:10.1016/j.neuropsychologia.2014.11.019
- Buckner, R. L., Andrews-Hanna, J. R., & Schacter, D. L. (2008). The brain's default network: Anatomy, function, and relevance to disease. *Annals of the New York Academy of Sciences*, *1124*(1), 1-38. doi:10.1196/annals.1440.011
- Buzzell, G. A., Roberts, D. M., Fedota, J. R., Thompson, J. C., Parasuraman, R., & McDonald, C. G. (2016). Uncertainty-dependent activity within the ventral striatum predicts task-related changes in response strategy. *Cognitive, Affective, & Behavioral Neuroscience*, *16*, 219-233. doi:10.3758/s13415-015-0383-2
- Cavanagh, J. F., & Shackman, A. J. (2015). Frontal midline theta reflects anxiety and cognitive control: Meta-analytic evidence. *Journal of Physiology - Paris*, *109*, 3-15. doi:10.1016/j.jphysparis.2014.04.003
- Churchland, A. K., & Ditterich, J. (2012). New advances in understanding decisions among multiple alternatives. *Current Opinion in Neurobiology*, *22*(6), 920-926. doi:10.1016/j.conb.2012.04.009
- Cohen, M. X., Elger, C. E., & Ranganath, C. (2007). Reward expectation modulates feedback-related negativity and EEG spectra. *Neuroimage*, *35*(2), 968-978. doi:10.1016/j.neuroimage.2006.11.056
- Cohen, M., Heller, A., & Ranganath, C. (2005). Functional connectivity with anterior cingulate and orbitofrontal cortices during decision-making. *Cognitive Brain Research*, *23*, 61-70. doi:10.1016/j.cogbrainres.2005.01.010
- Cooper, N. R., Croft, R. J., Dominey, S. J., Burgess, A. P., & Gruzelier, J. H. (2003). Paradox lost? exploring the role of alpha oscillations during externally vs. internally directed attention and the implications for idling and inhibition hypotheses. *International Journal of Psychophysiology*, *47*, 65-74.
- Cui, J., Chen, Y., Wang, Y., Shum, D. H. K., & Chan, R. C. K. (2013). Neural correlates of uncertain decision making: ERP evidence from the iowa gambling task. *Frontiers in Human Neuroscience*, *7*, 1-14. doi:10.3389/fnhum.2013.00776
- Daw, N. D., & Doya, K. (2006). The computational neurobiology of learning and reward. *Current Opinion in Neurobiology*, *16*, 199-204. doi:10.1016/j.conb.2006.03.006

- Demanele, C., Kirsch, P., Esslinger, C., Zink, M., Meyer-Lindenberg, A., & Durstewitz, D. (2013). Activation of midbrain and ventral striatal regions implicates salience processing during a modified beads task. *Public Library of Science One*, 8(3), 1-14. doi:10.1371/journal.pone.0058536.t004
- Desikan, R. S., Segonne, F., Fischl, B., Quinn, B. T., Dickerson, B. C., Blacker, D., . . . Killiany, R. J. (2006). An automated labeling system for subdividing the human cerebral cortex on MRI scans into gyral based regions of interest. *Neuroimage*, 31, 968-980. doi:10.1016/j.neuroimage.2006.01.021
- Esposito, R., Mosca, A., Pieramico, V., Cieri, F., Cera, N., & Sensi, S. L. (2013). Characterization of resting state activity in MCI individuals. *Peerj*, 1(e135), 1-17. doi:10.7717/peerj.135/supp-1
- Ferreira, L. K., Diniz, B. S., Forlenza, O. V., Busatto, G. F., & Zanetti, M. V. (2011). Neurostructural predictors of alzheimer's disease: A meta-analysis of VBM studies. *Neurobiology of Aging*, 32(10), 1733-1741. doi:10.1016/j.neurobiolaging.2009.11.008
- Fiorillo, C. D., Tobler, P. N., & Schultz, W. (2003). Discrete coding of reward probability and uncertainty by dopamine neurons. *Science*, 299, 1898-1902.
- Franko, E., & Joly, O. (2013). Evaluating alzheimer's disease progression using rate of regional hippocampal atrophy. *Public Library of Science One*, 8(8), e71354. doi:10.1371/journal.pone.0071354.t002
- Garrido, M. I., Barnes, G. R., Kumaran, D., Maguire, E. A., & Dolan, R. J. (2015). Ventromedial prefrontal cortex drives hippocampal theta oscillations induced by mismatch computations. *Neuroimage*, 120(C), 362-370. doi:doi:10.1016/j.neuroimage.2015.07.016
- Gibbons, L. E., Carle, A. C., Mackin, R. S., Harvey, D., Mukherjee, S., Insel, P., . . . Crane, P. K. (2012). A composite score for executive functioning, validated in alzheimer's disease neuroimaging initiative (ADNI) participants with baseline mild cognitive impairment. *Brain Imaging and Behavior*, 6(4), 517-527. doi:10.1007/s11682-012-9176-1
- Gloor, P. (1994). Berger lecture. is berger's dream coming true? *Electroencephalography and Clinical Neurophysiology*, 90, 253-266.
- Gold, B. T., Johnson, N. F., Powell, D. K., & Smith, C. D. (2012). White matter integrity and vulnerability to alzheimer's disease: Preliminary findings and future directions. *Biochimica Et Biophysica Acta*, 1822(3), 416-422. doi:doi:10.1016/j.bbadis.2011.07.009



- Goldman, R. I., Stern, J. M., Engel, J., & Cohen, M. S. (2002). Simultaneous EEG and fMRI of the alpha rhythm. *Neuroreport*, *13*, 2487-2492. doi:10.1097/01.wnr.0000047685.08940.d0
- Gorisek, V. R., Belic, A., Manouilidou, C., Koritnik, B., Repovs, G., Bon, J., . . . Zidar, J. (2015). The electrophysiological correlates of the working memory subcomponents: Evidence from high-density EEG and coherence analysis. *Neurological Sciences*, *36*(12), 2199-2207. doi:10.1007/s10072-015-2337-4
- Goveas, J., O'dwyer, L., Mascalchi, M., Cosottini, M., Diciotti, S., Santis, S. D., . . . Giannelli, M. (2015). Diffusion-MRI in neurodegenerative disorders. *Magnetic Resonance Imaging*, *33*(7), 853-876. doi:doi:10.1016/j.mri.2015.04.006
- Hutchinson, J. B., Uncapher, M. R., & Wagner, A. D. (2015). Increased functional connectivity between dorsal posterior parietal and ventral occipitotemporal cortex during uncertain memory decisions. *Neurobiology of Learning and Memory*, *117*, 71-83. doi:10.1016/j.nlm.2014.04.015
- Jenkinson, M., Bannister, P., Brady, M., & Smith, S. (2002). Improved optimization for the robust and accurate linear registration and motion correction of brain images. *Neuroimage*, *17*(2), 825-841. doi:10.1006/nimg.2002.1132
- Johnson, J. K., Lui, L., & Yaffe, K. (2007). Executive function, more than global cognition, predicts functional decline and mortality in elderly women. *The Journals of Gerontology: Series A*, *62*(10), 1134-1141.
- Kepecs, A., Uchida, N., Zariwala, H. A., & Mainen, Z. F. (2008). Neural correlates, computation and behavioural impact of decision confidence. *Nature*, *455*(7210), 227-231. doi:10.1038/nature07200
- Kiani, R., & Shadlen, M. N. (2009). Representation of confidence associated with a decision by neurons in the parietal cortex. *Science*, *324*(8), 759-776.
- Klein-Flugge, M. C., Barron, H. C., Brodersen, K. H., Dolan, R. J., & Behrens, T. E. J. (2013). Segregated encoding of reward-identity and stimulus-reward associations in human orbitofrontal cortex. *Journal of Neuroscience*, *33*(7), 3202-3211. doi:10.1523/JNEUROSCI.2532-12.2013
- Klimesch, W. (1999). EEG alpha and theta oscillations reflect cognitive and memory performance: A review and analysis. *Brain Research Reviews*, *29*, 169-195.
- Klimesch, W., Sauseng, P., & Hanslmayr, S. (2007). EEG alpha oscillations: The inhibition--timing hypothesis. *Brain Research Reviews*, *63*-88. doi:10.1016/j.brainresrev.2006.06.003

- Kramer, M. A. (2014). *An introduction to field analysis techniques: The power spectrum and coherence*. Unpublished manuscript. Retrieved November 1, 2015, Retrieved from <http://www.sfn.org/Careers-and-Training/Career-Tools-and-Resources/Short-Courses/2013-Short-Course-II>
- Krug, A., Cabanis, M., Pyka, M., Pauly, K., Walter, H., Landsberg, M., . . . Kircher, T. (2014). Investigation of decision-making under uncertainty in healthy subjects: A multi-centric fMRI study. *Behavioural Brain Research*, *261*, 89-96. doi:10.1016/j.bbr.2013.12.013
- Lebreton, M., Bertoux, M., Boutet, C., Lehericy, S., Dubois, B., Fossati, P., & Pessiglione, M. (2013). A critical role for the hippocampus in the valuation of imagined outcomes. *Public Library of Science Biology*, *11*(10), e1001684. doi:10.1371/journal.pbio.1001684.s002
- Lo, C., Wang, P., Chou, K., Wang, J., He, Y., & Lin, C. (2010). Diffusion tensor tractography reveals abnormal topological organization in structural cortical networks in alzheimer's disease. *Journal of Neuroscience*, *30*(50), 16876-16885. doi:10.1523/JNEUROSCI.4136-10.2010
- Logothetis, N. K. (2002). The neural basis of the blood-oxygen-level-dependent functional magnetic resonance imaging signal. *Philosophical Transactions of the Royal Society B: Biological Sciences*, *357*(1424), 1003-1037. doi:10.1098/rstb.2002.1114
- Logothetis, N. K. (2008). What we can do and what we cannot do with fMRI. *Nature*, *453*(7197), 869-878. doi:10.1038/nature06976
- Madelaine Daianu, Neda Jahanshad, Talia M Nir, Arthur W Toga, Clifford R Jack, Michael W Weiner, & Paul M Thompson, A. (2013). Breakdown of brain connectivity between normal aging and alzheimer's disease: A structural k-core network analysis. *Brain Connectivity*, *3*(4), 407-422. doi:10.1089/brain.2012.0137
- Matsuzawa, D., Shirayama, Y., Niitsu, T., Hashimoto, K., & Iyo, M. (2015). Deficits in emotion based decision-making in schizophrenia; a new insight based on the iowa gambling task. *Progress in Neuropsychopharmacology & Biological Psychiatry*, *57*(C), 52-59. doi:doi:10.1016/j.pnpbp.2014.10.007
- Nieuwenhuys, R., Voogd, J., & van Huijzen, C. (2008). *The human central nervous system* (4th ed.). Germany: Springer Berlag.
- Nowrangi, M. A., Lyketsos, C. G., Leoutsakos, J. S., Oishi, K., Albert, M., Mori, S., & Mielke, M. M. (2013). Longitudinal, region-specific course of diffusion tensor

- imaging measures in mild cognitive impairment and alzheimer's disease. *Alzheimer's & Dementia*, 9(5), 519-528. doi:10.1016/j.jalz.2012.05.2186
- Nowrangi, M. A., Okonkwo, O., Lyketsos, C., Oishi, K., Mori, S., Albert, M., & Mielke, M. M. (2015). Atlas-based diffusion tensor imaging correlates of executive function. *Journal of Alzheimer's Disease*, 44(2), 585-598.
- Nowrangi, M. A., & Rosenberg, P. B. (2015). The fornix in mild cognitive impairment and alzheimer's disease. *Frontiers in Aging Neuroscience*, 7, 1-7. doi:10.3389/fnagi.2015.00001
- O'gorman, R. L., Poil, S. -, Brandeis, D., Klaver, P., Bollmann, S., Ghisleni, C., . . . Michels, L. (2013). Coupling between resting cerebral perfusion and EEG. *Brain Topography*, 26(3), 442-457. doi:10.1007/s10548-012-0265-7
- Palva, S., & Palva, J. M. (2007). New vistas for alpha-frequency band oscillations. *Trends in Neurosciences*, 30(4), 150-158. doi:10.1016/j.tins.2007.02.001
- Pandey, A. K., Kamarajan, C., Manz, N., Chorlian, D. B., Stimus, A., & Porjesz, B. (2016). Delta, theta, and alpha event-related oscillations in alcoholics during Go/NoGo task: Neurocognitive deficits in execution, inhibition, and attention processing. *Progress in Neuropsychopharmacology & Biological Psychiatry*, 65(C), 158-171. doi:doi:10.1016/j.pnpbp.2015.10.002
- Pereiro, A. X., Juncos-Rabadan, O., & Facal, D. (2014). Attentional control in amnesic MCI subtypes: Insights from a simon task. *Neuropsychology*, 28(2), 261-272. doi:10.1037/neu0000047
- Philiastides, M. G., Biele, G., & Heekeren, H. R. (2010). A mechanistic account of value computation in the human brain. *Proceedings of the National Academy of Sciences*, 107(20), 9430-9435. doi:10.1073/pnas.1001732107
- Philiastides, M. G., Biele, G., Vavatzanidis, N., Kazzer, P., & Heekeren, H. R. (2010). Temporal dynamics of prediction error processing during reward-based decision making. *Neuroimage*, 53(1), 221-232. doi:10.1016/j.neuroimage.2010.05.052
- Pizzagalli, D. A., Oakes, T. R., Fox, A. S., Chung, M. K., Larson, C. L., Abercrombie, H. C., . . . Davidson, R. J. (2004). Functional but not structural subgenual prefrontal cortex abnormalities in melancholia. *Molecular Psychiatry*, 9(4), 393-405. doi:10.1038/sj.mp.4001469
- Pizzagalli, D. A. (2007). Electroencephalography and high-density electrophysiological source localization. In J. T. Cacioppo, L. G. Tassinary & G. Berntson (Eds.),

*Handbook of psychophysiology* (3rd ed., pp. 56-84). Cambridge, England: Cambridge University Press.

- Polania, R., Krajbich, I., Grueschow, M., & Ruff, C. C. (2014). Neural oscillations and synchronization differentially support evidence accumulation in perceptual and value-based decision making. *Neuron*, *82*(3), 709-720. doi:10.1016/j.neuron.2014.03.014
- Polich, J. (2007). Updating P300: An integrative theory of P3a and P3b. *Clinical Neurophysiology*, *118*, 2128-2148. doi:10.1016/j.clinph.2007.04.019
- Pouget, A., Drugowitsch, J., & Kepecs, A. (2016). Confidence and certainty: Distinct probabilistic quantities for different goals. *Nature Neuroscience*, *19*(3), 366-374. doi:10.1038/nn.4240
- Reuman, L., Jacoby, R. J., Fabricant, L. E., Herring, B., & Abramowitz, J. S. (2015). Uncertainty as an anxiety cue at high and low levels of threat. *Journal of Behavior Therapy and Experimental Psychiatry*, *47*, 111-119. doi:10.1016/j.jbtep.2014.12.002
- Rosen, N. O., & Knauper, B. (2009). A little uncertainty goes a long way: State and trait differences in uncertainty interact to increase information seeking but also increase worry. *Health Communication*, *24*(3), 228-238. doi:10.1080/10410230902804125
- Rosler, F. (2005). From single-channel recordings to brain-mapping devices: The impact of electroencephalography on experimental psychology. *History of Psychology*, *8*(1), 95-117. doi:10.1037/1093-4510.8.1.95
- Rubinov, M., & Sporns, O. (2010). Complex network measures of brain connectivity: Uses and interpretations. *Neuroimage*, *52*(3), 1059-1069. doi:10.1016/j.neuroimage.2009.10.003
- Samejima, K., Ueda, Y., Doya, K., & Kimura, M. (2005). Representation of action-specific reward values in the striatum. *Science*, *310*(5752), 1337-1340.
- Selimbeyoglu, A., Keskin-Ergen, Y., & Demiralp, T. (2012). What if you are not sure? electroencephalographic correlates of subjective confidence level about a decision. *Clinical Neurophysiology*, *123*(6), 1158-1167. doi:10.1016/j.clinph.2011.10.037
- Smith, E. H., Banks, G. P., Mikell, C. B., Cash, S. S., Patel, S. R., Eskandar, E. N., & Sheth, S. A. (2015). Frequency-dependent representation of reinforcement-related information in the human medial and lateral prefrontal cortex. *Journal of Neuroscience*, *35*(48), 15827-15836. doi:10.1523/JNEUROSCI.1864-15.2015

- Smith, S. M., Jenkinson, M., Woolrich, M. W., Beckmann, C. F., Behrens, T. E., Johansen-Berg, H., . . . Matthews, P. M. (2004). Advances in functional and structural MR image analysis and implementation as FSL. *Neuroimage*, *23*, S208-S219. doi:10.1016/j.neuroimage.2004.07.051
- Speckmann, E., Elger, C. E., & Gorji, A. (2010). Introduction to the neurophysiologic basis of EEG and DC potentials. In E. Niedermeyer, & F. Lopes da Silva (Eds.), *Electroencephalography: Basic principles, clinical applications, and related fields* (5th ed., pp. 1-16). Philadelphia, PA: Lippincott Williams and Wilkins.
- Stalnaker, T. A., Calhoun, G. G., Ogawa, M., Roesch, M. R., & Schoenbaum, G. (2012). Reward prediction error signaling in posterior dorsomedial striatum is action specific. *Journal of Neuroscience*, *32*(30), 10296-10305. doi:10.1523/JNEUROSCI.0832-12.2012
- Styliadis, C., Ioannides, A. A., Bamidis, P. D., & Papadelis, C. (2014). Amygdala responses to valence and its interaction by arousal revealed by MEG. *International Journal of Psychophysiology*, *93*(1), 121-133. doi:doi:10.1016/j.ijpsycho.2013.05.006
- Terada, S., Sato, S., Nagao, S., Ikeda, C., Shindo, A., Hayashi, S., . . . Uchitomi, Y. (2013). Trail making test B and brain perfusion imaging in mild cognitive impairment and mild alzheimer's disease. *Psychiatry Research: Neuroimaging*, *213*(3), 249-255. doi:10.1016/j.psychresns.2013.03.006
- Triebel, K., Martin, R., Griffith, H., Marceaux, J., Okonkwo, O., Harrell, L., . . . Marson, D. (2009). Declining financial capacity in mild cognitive impairment. *Neurology*, *73*, 928-934.
- Trujillo, L. T., & Allen, J. J. (2007). Theta EEG dynamics of the error-related negativity. *Clinical Neurophysiology*, *118*, 645-668. doi:10.1016/j.clinph.2006.11.009
- Vecchiato, G., Susac, A., Margeti, S., Fallani, F. D. V., Maglione, A. G., Supek, S., . . . Babiloni, F. (2013). High-resolution EEG analysis of power spectral density maps and coherence networks in a proportional reasoning task. *Brain Topography*, *26*(2), 303-314. doi:10.1007/s10548-012-0259-5
- Ward, L. M. (2003). Synchronous neural oscillations and cognitive processes. *Trends in Cognitive Sciences*, *17*(12), 553-559. doi:10.1016/j.tics.2003.10.012
- White, T. P., Engen, N. H., Sorensen, S., Overgaard, M., & Shergill, S. S. (2014). Uncertainty and confidence from the triple-network perspective: Voxel-based meta-analyses. *Brain and Cognition*, *85*, 191-200. doi:10.1016/j.bandc.2013.12.002

- Xia, M., Wang, J., & He, Y. (2013). BrainNet viewer: A network visualization tool for human brain connectomics. *Public Library of Science One*, 8(7), e68910. doi:10.1371/journal.pone.0068910.t001
- Ye, B. S., Seo, S. W., Yang, J. -, Kim, H. J., Kim, Y. J., Yoon, C. W., . . . Na, D. L. (2013). Comparison of cortical thickness in patients with early-stage versus late-stage amnesic mild cognitive impairment. *European Journal of Neurology*, 21(1), 86-92. doi:10.1111/ene.12251
- Yendiki, A. (2011). Automated probabilistic reconstruction of white-matter pathways in health and disease using an atlas of the underlying anatomy. *Frontiers in Neuroinformatics*, 5, 1-12. doi:10.3389/fninf.2011.00023
- Zalesky, A., Fornito, A., & Bullmore, E. T. (2010). Network-based statistic: Identifying differences in brain networks. *Neuroimage*, 53(4), 1197-1207. doi:10.1016/j.neuroimage.2010.06.041
- Zhang, L., Dong, Y., Ji, Y., Zhu, C., Yu, F., Ma, H., . . . Wang, K. (2015). Dissociation of decision making under ambiguity and decision making under risk: A neurocognitive endophenotype candidate for obsessive--compulsive disorder. *Progress in Neuropsychopharmacology & Biological Psychiatry*, 57(C), 60-68. doi:doi:10.1016/j.pnpbp.2014.09.005
- Zheng, D., Sun, H., Dong, X., Liu, B., Xu, Y., Chen, S., . . . Wang, X. (2014). Executive dysfunction and gray matter atrophy in amnesic mild cognitive impairment. *Neurobiology of Aging*, 35(3), 548-555. doi:10.1016/j.neurobiolaging.2013.09.007
- Zhuang, L., Sachdev, P. S., Trollor, J. N., Kochan, N. A., Reppermund, S., Brodaty, H., & Wen, W. (2012). Microstructural white matter changes in cognitively normal individuals at risk of amnesic MCI. *Neurology*, 79, 748-754.

## CURRICULUM VITAE

Danielle Farrar

Address: 140 Saratoga St #3  
Boston MA 02128

Phone: 206-660-8878

Email: dfarrar@bu.edu

Year of Birth: 1980

### Education

Doctor of Philosophy

Boston University, Department of Anatomy and Neurobiology  
August 2008 – May 2018 (Anticipated)

Doctor of Medicine

Boston University, August 2008-May 2018 (Anticipated)

Master of Arts, Medical Sciences

Boston University, Jan 2007-May 2008

Bachelor of Science, Computer Science

University of Washington, Seattle, WA, March 2000-June 2003

Harvey Mudd College, Claremont, CA

September 1998-December 1999

### Research Experience

Center for Biomedical Imaging

Boston University School of Medicine, Department of Anatomy and Neurobiology  
January 2013 - Current

*Decision-Making Under Uncertainty:* Currently investigating rule learning and rule application during a custom-developed card-sorting task, using electroencephalography (EEG) and functional magnetic resonance imaging (fMRI).

*Functional Connectivity Differences in MCI patients with High versus Low Executive Abilities:* Network analysis of functional resting state networks in individuals with mild cognitive impairment with high versus low executive abilities.

*Structural Connectivity Differences in MCI patients with High versus Low Executive Abilities:* Network analysis of structural diffusion data in individuals with mild cognitive impairment with high versus low executive abilities.

Neuroscience Interdisciplinary Modeling and Simulation Center,  
 Boston University School of Medicine, Department of Anatomy and Neurobiology  
 July 2010 – December 2012

*Rule Application:* Investigation of rule learning and rule application during a custom-developed card-sorting task, using electroencephalography and source localization techniques.

*CityLab Patient Simulator.* “They Mystery of the Crooked Cell” project. Developed a patient simulator using Java and MySQL. The application creates dynamic patient physiologic variables based on patient sickle cell anemia genotype. Front-end display includes a basic patient medical record and plots of physiological variables over time.

Neuroscience Interdisciplinary Modeling and Simulation Center,  
 Boston University School of Medicine, Department of Anatomy and Neurobiology.  
 March 2009-August 2009

Worked on preliminary investigation of neural suppression of noisy information in normal subjects using EEG recordings of the p300 signal.

Summer Internship in Addiction Medicine  
 Department of General Internal Medicine at Boston Medical Center  
 Summer 2007

Completed a chart review of methadone maintenance patients and the level of prescribed potentially dangerous medication interactions in the patient’s primary care record.

Summer Undergraduate Research Program  
 Department of Biomedical and Health Informatics  
 Summer 2002

Developed a tool assist the GeneReviews clinical staff that displayed database information as a productivity chart dynamically. (Java servlets, Perl, and SQL).

Summer Institute in Mathematics for Undergraduates,  
 University of Puerto Rico  
 Summer 2000

Completed a group research project proving theorems about relationships between graph theory and computational algebra.

Associated Western Universities Undergraduate Fellow  
 Pacific Northwest National Laboratories  
 High Performance Computational Chemistry Group  
 Summer 1998, 1999

Completed GUI applications in Java to aid the simulation of chemical scenarios.



### **Publications**

Walley, A. Y., Farrar, D. C., Cheng, D. M., Alford, D. P., & Samet, J. H. (2009). *Are Opioid Dependence and Methadone Maintenance Treatment (MMT) Documented in the Medical Record? A Patient Safety Issue*. *Journal of General Internal Medicine*, 24 (9), 1007-1011.

### **Posters**

Farrar D., Moss, M., Killiany, R. (2016, February) Structural Network Differences in Individuals with High versus Low Executive Abilities in Mild Cognitive Impairment. International Neuropsychological Society Conference.

Farrar D., Moss, M., Killiany, R. (2014, September) Functional network correlates of impaired executive function in mild cognitive impairment. Resting State and Brain Connectivity Conference.

Farrar, D., & Bergethon, P. (2012, April). Evoked Potentials Reflecting the Rule State During the Wisconsin Card Sort Task. American Academy of Neurology .

Farrar, D., & Bergethon, P. (2011, July). An Analysis of Evoked Potentials Demonstrated During the Wisconsin Card Sort. National MD/PhD Student Conference .

Farrar, D., Mazano, Y., & Torres Acevedo, J. M. (2001, January). Binomial Ideals from Graphs. Joint Mathematics Meetings .

Farrar, D., Manzano, Y., & Torres-Acevedo, J. M. (2000, October). Binomial Ideals from Graphs. Society for the Advancement of Chicanos and Native Americans in Science .

### **Work Experience**

#### Tutor

Wyzant Tutoring, Private Tutor

January 2013 – May 2016

- Private tutor at the middle school, high school, college and graduate level.
- Subjects tutored: Biology, Chemistry, Computer Science, Math (Algebra, Trigonometry, Pre-calculus), Spanish, Test Prep (GRE, MCAT, SAT, SSAT)

#### Tutor

Chyten Tutoring

July 2010-July 2012

- Private SAT and subject tutor to high school students

#### Consulting Engineer

Teranode Corporation

April 2005-December 2006

Responsibilities:

- Developed project plans for multiple projects, prioritizing requirements and adhering to deadlines through all phases of project cycle.

- Understood complex user requirements involving modeling laboratory workflow in a large pharmaceutical company, and determined how to meet the end-user needs using the Teranode Design Suite platform.
- Implemented software solutions using Teranode Design Suite and java plug-ins to optimize the drug discovery process for teams of scientists at the Pfizer Research Technology Center.

#### Software Engineer

Ursus Technologies

September 2004-April 2005

Responsibilities:

- Software planning, design and implementation in PHP and Perl for a MySQL database-driven web-based shopping cart and a web-based customer resource management system.
- Development of database maintenance and remote server communication scripts written in Perl.

#### Web Computing Specialist

University of Washington - GeneTests

Feb 2004 – August 2004

Responsibilities:

- Developed and enhanced the GUI for database content maintenance.
- Provided network support and workstation system administration for the content team.

#### Information Technologist Tech I/Computer Support Analyst I

University of Washington – Department of Pediatrics

January 2003-February 2004

Responsibilities:

- Assisted with various programming applications to improve features on the GeneTests website.
- Network administration.
- Designed and implemented an automation tool that takes user specifications and auto-generates Java swing forms for submitting patient information into a MySQL database.

#### Teaching Experience

##### Teaching Fellow

Boston University – Department of Anatomy and Neurobiology

*Cognitive Neuroscience*, Spring 2013, 2014, 2015, 2016

*Cellular Organization of Tissues*, Fall 2011

*Medical Histology, Spring 2011*

Tutor, Boston University:

Department of Biochemistry, Medical Biochemistry, Fall 2008

Department of Physiology, Medical Physiology, Spring 2009

Department of Anatomy and Neurobiology, Medical Histology, Spring 2011

Teaching Assistant

University of Washington – Department of Computer Science

September 2002 - March 2003

Intro to Computer Programming 1 and 2

Responsibilities:

- Taught Java programming language twice weekly to a quiz section of students for Computer Programming II.
- Graded programming and written assignments
- Held weekly office hours.

Research Skills

Methods: Electroencephalography, Magnetic Resonance Imaging, functional Magnetic Resonance Imaging, Diffusion Tensor Imaging.

Programming: Java, MATLAB scripting, SQL, Stella Modeling, Perl, C++

Coursework

Graduate School:

Advanced Topics in Writing, Journal Club (2 semesters), Cognitive Neuroscience, Computational Modeling, Systems Neurobiology, Elementary Statistics

Medical School:

Second Year, Disease and Therapy: 8 Modules of System based Pharmacology, Pathology and Treatment

First Year: Medical Physiology, Genetics, Gross Anatomy, Medical Biochemistry, Medical Histology, Medical Neuroscience, Endocrinology, Immunology

Undergraduate:

Computer Graphics, Methods in Applied Mathematics, Machine Organization and Assembly Language, Intro to Artificial Intelligence, Data Structures, Intro to the Theory of Computing, Intro to Digital Design, Intro to Formal Models, Programming Languages, Intro to Programming I/II

Personal Activities

PhD Student representative, Anatomy and Neurobiology Department, Fall 2013- Spring 2014

Ran graduate student sessions, helped organize student activities.

Planning Committee, 2012 Guisippina d’Raviola Memorial Seminar.

Organized yearly seminar, invited speaker, arranged facilities and advertising.

Clinical Neuroscience Society MD/PhD Representative, Fall 2010-Spring 2012

Helped organize Clinical Neuroscience talks and events on the Boston University Medical Campus.

Graduate Medical Sciences Student Organization Representative, Fall 2010, Spring 2011

Attended monthly meetings and participated in campus events and volunteer activities.

Data Manager, Medical Student Team, Project Trust, April 2009-April 2010

Collected and submitted monthly data collected by the Boston University School of Medicine Project Trust Team of Medical Student Volunteers.

Volunteer, Project Trust, February 2009 – April 2010

Performed rapid HIV tests and counseling on patients in Boston Medical Center and at CAB detox

Intensive Medical Spanish Program, Pop-Wuj, Quetzaltenango Guatemala, May-June 2008

Completed 5 weeks of intensive language instruction.

Volunteer, Atención Primaria en Salud, Nicaragua, July 2008

Assisted in interviewing and assessing community health workers in rural Nicaragua.

Volunteer, Boston Medical Center, September 2007-December 2007

Participated as a disability advocate for the “Here to Help” Program, by sitting weekly with a patient during dialysis sessions.

Volunteer, Massachusetts Screening, Brief Intervention, Referral, and Treatment (MASBIRT), June 2007-December 2007

Screened patients for unhealthy drug, alcohol, and tobacco use, and performed brief interventions and provided referrals to treatment when indicated.

Volunteer, Brigham and Women’s hospital, June 2006-June 2007

Weekly shifts, first volunteering in Central Transport, then in the Neonatal Intensive Care Unit, then in the Multiple Sclerosis Infusion Clinic.